

DISSERTATION

On the Dynamics of an Axially Moving Cable with Application to Ropeways

ausgeführt zum Zwecke der Erlangung des akademischen Grades eines
Doktors der technischen Wissenschaften unter der Leitung von

Ao.Univ.Prof. Dipl.-Ing. Dr.techn. Alois Steindl
E325
Institut für Mechanik und Mechatronik

eingereicht an der Technischen Universität Wien
Fakultät für Maschinenbau und Betriebswissenschaften

von

Dipl.-Ing. Hans Christian Renezeder
9325710
Davidgasse 39/28
A - 1100 Wien

Wien, am 25. Jänner 2006

Kurzfassung

Seilschwebbahnen stellen ein wichtiges Transportmittel in gebirgigen Regionen dar. Dennoch kommt es jährlich, trotz hoher Sicherheitsmaßnahmen, zu mehreren unverhergesehenen Zwischenfällen und leider auch zu Unfällen. Einige davon haben ihre Ursache in menschlichen Versagen, aber andere passieren auch aufgrund eines ungünstigen Zusammenwirkens von Anordnung und Betriebsbedingungen der Seilbahnen. Das hat zur Folge, daß manchmal große unerwünschte Schwingungen des Seiles (Pumpschwingungen) auftreten. Diese gefährden aber nicht nur den Fahrkomfort sondern auch die Sicherheit. Selbst bei der Planung moderner Einseilumlaufbahnen greift man auf ziemlich einfache Modelle zurück, wenn man mögliche Pumpschwingungen vorhersagen oder analysieren möchte. Manche dieser Modelle reduzieren das komplexe mechanische System der gesamten Seilbahn auf ein System mit nur sehr wenig Freiheitsgraden. Dieser starken Vereinfachung gehen klarerweise eine Vielzahl von Annahmen voraus deren Gültigkeit aber fraglich ist. Dennoch bietet bereits das Seil alleine - als eindimensionale kontinuierliche Struktur betrachtet - mit seinen unendlich vielen Freiheitsgraden eine sehr facettenreiche und interessante Dynamik. Da diese daher auch bei der Erklärung von Pumpschwingungen berücksichtigt werden sollte, ist der Ausgangspunkt dieser Untersuchung die Dynamik eines axial bewegten Seiles.

Nach Aufstellung der allgemeinen Bewegungsgleichungen eines zwischen zwei Ösen in einem äußeren Kraftfeld räumlich und axial bewegten Seiles wird der Fall des konstanten Schwerfeldes diskutiert. Es werden die möglichen stationären Bewegungszustände beschrieben und die Abhängigkeit dieser von der axialen Geschwindigkeit erläutert, wenn die Seilkraft in einer der Ösen vorgegeben wird. Das entspricht auch der Situation in den Seilfeldern einer Einseilumlaufbahn. In weiterer Folge wird das entsprechende linearisierte Problem diskutiert und damit die Eigenfrequenzen und Eigenmoden, wobei auch hier die Abhängigkeit von der axialen Geschwindigkeit behandelt wird. Außerdem wird erläutert warum nicht zu erwarten ist, dass Pumpschwingungen auf Grund von Selbsterregung entstehen.

Nach Aufstellung der stationären Bewegungsgleichungen eines axial bewegten biegesteifen Seiles zwischen zwei Rollen, wird die Biegesteifigkeit als mathematische Störung behandelt. Dies führt auf ein reguläres singular gestörtes Randwertproblem, welches formal mit einer asymptotischen Entwicklung approximiert wird. Dieses analytische Ergebnis wird mit der numerischen Lösung dieses Randwertproblems verglichen. Weiters werden die Ergebnisse für die stationäre Bewegung mit Finite Elemente Simulationen verglichen.

Die Seilbewegungsformen zweier benachbarter Seilfelder sind nicht voneinander unabhängig, sondern werden durch die Seilkraft auf der dazwischen liegenden Stütze gekoppelt. Daher werden die möglichen konvexen stationären Bewegungszustände in einem Seilfeld erörtert, wenn die Kraft auf einer angrenzenden Stütze vorgegeben ist. Durch konsequente Weiterführung

dieser Überlegung erhält man den mechanisch stabilen stationären Bewegungszustand der Seilschleife einer Einseilumlaufbahn, bei der die Seilkraft in der Spannstation festgelegt wird. Mit Hilfe dieses stationären Zustands der Seilschleife einer Einseilumlaufbahn kann ein dreidimensionales Finite Elemente Modell einer solchen Seilbahn aufgestellt werden. An Hand von Simulationsbeispielen wird erklärt, wie Pumpschwingungen durch Resonanzen zustandekommen können und wie praktische Probleme analysiert werden können.

Abstract

Aerial ropeways play an important role for transportation in mountainous regions. Unfortunately, even if utmost care is taken of their operation, every year several accidents occur. Some due to human mistakes, but some others also due to a combination of bad design and bad operational conditions that might lead to sometimes large, undesired oscillations of the cable(sag-oscillations). These oscillations are not only a problem of comfort for the passengers but can also be a safety problem. Nowadays, when ropeways are constructed, rather simple models are used to predict and analyse sag-oscillations. Some of these models in fact reduce the complex mechanical system of the entire ropeway to a few degrees of freedom which implies a lot of underlying questionable assumptions. Moreover, the mere cable as a one-dimensional continuous structure offers a variety of phenomena due to its infinite number of degrees of freedom. Therefore, in this work the problem of sag-oscillations of the hauling rope is approached by investigating the dynamics of axially moving cables.

First of all the equations of motion of the axially moving cable between two eyelets in an external force field in a three-dimensional space are derived. After specializing in the constant gravitational field, a survey of the different steady-state motions is given and the dependence of the configuration on the line speed is illustrated when the cable tension is prescribed in one of the eyelets. This comes up to the situation in the span between the towers of a monocable ropeway. Subsequently the corresponding linearized problem is studied and the influence of different line-speeds on the in-plane eigenfrequencies in a ropeway span is illustrated. Furthermore, it is explained why solely external excitations are assumed to be the reason for sag-oscillations. After deriving the steady-state equations of motion for the not completely flexible cable between two rolls, the slight bending stiffness is treated as a perturbation. This yields a regular singularly perturbed boundary value problem for which a formal approximation of the solution is showed. This analytical result is compared with the numerical result of the boundary value problem. Moreover, the steady-state configurations of the cable between two rolls are checked by Finite Element simulations.

The interaction of the configurations of two adjacent cable spans is controlled by the cable tension at the sheave assembly of the interjacent tower. Hence the possible convex steady-state configurations in a span for a given cable tension at one of the adjacent towers are discussed. Based on this idea a steady-state configuration for a whole cable loop of a circulating monocable ropeway for a prescribed tension in the haulage device can be obtained. Subsequently this configuration is used to perform three-dimensional Finite Element simulations of arbitrary monocable ropeways and finally, it is also discussed how sag-oscillations can be caused by resonances as well as how real ropeways can be simulated.

Notations

Symbol	Meaning
Chapter 2	
v	constant velocity (line speed) of the cable in the eyelets
l	cable length between the in- and the outlet
t	time
$\chi(t)$	cable configuration at time t
$E = (\mathbf{e}_1, \mathbf{e}_2, \mathbf{e}_3)$	fixed orthonormal vector basis
x_1, x_2, x_3	Cartesian coordinates corresponding to E
g	constant gravitational acceleration
\mathbf{g}	$-g\mathbf{e}_2$
s	arc length
$\mathbf{r}(s, t)$	position of $\chi(t)$
τ	reference time
ξ	reference arc length
$s(\xi, t)$	bijection between cable points and configuration points
$\mathbf{R}(\xi, t)$	position of the cable
h	cable segment length
$\mathbf{P}(\xi, t)$	section force of the cable (cable tension)
$\mathbf{F}(\xi, t)$	the resultant external force per unit length
ξ_c	center of mass of a small cable segment
O	Landau order symbol
ρ	mass density
A	section area
$\mathbf{p}(s, t)$	section force of the configuration
$\mathbf{f}(s, t)$	external force per unit length function
D/Dt	$(v \partial/\partial s + \partial/\partial t)$
$\mathbf{r}_B = (x_B, y_B, 0)$	position of the outlet
Chapter 3	
$\hat{s}, \hat{t}, \hat{\mathbf{r}}, \hat{\mathbf{p}}, c$	dimensionless quantities instead of $s, t, \mathbf{r}, \mathbf{p}, v$
χ_0	steady-state configuration
$\mathbf{r}_0(s) = (x_0(s), y_0(s), 0)$	position of χ_0
$\mathbf{p}_0(s)$	steady-state section force function
$(\dots)'$	$\partial/\partial s(\dots)$
(\dots)	$\partial/\partial t(\dots)$

Symbol	Meaning
$\mathbf{t}_0(s)$ $\mathbf{n}_0(s)$ $\mathbf{a}_0 = (a, b, 0)$ $\ \cdot\ $ \tilde{p} $\tilde{p}^{(\pm)}$ $\alpha_0(s)$ $\kappa_0(s)$ c_x, c_y p_{\min} v_{crit} ε $\mathbf{r}_1(s, t)$ $\mathbf{p}_1(s, t)$ u_1, u_2, u_3 q_1, q_2, q_3 $\gamma(s)$ \Re (z_1, z_2, z_3, z_4) (z_5, z_6) $\zeta_k(s) = \xi_k(s) + i\eta_k(s)$ $\mu = \lambda + i\omega$ $\nu = \bar{\lambda} + i\bar{\omega}$ $\mathbf{r}_1^{(\text{in})}$ $\mathbf{r}_1^{(\text{out})}$ $\mathbf{A}^{(\text{in})}, \mathbf{B}^{(\text{in})}$ $\mathbf{A}^{(\text{out})}, \mathbf{B}^{(\text{out})}$ f f_1	tangential vector of χ_0 normal vector of χ_0 integration constant vector Euclidean norm on \mathbb{R}^3 $\ \mathbf{p}_0\ - c^2$ two solutions for \tilde{p} inclination angle of χ_0 curvature of χ_0 integration constants $\min_{s \in [0,1]} \ \mathbf{p}_0(s)\ $ minimal velocity that is necessary for concave configurations small perturbation parameter linear correction of $\mathbf{r}(s, t)$ linear correction of $\mathbf{p}(s, t)$ tangential, normal and binormal component of \mathbf{r}_1 tangential, normal and binormal component of \mathbf{p}_1 $1 - c^2 / \ \mathbf{p}_0(s)\ $ real part has to fulfill $(u_1, u_2, q_1, q_2) = \Re(z_1, z_2, z_3, z_4)$ has to fulfill $(u_3, q_3) = \Re(z_5, z_6)$ components of the in-plane eigenfunction ($k = 1, \dots, 4$) and of the out-of-plane eigenfunction ($k = 5, 6$) in-plane eigenvalue out-of-plane eigenvalue projection of \mathbf{r}_1 onto the x_1, x_2 -plane x_3 -component of \mathbf{r}_1 the two independent components of an in-plane eigenmode the two independent components of an out-of-plane eigenmode (dimensional) eigenfrequency lowest eigenfrequency
Chapter 4	
l \mathcal{C}_A r_A, \mathbf{m}_A x_A, y_A, ϕ, s_A \mathcal{C}_B r_B, \mathbf{m}_B x_B, y_B, ψ, s_B $T\mathcal{C} _{\mathbf{r}}$ $s_{A,0}, s_{B,0}$	reference length (redefinition) circle line representing the inlet roll radius and centre of \mathcal{C}_A x_1 -coordinate, x_2 -coordinate, inclination angle and arclength at the point where the cable loses the contact with the roll \mathcal{C}_A circle line representing the outlet roll radius and centre of \mathcal{C}_B x_1 -coordinate, x_2 -coordinate, inclination angle and arclength at the point where the cable touches the roll \mathcal{C}_B first tangential manifold on \mathcal{C} at the point $\mathbf{r} \in \mathcal{C}$ steady-state part of s_A, s_B

Symbol	Meaning
$s_{A,1}, s_{B,1}$ P_0, Q_0 \mathbf{p}_0^* P_0^* H_0^*, V_0^* $\mathbf{M}_0 = M_0 \mathbf{e}_3$ B $\hat{s}_{A,0}, \hat{s}_{B,0}, \hat{x}_0, \hat{y}_0$ $\hat{\kappa}_0, \hat{H}_0^*, \hat{Q}_0, \beta$ $x_A^{(k)}, x_B^{(k)}, y_A^{(k)}, y_B^{(k)}$ $s_{A,0}^{(k)}, s_{B,0}^{(k)}, \phi^{(k)}, \psi^{(k)}$ $l^{(k)}$ t $(\cdot)'$ \mathbf{y} \mathbf{z} \mathbf{f} \mathbf{g} \mathbf{b} $(\bar{\mathbf{y}}, \bar{\mathbf{z}}) = (\bar{\kappa}, \bar{Q}_0, \bar{y}_0, \bar{\alpha}_0)$ φ μ_-, \mathbf{e}_- μ_+, \mathbf{e}_+ τ, σ $\mathbf{L}\mathbf{y} = (L\kappa_0, LQ_0)$ $\mathbf{R}\mathbf{y} = (R\kappa_0, RQ_0)$	<p>linear correction of s_A, s_B</p> <p>tangential and normal component of \mathbf{p}_0</p> <p>fictitious cable section force</p> <p>tangential component of \mathbf{p}_0^*</p> <p>horizontal and vertical component of \mathbf{p}_0^*</p> <p>sectional bending moment</p> <p>bending stiffness</p> <p>dimensionless quantities instead of $s_{A,0}, s_{B,0}, x_0, y_0$</p> <p>dimensionless quantities instead of κ_0, H_0^*, Q_0, B</p> <p>x_A, x_B, y_A, y_B in the k-th iteration step</p> <p>$s_{A,0}, s_{B,0}, \phi, \psi$ in the k-th iteration step</p> <p>configuration length in the k-th iteration step</p> <p>scaled arclength variable during an iteration step</p> <p>$d(\cdot)/dt$ (redefinition)</p> <p>(κ_0, Q_0)</p> <p>(y_0, α_0)</p> <p>right hand side of the the singular part of the ODE</p> <p>right hand side of the the regular part of the ODE</p> <p>boundary conditions of the singularly perturbed BVP</p> <p>solution of the reduced equation</p> <p>auxiliary function for expressing $\bar{\mathbf{y}}$</p> <p>stable eigenvalue and the corresponding eigenvector</p> <p>unstable eigenvalue and the corresponding eigenvector</p> <p>boundary layer variables</p> <p>left boundary layer term</p> <p>right boundary layer term</p>
Chapter 6	
Y_0 p_A $f(a, c)$ $\mathcal{M}_0, \mathcal{M}_1$ p_{crit} a_{crit}	<p>catenary as a function of the x-value</p> <p>fictitious cable tension at the inlet</p> <p>$a \cosh(c/a)$ (redefinition)</p> <p>manifolds associated with the boundary conditions</p> <p>critical cable tension</p> <p>critical catenary parameter</p>
Chapter 7	
d f N l m_{cab} I_{ij} E Δt_{max}	<p>is the distance between two adjacent cabins</p> <p>frequency of cabins entering the span (redefinition)</p> <p>number of cabins</p> <p>length of the cable loop</p> <p>mass of a cabin</p> <p>tensor of rotational inertia</p> <p>Young's modulus</p> <p>maximal time increment</p>

Contents

1	Introduction	12
2	Mechanical Model and Equations of Motion for the Cable	15
3	The Cable in a Constant Gravitational Field	18
3.1	The Steady-State Problem	18
3.1.1	Curved configurations	19
3.1.2	Straight configurations	20
3.1.3	Remarks	21
3.1.4	Example	21
3.1.5	Example	21
3.2	The Linearized Problem	23
3.2.1	Eigenmodes of the In-plane-motion	26
3.2.2	Eigenmodes of the Out-of-plane-motion	29
3.2.3	Remarks	30
3.2.4	Example	31
3.2.5	Remarks	34
4	Rolls as boundaries	35
4.1	The Steady-State Problem	36
4.2	The linearized problem	37
4.3	A Not Perfectly Flexible Cable	38
4.3.1	A Singularly Perturbed Boundary Value Problem	42
4.3.2	Example	45
5	Numerical Simulation of the Steady-State Solution	50
6	Coupled Cable Spans	58
6.1	How the Cable Tension at the Border of a Span Influences the Sag	58
7	Numerical Simulation of The Dynamics of Ropeways with Finite Elements	63
7.1	The components of the model	63
7.2	Sag-Oscillations due to Resonances	66
7.3	Preprocessing	70
7.4	Example	70

7.5	Remarks	72
7.6	Example	72
8	Conclusion	74
A	Regular Singularly Perturbed Boundary Value Problem	77
B	Properties of $f(a, c) = a \cosh(c/a)$	79

List of Figures

1.1	Scheme of a circulating monocable aerial ropeway, e.g. a ski-lift.	12
1.2	On each tower a sheave assembly, that is an assembly of rolls, constrains the cable to stay in its track. That means that the cable is forced to move over (Figs. 1.2(a) & 1.2(b)), under (Fig. 1.2(c)) or between sheave assemblies (Fig. 1.2(d)).	13
3.1	Scheme of the ropeway span in example 3.1.5.	22
3.2	Example 3.1.5: The curve length l of the convex steady-state configuration in dependence on the cable line speed v	22
3.3	The sag of the convex steady-state configuration in the span of example 3.1.5 increases with the increasing line speed v . For $v = 169.74 \text{ m/s}$, the maximal sag is reached.	23
3.4	The lowest eigenfrequency of the cable span in the ropeway of example 3.2.4 (or 3.1.5) in dependence on the line speed.	31
3.5	Example 3.2.4: The first component (3.52) of the lowest eigenmode and the corresponding steady-state configuration for three different line speeds v	32
3.6	Example 3.2.4: The second component (3.53) of the lowest eigenmode and the corresponding steady-state configuration for four different line speeds v	32
3.7	Example 3.2.4: The lower part of the eigenfrequency-spectrum varying with the line speed v	33
3.8	Example of Perkins and Mote in [18]: The figure shows the lowest non-dimensional in-plane eigenfrequencies of an elastic cable in dependency on the non-dimensional line speed. Here the cable mass between the in- and the outlet is conserved. . .	33
4.1	In many technical applications - not only in aerial ropeways - the cable at the boundaries moves over rolls.	35
4.2	The left roll: the location of the cable configuration point where the cable loses contact with the roll is time-dependent.	36
4.3	The eigenvector \mathbf{e}_- (\mathbf{e}_+) of the linearized problem at $t=0$ ($t=1$) has a component transversal to the hyperplane $\kappa = -1/r_A$ ($\kappa = -1/r_B$). Thus the problem (4.15) is well posed.	43
4.4	Example 4.3.2: A slightly bending-stiff cable moves axially between two rolls which have the same radius and are at the same elevation.	45
4.5	Steady-state curvature κ_0 of the symmetric ex. 4.3.2 with the roll-radius $r = l/20$ and the bending stiffnesses β . The different solution methods yield very well coinciding results.	47

4.6	Example 4.3.2: The figure shows how the steady-state shape of the configuration varies when the curvature in (4.26) is integrated and consequently a matching iteration procedure is performed. The configurations with ($\beta^2 > 0$, solid line) and without ($\beta^2 = 0$, dashed line) bending stiffness are depicted. It also becomes clear how the bending stiffness forces the variation of the point on the roll where it loses contact.	48
4.7	Results of the iterative boundary value problem (4.15) using COLSYS [2]. . . .	49
5.1	Different two-dimensional FE-models used to simulate a steady-state cable motion over rolls. The cable is modelled as a combination of hybrid truss- and beam- Elements. The latter have a slight bending stiffness. The rolls and tables are modelled as analytical rigid bodies. The contact between this bodies and the cable is frictionless. The cable has no self-contact.	51
5.2	Initial configuration of the FE-Simulation with the model of Fig. 5.1(g). The red part of the cable is built up of two-dimensional hybrid beam elements B21H.	53
5.3	The cable in the span: the configuration after 0.86s of the simulation time is depicted in red, the completely flexible initial configuration in blue.	55
5.4	The configuration with bending stiffness approximated by a matched asymptotic expansion.	56
5.5	Comparison between the FE-simulation configuration after 0.86s and the numerical steady-state solution with COLSYS [2] for different bending stiffness values β	57
6.1	The two eqs. in (6.6) define implicitly the two curves \mathcal{M}_0 and \mathcal{M}_1 (s. Figs. 6.1(a)-6.1(c)) in the a, c_x -plane. Here the curves are depicted for $y_B = 0.3$ and intersect only if p_A , the prescribed cable tension at the left eyelet is equal to (s. Fig. 6.1(b)) or greater than (s. Fig. 6.1(c)) a critical value $p_{crit} = 0.6255$. The figures 6.1(d)-6.1(f) show the dependence of a on p_A	60
6.2	The convex function $p(a)$ is enclosed by two asymptotes and has a local minimum at $a = a_{crit}$. The steady-state solutions for $0 < a < a_{crit}$ are the unstable solutions and the solutions for $a_{crit} < a$ are stable.	61
6.3	In this plots for $y_B = 0.3$ and $p_A = 3.1$ we see how different the resulting steady-state configurations are if p_A is perspicuously higher than p_{crit} (here $p_{crit} = 0.6255$). In particular one of the solutions is always mechanically stable and the other unstable.	62
7.1	A generalized sheave assembly can be modelled by a three-dimensional surface of revolution: a semicircle that has a radius which depends on the envelope of the rolls rotates around a non-intersecting axis of the same plane.	64
7.2	The generalized sheave assemblies on the towers and the haulage and drive pulleys of the bottom and top terminals are modelled by analytical rigid surfaces.	65
7.3	An illustrative Finite Element model of a ropeway with two spans used to simulate sag-oscillations. The drive pulley is located in the top terminal (on the right).	66

7.4	The model from Fig. 7.3 with different numbers of cabins ($N=0, 1, 2 \dots 7$) after an elapsed simulation time $t=40.4s$. In this series of simulations the line speed is $v=4.5m/s$	67
7.5	Like Fig. 7.4, but now after an elapsed simulation time $t=40.9s$ and for a line speed $v=6m/s$	68
7.6	Like Fig. 7.4, but now after an elapsed simulation time $t=22.8s$ and for a line speed $v=9m/s$	69
7.7	The preprocessor program <i>fiat</i> for ABAQUS/Explicit attaches cabins or gondolas to the cable that are modelled as cylindrical rigid bodies with a prescribed mass and inertia tensor. They are connected to the cable by spring-dashpot elements.	70
7.8	Finite Element model of the Silvrettabahn in Ischgl (Austria) [12]	71
7.9	The cable of the ropeway is hit by a hopper not far away from a gondola (s. Fig. 7.9(b)). Due to the impact the coupling mechanism of the gondola opens in such a way that the cabin falls down.	73
B.1	Contour-plots of the function $f(a, c)$ in eq. (6.5) - light color means high value. The similarity between the two pictures of different 'zoom'-factor is typical for the parallel plane sections of a geometrically three-dimensional cone $\Gamma \subset \mathbb{R}^3$ for which $\Gamma \subset \lambda \Gamma$ holds with $\lambda > 0$	79
B.2	The domain enclosed by the line $\mathcal{C} = \{(a, c) f(a, c) = p\} \cup (0, 0)$ has the area p^2	80

Chapter 1

Introduction

Nowadays, in particular when people shall be carried, often *circulating monocable aerial ropeways* are projected. These are ropeways where the transporting units (e.g. chairs or little cabins) are attached to a single carrying and hauling rope or *cable*.¹ This cable is a closed loop and moves either through the air or over rolls. The latter is the case in the drive device, the haulage device and on the towers. (s. Fig. 1.1)

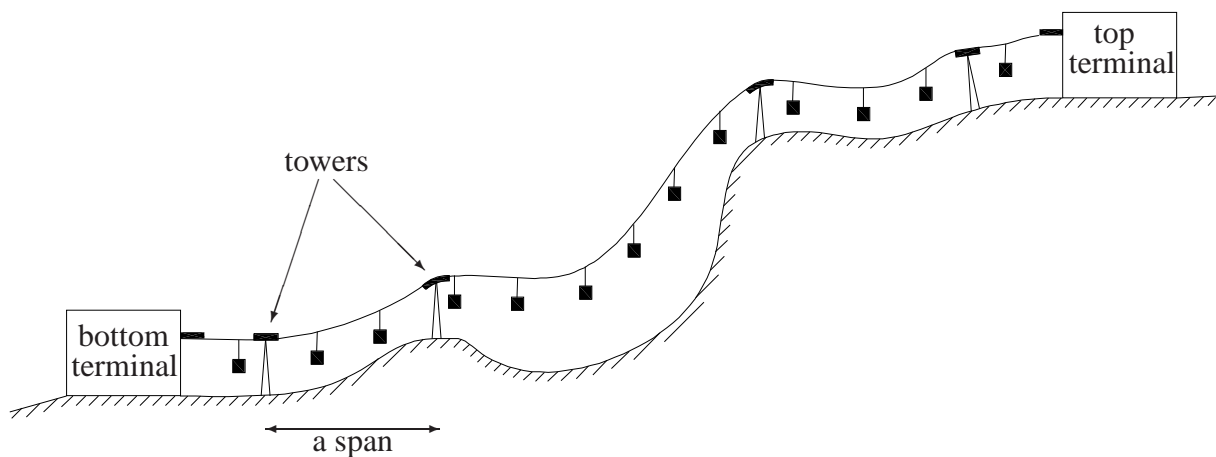


Figure 1.1: Scheme of a circulating monocable aerial ropeway, e.g. a ski-lift.

In the drive device the cable is constrained to an axial motion with a constant velocity, and in the haulage device the cable tension is prescribed. Finally if the ropeway is used as a means of transportation over a large distance, towers with *sheave assemblies*, which are assemblies of rolls (s. Fig. 1.2), are necessary along the track of the ropeway in order to reduce the sag of the cable that is hanging in the air. Therefore the drive device, the haulage device and the towers subdivide the track of the ropeway into several *spans*.

The terminals where people get in or off normally coincide with either a driving device or a haulage device. Usually the carrying units are attached to the cable with detachable grips, so

¹Here and in the following the words 'rope', 'cable' and 'string' are used as synonyms.



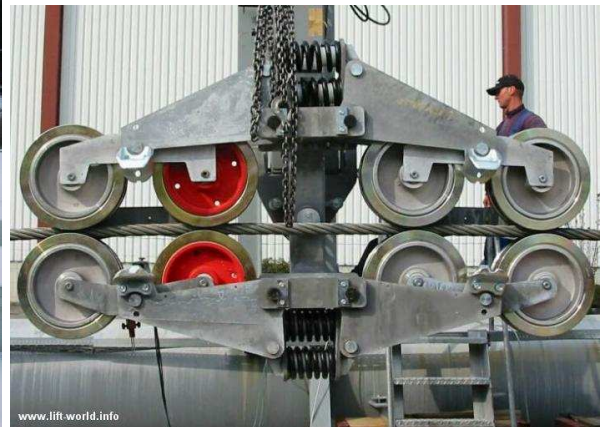
(a) A tower with a carrying sheave assembly.



(b) Another carrying sheave assembly.



(c) A holding-down sheave assembly.



(d) A sheave assembly that wedges the cable in.

Figure 1.2: On each tower a sheave assembly, that is an assembly of rolls, constrains the cable to stay in its track. That means that the cable is forced to move over (Figs. 1.2(a) & 1.2(b)), under (Fig. 1.2(c)) or between sheave assemblies (Fig. 1.2(d)).

that loading and unloading at low speed is possible, which is also more comfortable. Only in chair-lifts the chairs are sometimes permanently attached to the cable.

In ropeway engineering the transient dynamics of *sag-oscillations*² are of particular interest for circulating monocable aerial ropeways [12]. This is a nearly periodic change of the sag of the cable curve with amplitudes of some meters and time periods of some seconds. It is not only a problem of comfort for the passengers but can also be a safety problem.

Until now, when ropeways are constructed, rather simple models are used to predict and

²In German: *Pumpschwingungen*.

analyse sag-oscillations [4, 12, 11]. Some of these models in fact imply only a single degree of freedom for each span. Nevertheless, following literature, the cable as a one-dimensional continuous structure offers a variety of phenomena due to its infinite number of degrees of freedom. Therefore in our investigation on sag-oscillations we will primarily look at the dynamics of axially moving cables.

In the year 1851 Rohrs [25] first modelled the vibrations of a uniform, inextensible suspended chain hanging freely under its own weight. He obtained the approximate natural frequencies or eigenfrequencies and responses of a cable with a small sag to span ratio³ that is defined as a sag to span ratio less than 1 : 8. Then in 1868 Routh [26] considered the symmetric transverse vibration of a heterogeneous chain hanging in the form of a cycloid. He obtained an analytical solution and the application of this chain model to the uniform chain yielded Rohrs model. Their solutions for cable eigenfrequencies converged in the limit of a vanishing cable sag, but they failed to reproduce the spectrum of the classical taut string. This shortcoming was firstly explained by Irvine and Caughey [8] in 1974. They demonstrated that including cable elasticity allows the small sagged cable model of Rohr to pass smoothly to the taut string model in the limit of a vanishing cable sag. But also the earlier models of Soler [32] in 1970 and Simpson [30] in 1972 were already capable of this transition. Furthermore, Simpson was the first who analysed the linear in-plane vibration of a translating - that is an axially moving - cable. His cable was elastic, had a small sag and moved through two fixed eyelets at the same elevation. The small sag assumption guaranteed analytical solutions for the eigenfrequencies and for the eigenmode shapes. Simpson noted that the introduction of a cable line speed leads to complex vibration modes, that means to a non-constant phase shift in displacement along the cable span. In 1985 Triantafyllou [37] extended Simpson's plane travelling cable model to include either a very small or a very large cable sag and inclined eyelets. However, the cable in a ropeway may have an arbitrary sag - not only a small or a very large one - and also out-of-plane motions may occur. In 1987 Perkins and Mote [18] analysed the in-plane and the out-of-plane linear vibrations of translating elastic cables having an arbitrary initial sag and an arbitrary eyelet inclination after discretizing the equations by Galerkin's method. Since in this calculations the elasticity was crucial, they made some assumptions for the strain in the cable and the choice of the material cable parameters in order to get the equations of motion. In 2001 Miroshnik [13] analysed the steady-state motion of an inelastic axially moving cable. Besides the gravitational force, he also introduced a viscous force acting tangentially on the cable. His solutions for the inelastic cable were analytical. Two restrictions were made in all of the mentioned analysis: Firstly, the boundaries were always two eyelets, but in most of the applications for axially moving cables - such as in aerial ropeways - the boundaries are pulleys or rolls. Secondly, real ropes have a bending stiffness which may play an important role for the solutions, especially if the boundaries are not eyelets. As we shall see, in this case a slight bending stiffness can be introduced by means of a boundary layer solution using the singular perturbation theory.

³Instead of 'small sag to span ratio' we will just say 'small sag'.

Chapter 2

Mechanical Model and Equations of Motion for the Cable

Consider a *cable*, modelled as an inextensible homogeneous *one-dimensional structure* without bending stiffness or torsion rigidity, moving in an external force field in three-dimensional space. In our case this external force field consists of a constant gravitational force field and in some spatial regions of contact forces¹ between the cable and other materia, such as rolls or a viscous medium.

Let there be two *eyelets*, modelled as two different fixed points in space through which the cable always runs through and where as a consequence the motion of the cable can only be an axial one. Let v be a constant *velocity* of the purely axial motion in both of the two eyelets such that the mass of the connecting cable part always stays the same. Hence for $v \neq 0$ it makes sense to denote one eyelet as the *inlet* and the other one as the *outlet*. Furthermore due to the inextensibility of the cable, it has always the same *length* l between the in- and the outlet.

In some cases it is useful to define a *closed cable* identifying cable materia which runs through the inlet with the cable materia that simultaneously runs through the outlet. This situation becomes a physical one if the two eyelets are unified in a single one which drives the cable.

For every *time* $t \in \mathbb{R}$ the cable has a certain *configuration* $\chi(t)$ which is defined as the curve that is described by the cable part connecting the eyelets at t .

We introduce Cartesian coordinates x_1, x_2, x_3 corresponding to the orthonormal vector basis $E = (\mathbf{e}_1, \mathbf{e}_2, \mathbf{e}_3)$ so that the inlet coincides with the origin, that the outlet lies in the x_1, x_2 -plane with a non-negative x_1 -component and in such a way that the constant gravitational acceleration can be written as $\mathbf{g} = -g\mathbf{e}_2$. Then let $\chi(t)$ be located by $\mathbf{r}(s, t)$ with the arc length $s \in [0, l]$ so that $\mathbf{r}(0, t) = \mathbf{0}$ is valid for all t .

At a fixed *reference time* τ the cable material can be labelled by the *reference arc length* ξ in such a way that $\xi = 0$ denotes the material cable point which passes the inlet at $t = \tau$. Since v is constant and the cable is inextensible, a material cable point between the in- and the outlet which is labelled by ξ can be identified with the curve point of the configuration $\chi(t)$ at arc length

$$s(\xi, t) = \xi + v(t - \tau) \quad . \quad (2.1)$$

¹Here and in the following self-contact of the cable is not taken into account.

Let $\mathbf{R}(\xi, t)$ be the position of the material point (labelled by) ξ at time t in our coordinate system. Then the following relation holds:

$$\mathbf{R}(\xi, t) = \mathbf{r}(s(\xi, t), t) . \quad (2.2)$$

Consider at time t a very small cable material segment of length h on its path from the in- to the outlet and labelled by the interval $[\xi, \xi + h]$, so that the endpoints are located at $\mathbf{R}(\xi, t)$ and $\mathbf{R}(\xi + h, t)$. If we cut this segment out of the cable then let $\mathbf{P}(\xi + h, t)$ and $-\mathbf{P}(\xi, t)$ be the section forces acting on the right and left border. Due to the lack of bending stiffness the vector $\mathbf{P}(\xi, t)$ can only be tangential to the cable. This fact and the inextensibility of the cable can be expressed by:

$$\frac{\partial}{\partial \xi} \mathbf{R}(\xi, t) = \frac{\mathbf{P}(\xi, t)}{\|\mathbf{P}(\xi, t)\|}, \quad \forall \xi . \quad (2.3)$$

Equation (2.3) also implies that the cable tension and the cable tangential vector have always the same orientation. Furthermore we denote the function of the resultant external force per unit length by $\mathbf{F}(\xi, t)$. With the center of mass $\xi_c \in (\xi, \xi + h)$ of this cable segment, Newton's law yields:²

$$\rho A h \frac{\partial^2}{\partial t^2} \mathbf{R}(\xi_c, t) = h \mathbf{F}(\xi_c, t) + \mathbf{P}(\xi + h, t) - \mathbf{P}(\xi, t) + O(h^2) ,$$

where the constants ρ and A denote the mass density and the section area. After dividing this equation by h the limit $h \rightarrow 0$ yields:

$$\rho A \frac{\partial^2}{\partial t^2} \mathbf{R}(\xi, t) = \mathbf{F}(\xi, t) + \frac{\partial}{\partial \xi} \mathbf{P}(\xi, t) . \quad (2.4)$$

Eqs. (2.3) and (2.4) are the *equations of motion* for \mathbf{R} and \mathbf{P} - the state variables of the *material cable point* ξ . In the same way as in (2.2) we define a cable force function $\mathbf{p}(s, t)$ as well as an external force per unit length function $\mathbf{f}(s, t)$ so that $\mathbf{p}(s(\xi, t), t) = \mathbf{P}(\xi, t)$ and $\mathbf{f}(s(\xi, t), t) = \mathbf{F}(\xi, t)$. With eqs. (2.1) and (2.2) we get:

$$\begin{aligned} \frac{\partial}{\partial t} \mathbf{R}(\xi, t) &= \frac{d}{dt} \mathbf{r}(s(\xi, t), t) \\ &= \frac{\partial s(\xi, t)}{\partial t} \frac{\partial}{\partial s} \mathbf{r}(s(\xi, t), t) + \frac{\partial}{\partial t} \mathbf{r}(s(\xi, t), t) \\ &= \left(v \frac{\partial}{\partial s} + \frac{\partial}{\partial t} \right) \mathbf{r}(s(\xi, t), t) , \\ \frac{\partial}{\partial \xi} \mathbf{P}(\xi, t) &= \frac{\partial s(\xi, t)}{\partial \xi} \frac{\partial}{\partial s} \mathbf{p}(s(\xi, t), t) = \frac{\partial}{\partial s} \mathbf{p}(s(\xi, t), t) . \end{aligned}$$

²The (*Landau*) order symbol O has the following meaning: With $f(\varepsilon), g(\varepsilon) \in \mathbb{R}$ for $\varepsilon \in (0, \varepsilon_0]$ the relation $f(\varepsilon) = O(g(\varepsilon))$ for $\varepsilon \rightarrow 0$ holds, if there is a constant $C > 0$, which is independent of ε , in such a way that $|f(\varepsilon)| \leq C|g(\varepsilon)|$ for $\varepsilon \in (0, \varepsilon_0]$.

On the one hand, defining the operator $\frac{D^2}{Dt^2} = \left(v \frac{\partial}{\partial s} + \frac{\partial}{\partial t}\right)^2$ we get from eq. (2.4):

$$\rho A \frac{D^2}{Dt^2} \mathbf{r}(s, t) = \mathbf{f}(s, t) + \frac{\partial}{\partial s} \mathbf{p}(s, t), \quad \forall s \in [0, l] \quad (2.5)$$

and on the other hand we get from eq. (2.3):

$$\frac{\partial}{\partial s} \mathbf{r}(s, t) = \frac{\mathbf{p}(s, t)}{\|\mathbf{p}(s, t)\|}, \quad \forall s \in [0, l]. \quad (2.6)$$

Thus (2.5) and (2.6) are the *equations of motion* for \mathbf{r} and \mathbf{p} - the state variables of the *cable configuration point* s . Furthermore, if \mathbf{r}_B with $\|\mathbf{r}_B\| \leq l$ denotes the position of the outlet (within the x_1, x_2 -plane) then the following six boundary conditions have to be fulfilled:

$$\mathbf{r}(0, t) = \mathbf{0}, \quad \mathbf{r}(l, t) = \mathbf{r}_B, \quad \forall t. \quad (2.7)$$

Hence we can summarize the whole problem:

$$\boxed{\begin{aligned} \forall s \in [0, l] : \begin{cases} \rho A \frac{D^2}{Dt^2} \mathbf{r}(s, t) = \mathbf{f}(s, t) + \frac{\partial}{\partial s} \mathbf{p}(s, t), \\ \frac{\partial}{\partial s} \mathbf{r}(s, t) = \frac{\mathbf{p}(s, t)}{\|\mathbf{p}(s, t)\|}, \end{cases} \\ \mathbf{r}(0, t) = \mathbf{0}, \\ \mathbf{r}(l, t) = \mathbf{r}_B. \end{aligned}} \quad (2.8)$$

Finally it should be remarked that the same system of forces is acting on the cable as it is acting on a streamtube fluid or on the fluid within a massless tube [38, 34, 7]. Therefore the linear momentum balance law and the angular momentum balance law can be applied in the same way as to the fluid within such a piece of tube. Obviously, a cable configuration point corresponds in this analogy to a point on the centerline of a fluid conveying tube.

Chapter 3

The Cable in a Constant Gravitational Field

The external force per unit length for a free - that is without any contact - moving cable in a constant gravitational field is $\mathbf{f}(s, t) = -\rho A g \mathbf{e}_2$ and therefore eq. (2.5) yields:

$$\rho A \frac{D^2}{Dt^2} \mathbf{r}(s, t) = -\rho A g \mathbf{e}_2 + \frac{\partial}{\partial s} \mathbf{p}(s, t), \quad \forall s \in [0, l].$$

This equation as well as the inextensibility eq. (2.6) can be brought into a dimensionless form by substituting

$$s = \hat{s}l, \quad t = \hat{t}\sqrt{l/g}, \quad \mathbf{r} = \hat{\mathbf{r}}l, \quad \mathbf{p} = \hat{\mathbf{p}}\rho A g l, \quad v = c\sqrt{gl} \quad (3.1)$$

and dropping afterwards the “^”-symbol as well as redefining $\frac{D^2}{Dt^2} = \left(c\frac{\partial}{\partial s} + \frac{\partial}{\partial t}\right)^2$. Thus we can summarize the whole problem:

$$\boxed{\begin{aligned} \forall s \in [0, 1] : \quad & \begin{cases} \frac{D^2}{Dt^2} \mathbf{r}(s, t) = -\mathbf{e}_2 + \frac{\partial}{\partial s} \mathbf{p}(s, t), \\ \frac{\partial}{\partial s} \mathbf{r}(s, t) = \frac{\mathbf{p}(s, t)}{\|\mathbf{p}(s, t)\|}, \end{cases} \\ & \mathbf{r}(0, t) = \mathbf{0}, \\ & \mathbf{r}(1, t) = \mathbf{r}_B, \quad \|\mathbf{r}_B\| \leq 1. \end{aligned}} \quad (3.2)$$

3.1 The Steady-State Problem

Now we look for a time-independent or *steady-state* solution of problem (3.2). We denote the time-independent configuration by χ_0 and the corresponding functions by $\mathbf{r}_0(s)$ and $\mathbf{p}_0(s)$. Thus

with the abbreviation $(\dots)' = \frac{\partial}{\partial s}(\dots)$ we get from problem (3.2) the steady-state subproblem:

$$\begin{aligned} \forall s \in [0, 1] : \begin{cases} c^2 \mathbf{r}_0''(s) = -\mathbf{e}_2 + \mathbf{p}_0'(s), \\ \mathbf{r}_0'(s) = \frac{\mathbf{p}_0(s)}{\|\mathbf{p}_0(s)\|}, \end{cases} \\ \mathbf{r}_0(0) = \mathbf{0}, \\ \mathbf{r}_0(1) = \mathbf{r}_B. \end{aligned} \quad (3.3)$$

Let χ_0 have the tangential vector $\mathbf{t}_0(s)$ and the normal vector $\mathbf{n}_0(s)$ - each of them has length one. Then because of $\mathbf{t}_0(s) = \mathbf{r}_0'(s)$, the two differential equations in (3.3) are equivalent to

$$\begin{aligned} \mathbf{p}_0(s) &= \|\mathbf{p}_0(s)\| \mathbf{t}_0(s), \\ [(\|\mathbf{p}_0(s)\| - c^2) \mathbf{t}_0(s)]' &= \mathbf{e}_2 \end{aligned}$$

We integrate the last equation and get

$$(\|\mathbf{p}_0(s)\| - c^2) \mathbf{t}_0(s) = s \mathbf{e}_2 + \mathbf{a}_0 \quad (3.4)$$

with the integration constant $\mathbf{a}_0 \in \mathbb{R}^3$. Eq. (3.4) shows that all the tangential vectors of χ_0 lie in the subspace that is spanned by \mathbf{e}_2 and \mathbf{a}_0 . If the inlet lies in the origin and the outlet in a point of the x_1, x_2 -plane, then \mathbf{a}_0 and therefore also χ_0 has to lie in the x_1, x_2 -plane.¹ It is useful to define the function $\tilde{p} = \|\mathbf{p}_0\| - c^2$, which doesn't have to be positive. Then eq. (3.4) can be written as

$$\tilde{p}(s) \mathbf{t}_0(s) = a \mathbf{e}_1 + (s + b) \mathbf{e}_2 \quad a, b \in \mathbb{R}. \quad (3.5)$$

Squaring eq. (3.5) yields

$$\tilde{p}^2 = a^2 + (s + b)^2$$

and hence there are obviously *two* solutions for \tilde{p} , namely:

$$\tilde{p}^{(\pm)} = \pm \sqrt{a^2 + (s + b)^2}. \quad (3.6)$$

Finally we choose the orientation of the x_1 -axis in such a way that the x_1 -component of the outlet is a non-negative value. As a consequence the x_1 -component of the tangential vector, which never changes its sign also has to be a non-negative value. Therefore we have to distinguish the four cases $a > 0$, $a \searrow 0^+$, $a \nearrow 0^-$ and $a < 0$.

3.1.1 Curved configurations

This is the case when the outlet doesn't lie on the x_2 -axis. From eq. (3.5) and (3.6) we get the tangential vector. We have to distinguish *two* cases:

$$\mathbf{t}_0(s) = \begin{pmatrix} x_0'(s) \\ y_0'(s) \\ z_0'(s) \end{pmatrix} = \frac{1}{\sqrt{a^2 + (s + b)^2}} \begin{pmatrix} a \\ s + b \\ 0 \end{pmatrix} \cdot \begin{cases} (+1), & a > 0, \tilde{p} = \tilde{p}^{(+)} \\ (-1), & a < 0, \tilde{p} = \tilde{p}^{(-)} \end{cases} \quad (3.7)$$

¹Hence we will not care about the x_3 -component in the notation of this section.

If we divide the x_2 -component of \mathbf{t}_0 by the x_1 -component, we get the slope of \mathbf{t}_0 relative to the x_1 -axis. Thus the inclination angle and the curvature are:

$$\alpha_0(s) = \arctan\left(\frac{s+b}{a}\right), \quad \kappa_0(s) = \frac{a}{a^2 + (s+b)^2}.$$

In both of the cases integration of eq. (3.7) yields

$$x_0(s) = a \operatorname{arsinh}\left(\frac{s+b}{a}\right) + c_x, \quad c_x \in \mathbb{R} \quad (3.8)$$

$$y_0(s) = a \sqrt{1 + \left(\frac{s+b}{a}\right)^2} + c_y, \quad c_y \in \mathbb{R} \quad (3.9)$$

and with $\mathbf{r}_B = (x_B, y_B, 0)$ the constants a, b, c_x, c_y have to be chosen in such a way that the boundary conditions

$$x_0(0) = 0, \quad y_0(0) = 0, \quad x_0(1) = x_B, \quad y_0(1) = y_B \quad (3.10)$$

are fulfilled. If we express y_0 by x_0 using eq. (3.8) and eq. (3.9) then we get

$$y_0 = c_y + a \cosh\left(\frac{x_0 - c_x}{a}\right). \quad (3.11)$$

3.1.2 Straight configurations

This can only be the case when the outlet lies on the x_2 -axis. From eq. (3.5) and (3.6) we get the tangential vector for $s \neq -b$. Here we have to distinguish *two* cases:

$$\mathbf{t}_0(s) = \begin{pmatrix} x'_0(s) \\ y'_0(s) \\ z'_0(s) \end{pmatrix} = \frac{1}{|s+b|} \begin{pmatrix} 0 \\ s+b \\ 0 \end{pmatrix} \cdot \begin{cases} (+1), & a \searrow 0^+, \tilde{p} = \tilde{p}^{(+)} \\ (-1), & a \nearrow 0^-, \tilde{p} = \tilde{p}^{(-)} \end{cases} \quad (3.12)$$

Integration yields:

$$y_0(s) = c_y + |s+b| \cdot \begin{cases} (+1), & a \searrow 0^+, \tilde{p} = \tilde{p}^{(+)} \\ (-1), & a \nearrow 0^-, \tilde{p} = \tilde{p}^{(-)} \end{cases}, \quad c_y \in \mathbb{R}. \quad (3.13)$$

With $\mathbf{r}_B = (0, y_B, 0)$ the constants b, c_y have to be chosen in such a way that the boundary conditions

$$y_0(0) = 0, \quad y_0(1) = y_B$$

are fulfilled.

3.1.3 Remarks

The cable configuration or curve that connects the two eyelets in a gravitational field can be only one of the four types described above, but not a combination of them, since due to eq. (3.6) this would imply a jump in the cable tension $\|\mathbf{p}_0\|$. Such a jump is impossible without an external point load.

For $a \neq 0$ we notice from eq. (3.11) that y_0 as a function of x_0 is *convex* if $a > 0$ and *concave* if $a < 0$. For all a the *cable configurations are independent of the velocity c* . In particular the convex curve connecting the eyelets for an arbitrary velocity c is exactly the same as in statics. Unlike in statics the existence of concave configurations is possible. Since the cable has to be under tension as a matter of fact, concave configurations are only possible if for the cable configuration points $\tilde{p} < 0$ and simultaneously $\|\mathbf{p}_0\| = \tilde{p} + c^2 > 0$ can be satisfied. Hence $c > 0$ must hold and that is why in the case of elastic cables Perkins and Mote [18] called this phenomenon *speed tensioning*.

Comparing eq. (3.6) with eq. (3.9) and (3.13), we notice that in any case the relation

$$\|\mathbf{p}_0\| = y_0 - c_y + c^2 \quad (3.14)$$

holds. Obviously the cable-tension $\|\mathbf{p}_0\|$ is linearly dependent on the 'height' y_0 and thus in the same way as the hydrostatical pressure depends on height in fluid mechanics.

3.1.4 Example

We want to check whether the concave steady-state configuration is relevant for the application of cable dynamics to circulating monocable aerial ropeways. As mentioned above, \tilde{p} must become less than zero. Therefore the critical value for the \tilde{p} is given, if $\|\mathbf{p}_0\| = c^2$ or after substituting back into dimensional quantities $\mathbf{p}_0 \rightarrow \hat{\mathbf{p}}_0 \rightarrow \mathbf{p}_0/(\rho Ag)$, $c \rightarrow v/\sqrt{gl}$:

$$\|\mathbf{p}_0\| = \rho A v^2 .$$

Hence, if we know the tension $\|\mathbf{p}_0\| = p_{\min}$ at the lower eyelet, we can calculate the critical velocity

$$v_{\text{crit}} = \sqrt{\frac{p_{\min}}{\rho A}} . \quad (3.15)$$

Concave configurations do exist only for $v > v_{\text{crit}}$. The value of v_{crit} becomes small, if p_{\min} is small or if ρA is big. For monocable aerial ropeways $p_{\min} > 10^4 \text{ N}$ and $\rho A < 10 \text{ kg/m}$. From eq. (3.15) follows that $v_{\text{crit}} > 31.6 \text{ m/s}$. Nowadays even the fastest monocable ropeways do not surpass a velocity of 10 m/s . This means we are at least at factor three under the critical velocity, and therefore the concave steady-state configuration is nowadays not relevant for this kind of ropeways.

3.1.5 Example

The first large span for the outgoing rope after the bottom terminal of a circulating monocable gondola ropeway that carries ski-tourists to a mountain (s. Fig.3.1) shall be bordered by two

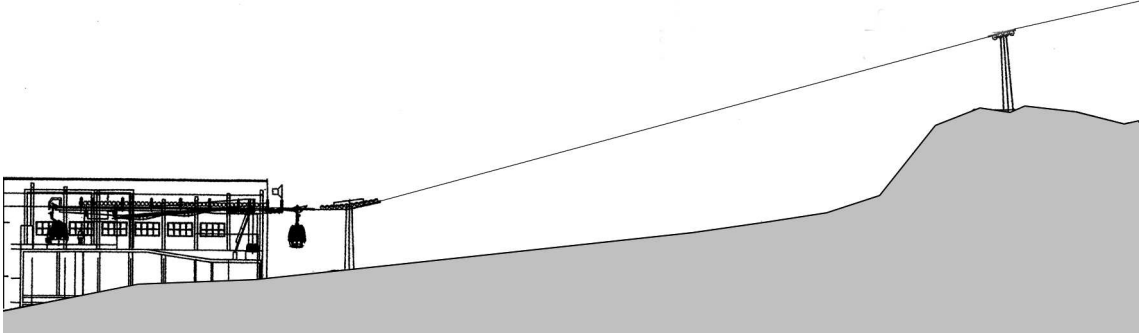
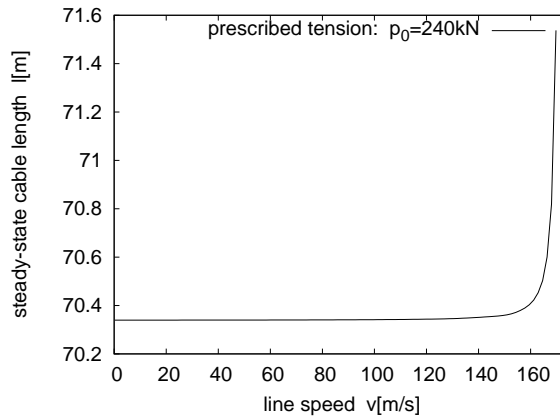


Figure 3.1: Scheme of the ropeway span in example 3.1.5.

towers, so that the horizontal distance of the cable in the air is 67.65 m and the vertical distance is 19.25 m . The haulage device shall be installed at the bottom terminal of the ropeway prescribing there a cable tension $\|\mathbf{p}_0\| = 240000\text{ N}$. Since the lower tower lies at the same height as the hauling device, the cable tension there is the same. In absence of gondolas, the sag and the length of the steady-state cable configuration are uniquely given by the cable tension on the lower tower. Using the equations of section 3.1.1, we want to analyse to what extent the cable line speed v in the steady-state convex configuration influences the curve length if the prescribed cable tension on the lower tower is kept constant. In our case Fig.3.2 shows that up to a cable

Figure 3.2: Example 3.1.5: The curve length l of the convex steady-state configuration in dependence on the cable line speed v .

line speed of 120 m/s the curve length and therefore also the sag (s. Fig.3.3) of the rope is approximately constant. Then the length increases rapidly until it reaches a maximum at a cable velocity of 169.74 m/s . Above this speed value the tensioning device is not able anymore to support the cable tension of the span. As was stated in the example before: nowadays even the fastest monocable ropeways do not surpass a line speed of 10 m/s . This means that in our application the sag would practically not depend on the line speed.

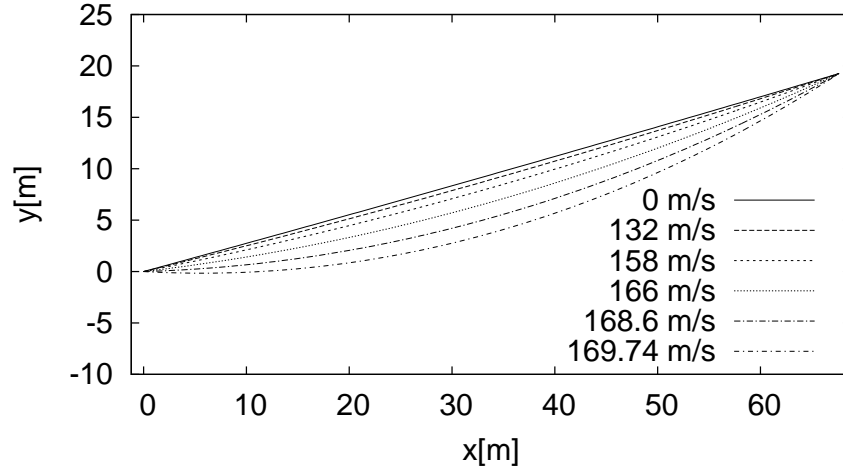


Figure 3.3: The sag of the convex steady-state configuration in the span of example 3.1.5 increases with the increasing line speed v . For $v = 169.74$ m/s, the maximal sag is reached.

3.2 The Linearized Problem

We now want to study the dynamics of the cable if it is almost but not exactly in the steady-state motion.

Let χ_0 be a steady-state configuration of (3.2) and let ε be the distance between the state of a general configuration $\chi(t)$ and the state of χ_0 , both elements of a suitable Banachspace. Assuming that ε is very small, we make the following ansatz:

$$\begin{aligned}\mathbf{r}(s,t) &= \mathbf{r}_0(s) + \varepsilon \mathbf{r}_1(s,t) + O(\varepsilon^2), \\ \mathbf{p}(s,t) &= \mathbf{p}_0(s) + \varepsilon \mathbf{p}_1(s,t) + O(\varepsilon^2),\end{aligned}$$

Plugging this into the first equation in (3.2) and comparing coefficients of ε , we come to

$$\frac{D^2}{Dt^2} \mathbf{r}_1(s,t) = \mathbf{p}'_1(s,t), \quad \forall s \in [0,1]. \quad (3.16)$$

Furthermore we have

$$\begin{aligned}\frac{1}{\|\mathbf{p}\|} &= [(\mathbf{p}_0 + \varepsilon \mathbf{p}_1 + \dots) \cdot (\mathbf{p}_0 + \varepsilon \mathbf{p}_1 + \dots)]^{-\frac{1}{2}} \\ &= [\mathbf{p}_0^2 + 2\varepsilon \mathbf{p}_0 \cdot \mathbf{p}_1 + O(\varepsilon^2)]^{-\frac{1}{2}} \\ &= \frac{1}{\|\mathbf{p}_0\|} \left[1 + 2\varepsilon \frac{\mathbf{p}_0 \cdot \mathbf{p}_1}{\mathbf{p}_0^2} + O(\varepsilon^2) \right]^{-\frac{1}{2}},\end{aligned}$$

so that if the absolute value of the term $2\varepsilon \frac{\mathbf{p}_0 \cdot \mathbf{p}_1}{\mathbf{p}_0^2} + O(\varepsilon^2)$ within the brackets is smaller than

one, it makes sense to write:

$$\begin{aligned}\frac{\mathbf{p}}{\|\mathbf{p}\|} &= \frac{(\mathbf{p}_0 + \varepsilon \mathbf{p}_1 + \dots)}{\|\mathbf{p}_0\|} \left[1 - \varepsilon \frac{\mathbf{p}_0 \cdot \mathbf{p}_1}{\|\mathbf{p}_0\|^2} + \dots \right] \\ &= \frac{\mathbf{p}_0}{\|\mathbf{p}_0\|} + \varepsilon \left(\frac{\mathbf{p}_1}{\|\mathbf{p}_0\|} - \frac{\mathbf{p}_0}{\|\mathbf{p}_0\|} \left(\frac{\mathbf{p}_0}{\|\mathbf{p}_0\|} \cdot \frac{\mathbf{p}_1}{\|\mathbf{p}_0\|} \right) \right) + O(\varepsilon^2).\end{aligned}$$

Plugging this into the second equation in (3.2) and comparing coefficients of ε , we come to

$$\mathbf{r}'_1 = \frac{\mathbf{p}_1}{\|\mathbf{p}_0\|} - \frac{\mathbf{p}_0}{\|\mathbf{p}_0\|} \left(\frac{\mathbf{p}_0}{\|\mathbf{p}_0\|} \cdot \frac{\mathbf{p}_1}{\|\mathbf{p}_0\|} \right). \quad (3.17)$$

In the same way we get the homogeneous boundary conditions and we summarize:

$$\begin{aligned}\forall s \in [0, 1]: \quad & \begin{cases} \frac{D^2}{Dt^2} \mathbf{r}_1 = \mathbf{p}'_1, \\ \mathbf{r}'_1 = \frac{\mathbf{p}_1}{\|\mathbf{p}_0\|} - \frac{\mathbf{p}_0}{\|\mathbf{p}_0\|} \left(\frac{\mathbf{p}_0}{\|\mathbf{p}_0\|} \cdot \frac{\mathbf{p}_1}{\|\mathbf{p}_0\|} \right), \end{cases} \\ \mathbf{r}_1(0, t) &= \mathbf{0}, \\ \mathbf{r}_1(1, t) &= \mathbf{0}.\end{aligned} \quad (3.18)$$

We make the following ansatz

$$\mathbf{r}_1(s, t) = u_1(s, t) \mathbf{t}_0(s) + u_2(s, t) \mathbf{n}_0(s) + u_3(s, t) \mathbf{e}_3, \quad (3.19)$$

$$\mathbf{p}_1(s, t) = q_1(s, t) \mathbf{t}_0(s) + q_2(s, t) \mathbf{n}_0(s) + q_3(s, t) \mathbf{e}_3 \quad (3.20)$$

and using the relations

$$\mathbf{t}'_0(s) = \kappa_0(s) \mathbf{n}_0(s), \quad \mathbf{n}'_0(s) = -\kappa_0(s) \mathbf{t}_0(s),$$

we get

$$\mathbf{r}'_1 = (u'_1 - \kappa_0 u_2) \mathbf{t}_0 + (u'_2 + \kappa_0 u_1) \mathbf{n}_0 + u'_3 \mathbf{e}_3, \quad (3.21)$$

$$\mathbf{p}'_1 = (q'_1 - \kappa_0 q_2) \mathbf{t}_0 + (q'_2 + \kappa_0 q_1) \mathbf{n}_0 + q'_3 \mathbf{e}_3. \quad (3.22)$$

Besides, due to the inextensibility and due to (3.3) we have

$$\mathbf{t}_0 = \mathbf{r}'_0 = \frac{\mathbf{p}_0}{\|\mathbf{p}_0\|}$$

and plugging (3.20) into eq. (3.17) we come to

$$\begin{aligned}\mathbf{r}'_1 &= \frac{\mathbf{p}_1}{\|\mathbf{p}_0\|} - \mathbf{t}_0 \left(\mathbf{t}_0 \cdot \frac{\mathbf{p}_1}{\|\mathbf{p}_0\|} \right) \\ &= \mathbf{n}_0 \left(\mathbf{n}_0 \cdot \frac{\mathbf{p}_1}{\|\mathbf{p}_0\|} \right) + \mathbf{e}_3 \left(\mathbf{e}_3 \cdot \frac{\mathbf{p}_1}{\|\mathbf{p}_0\|} \right) \\ &= \frac{1}{\|\mathbf{p}_0\|} (q_2 \mathbf{n}_0 + q_3 \mathbf{e}_3).\end{aligned} \quad (3.23)$$

Comparing (3.23) with (3.21), we get the following three equations:

$$u'_1 - \kappa_0 u_2 = 0, \quad (3.24)$$

$$u'_2 + \kappa_0 u_1 = \frac{q_2}{\|\mathbf{p}_0\|}, \quad (3.25)$$

$$u'_3 = \frac{q_3}{\|\mathbf{p}_0\|}. \quad (3.26)$$

The homogeneous boundary conditions in (3.18) are equal to:

$$\begin{aligned} u_1(0, t) &= 0, & u_1(1, t) &= 0, \\ u_2(0, t) &= 0, & u_2(1, t) &= 0, \\ u_3(0, t) &= 0, & u_3(1, t) &= 0. \end{aligned}$$

With the abbreviation $\dot{A} = \frac{\partial}{\partial t}A$ for an arbitrary quantity A we get from (3.19) and (3.23)

$$\begin{aligned} \ddot{\mathbf{r}}_1 &= \ddot{u}_1 \mathbf{t}_0 + \ddot{u}_2 \mathbf{n}_0 + \ddot{u}_3 \mathbf{e}_3, \\ \dot{\mathbf{r}}'_1 &= \frac{1}{\|\mathbf{p}_0\|} (\dot{q}_2 \mathbf{n}_0 + \dot{q}_3 \mathbf{e}_3), \\ \mathbf{r}''_1 &= \frac{1}{\|\mathbf{p}_0\|} \left[-q_2 \kappa_0 \mathbf{t}_0 + \left(q'_2 - \frac{\|\mathbf{p}_0\|'}{\|\mathbf{p}_0\|} q_2 \right) \mathbf{n}_0 + \left(q'_3 - \frac{\|\mathbf{p}_0\|'}{\|\mathbf{p}_0\|} q_3 \right) \mathbf{e}_3 \right], \end{aligned}$$

so that

$$\begin{aligned} \frac{D^2}{Dt^2} \mathbf{r}_1 &= \ddot{\mathbf{r}}_1 + 2c \dot{\mathbf{r}}'_1 + c^2 \mathbf{r}''_1 \\ &= \ddot{u}_1 \mathbf{t}_0 + \ddot{u}_2 \mathbf{n}_0 + \ddot{u}_3 \mathbf{e}_3 + \frac{2c}{\|\mathbf{p}_0\|} \dot{q}_2 \mathbf{n}_0 + \frac{2c}{\|\mathbf{p}_0\|} \dot{q}_3 \mathbf{e}_3 \\ &\quad - \frac{c^2}{\|\mathbf{p}_0\|} q_2 \kappa_0 \mathbf{t}_0 + \frac{c^2}{\|\mathbf{p}_0\|} \left(q'_2 - \frac{\|\mathbf{p}_0\|'}{\|\mathbf{p}_0\|} q_2 \right) \mathbf{n}_0 + \frac{c^2}{\|\mathbf{p}_0\|} \left(q'_3 - \frac{\|\mathbf{p}_0\|'}{\|\mathbf{p}_0\|} q_3 \right) \mathbf{e}_3 \\ &= \left[\ddot{u}_1 - \frac{c^2}{\|\mathbf{p}_0\|} q_2 \kappa_0 \right] \mathbf{t}_0 + \left[\ddot{u}_2 + \frac{2c}{\|\mathbf{p}_0\|} \dot{q}_2 + \frac{c^2}{\|\mathbf{p}_0\|} \left(q'_2 - \frac{\|\mathbf{p}_0\|'}{\|\mathbf{p}_0\|} q_2 \right) \right] \mathbf{n}_0 \\ &\quad + \left[\ddot{u}_3 + \frac{2c}{\|\mathbf{p}_0\|} \dot{q}_3 + \frac{c^2}{\|\mathbf{p}_0\|} \left(q'_3 - \frac{\|\mathbf{p}_0\|'}{\|\mathbf{p}_0\|} q_3 \right) \right] \mathbf{e}_3 \end{aligned} \quad (3.27)$$

Due to (3.16) this should be equal to \mathbf{p}'_1 . Thus the comparison of (3.27) with (3.22) yields

$$q'_1 - \kappa_0 q_2 = \ddot{u}_1 - \frac{c^2}{\|\mathbf{p}_0\|} q_2 \kappa_0, \quad (3.28)$$

$$q'_2 + \kappa_0 q_1 = \ddot{u}_2 + \frac{2c}{\|\mathbf{p}_0\|} \dot{q}_2 + \frac{c^2}{\|\mathbf{p}_0\|} \left(q'_2 - \frac{\|\mathbf{p}_0\|'}{\|\mathbf{p}_0\|} q_2 \right), \quad (3.29)$$

$$q'_3 = \ddot{u}_3 + \frac{2c}{\|\mathbf{p}_0\|} \dot{q}_3 + \frac{c^2}{\|\mathbf{p}_0\|} \left(q'_3 - \frac{\|\mathbf{p}_0\|'}{\|\mathbf{p}_0\|} q_3 \right). \quad (3.30)$$

As we can see from eq. (3.26) and (3.30), the equations of (3.18) concerning the x_3 -direction can be decoupled. Therefore, defining the function

$$\gamma(s) = 1 - \frac{c^2}{\|\mathbf{p}_0(s)\|},$$

eqs. (3.24)-(3.26) and (3.28)-(3.30) with the homogeneous boundary conditions describe an *in-plane*-motion

$$\begin{aligned} \forall s \in [0, 1] : \begin{cases} u'_1 = \kappa_0 u_2, \\ u'_2 = -\kappa_0 u_1 + \frac{q_2}{\|\mathbf{p}_0\|}, \\ q'_1 = \ddot{u}_1 + \gamma \kappa_0 q_2, \\ q'_2 = \left[\ddot{u}_2 + \frac{2c}{\|\mathbf{p}_0\|} \dot{q}_2 - \frac{c^2 \|\mathbf{p}_0\|'}{\|\mathbf{p}_0\|^2} q_2 - \kappa_0 q_1 \right] \frac{1}{\gamma}, \end{cases} \\ u_1(0, t) = 0, \\ u_2(0, t) = 0, \\ u_1(1, t) = 0, \\ u_2(1, t) = 0 \end{aligned} \quad (3.31)$$

and an *out-of-plane*-motion

$$\begin{aligned} \forall s \in [0, 1] : \begin{cases} u'_3 = \frac{q_3}{\|\mathbf{p}_0\|}, \\ q'_3 = \left[\ddot{u}_3 + \frac{2c}{\|\mathbf{p}_0\|} \dot{q}_3 - \frac{c^2 \|\mathbf{p}_0\|'}{\|\mathbf{p}_0\|^2} q_3 \right] \frac{1}{\gamma}, \end{cases} \\ u_3(0, t) = 0, \\ u_3(1, t) = 0, \end{aligned} \quad (3.32)$$

which can be solved separately.

In the following sections it will be comfortable to use complex quantities. Therefore we denote by \Re_z the real part of $z \in \mathbb{C}$ or the vector of the real parts of the components of z if $z \in \mathbb{C}^n$, with $1 \leq n < \infty$.

3.2.1 Eigenmodes of the In-plane-motion

With

$(u_1, u_2, q_1, q_2) = \Re(z_1, z_2, z_3, z_4)$ we convert problem (3.31) into a complex one and try to find solutions using the complex ansatz

$$z_k(s, t) = e^{\mu t} \zeta_k(s), \quad \forall k, \quad (3.33)$$

choosing $\mu \in \mathbb{C}$ in such a way that the now ordinary differential equation system

$$\forall s \in [0, 1] : \begin{cases} \zeta_1' &= \kappa_0 \zeta_2, \\ \zeta_2' &= -\kappa_0 \zeta_1 + \frac{1}{\|\mathbf{p}_0\|} \zeta_4, \\ \zeta_3' &= \mu^2 \zeta_1 + \gamma \kappa_0 \zeta_4, \\ \zeta_4' &= \left[\mu^2 \zeta_2 + \frac{2c}{\|\mathbf{p}_0\|} \mu \zeta_4 - \frac{c^2 \|\mathbf{p}_0\|'}{\|\mathbf{p}_0\|^2} \zeta_4 - \kappa_0 \zeta_3 \right] / \gamma, \end{cases} \quad (3.34)$$

with the complex homogeneous boundary conditions

$$\zeta_1(0) = 0, \quad (3.35)$$

$$\zeta_2(0) = 0, \quad (3.36)$$

$$\zeta_1(1) = 0, \quad (3.37)$$

$$\zeta_2(1) = 0 \quad (3.38)$$

can be fulfilled. Obviously, solutions of the boundary value problem (3.34)-(3.38) are unique up to an arbitrary complex factor. Therefore we can demand one more complex equation (or two real equations) to be fulfilled at a boundary value - thus we choose the following normalization and phase condition:

$$\underbrace{|\zeta_1(0)|^2 + |\zeta_2(0)|^2}_{=0, \text{ eq. (3.35), (3.36)}} + |\zeta_3(0)|^2 + |\zeta_4(0)|^2 = 1, \quad \zeta_3(0) = \bar{\zeta}_3(0) \in \mathbb{R}. \quad (3.39)$$

By separating real- and imaginary-part for

$$\begin{aligned} \zeta_k(s) &= \xi_k(s) + i \eta_k(s), \\ \mu &= \lambda + i \omega, \end{aligned}$$

and also in the eqs. (3.34)-(3.38), we get the following *eight* coupled real ordinary differential equations:

$$\begin{aligned} \xi_1' &= \kappa_0 \xi_2, \\ \xi_2' &= -\kappa_0 \xi_1 + \frac{1}{\|\mathbf{p}_0\|} \xi_4, \\ \xi_3' &= (\lambda^2 - \omega^2) \xi_1 + \gamma \kappa_0 \xi_4 - 2\lambda \omega \eta_1, \\ \xi_4' &= \left[(\lambda^2 - \omega^2) \xi_2 - \kappa_0 \xi_3 + \left(\frac{2c\lambda}{\|\mathbf{p}_0\|} - \frac{c^2 \|\mathbf{p}_0\|'}{\|\mathbf{p}_0\|^2} \right) \xi_4 - 2\lambda \omega \eta_2 - \frac{2c\omega}{\|\mathbf{p}_0\|} \eta_4 \right] \frac{1}{\gamma}, \\ \eta_1' &= \kappa_0 \eta_2, \\ \eta_2' &= -\kappa_0 \eta_1 + \frac{1}{\|\mathbf{p}_0\|} \eta_4, \\ \eta_3' &= (\lambda^2 - \omega^2) \eta_1 + \gamma \kappa_0 \eta_4 + 2\lambda \omega \xi_1, \\ \eta_4' &= \left[(\lambda^2 - \omega^2) \eta_2 - \kappa_0 \eta_3 + \left(\frac{2c\lambda}{\|\mathbf{p}_0\|} - \frac{c^2 \|\mathbf{p}_0\|'}{\|\mathbf{p}_0\|^2} \right) \eta_4 + 2\lambda \omega \xi_2 + \frac{2c\omega}{\|\mathbf{p}_0\|} \xi_4 \right] \frac{1}{\gamma}, \end{aligned} \quad (3.40)$$

and as mentioned above the real parameters λ and ω have to be chosen in such a way that these *eight* boundary conditions

$$\xi_1(0) = 0, \quad (3.41)$$

$$\eta_1(0) = 0, \quad (3.42)$$

$$\xi_2(0) = 0, \quad (3.43)$$

$$\eta_2(0) = 0, \quad (3.44)$$

$$\xi_1(1) = 0, \quad (3.45)$$

$$\eta_1(1) = 0, \quad (3.46)$$

$$\xi_2(1) = 0, \quad (3.47)$$

$$\eta_2(1) = 0, \quad (3.48)$$

are fulfilled. The normalization-phase convention (3.39) can be formulated now as:

$$\xi_3^2(0) + \xi_4^2(0) + \eta_4^2(0) = 1, \quad (3.49)$$

$$\eta_3(0) = 0. \quad (3.50)$$

In order to find the right (λ, ω) -values, we look at the system (3.40) with *new* boundary conditions substituting *two* of the last four boundary conditions - let us say for instance eqs. (3.45) and (3.46) - by the eqs. (3.49) and (3.50). We solve this boundary value problem varying the values of λ and ω as long as the original boundary condition eqs. (3.45) and (3.46) are fulfilled. By evaluating the real part of (3.33) we get the solutions of (3.31):

$$\begin{aligned} u_1 &= e^{\lambda t} (\xi_1 \cos \omega t - \eta_1 \sin \omega t), \\ u_2 &= e^{\lambda t} (\xi_2 \cos \omega t - \eta_2 \sin \omega t), \\ q_1 &= e^{\lambda t} (\xi_3 \cos \omega t - \eta_3 \sin \omega t), \\ q_2 &= e^{\lambda t} (\xi_4 \cos \omega t - \eta_4 \sin \omega t). \end{aligned} \quad (3.51)$$

If we plug the expressions for u_1 and u_2 into eq. (3.19) and project it into the x_1, x_2 -plane, we get for the linear correction term $\mathbf{r}_1 = \mathbf{r}_1^{(\text{in})}$

$$\begin{aligned} \mathbf{r}_1^{(\text{in})} &= u_1 \mathbf{t}_0 + u_2 \mathbf{n}_0 \\ &= e^{\lambda t} [(\xi_1 \mathbf{t}_0 + \xi_2 \mathbf{n}_0) \cos \omega t - (\eta_1 \mathbf{t}_0 + \eta_2 \mathbf{n}_0) \sin \omega t] \end{aligned}$$

As a consequence for a particular eigenvalue $\lambda + i\omega$ the linear correction $\mathbf{r}_1^{(\text{in})}$ has two independent amplitudes, the coefficients of $e^{\lambda t} \cos \omega t$ and of $e^{\lambda t} \sin \omega t$:

$$\mathbf{A}^{(\text{in})} = \xi_1 \mathbf{t}_0 + \xi_2 \mathbf{n}_0,$$

$$\mathbf{B}^{(\text{in})} = \eta_1 \mathbf{t}_0 + \eta_2 \mathbf{n}_0.$$

Therefore every in-plane eigenmode is represented by these two components:

$$\mathbf{r}_0 + a \mathbf{A}^{(\text{in})}, \quad a \in \mathbb{R}, \quad (3.52)$$

$$\mathbf{r}_0 + b \mathbf{B}^{(\text{in})}, \quad b \in \mathbb{R}, \quad (3.53)$$

where a and b are arbitrary constants.

3.2.2 Eigenmodes of the Out-of-plane-motion

With $(u_3, q_3) = \Re(z_5, z_6)$ we convert problem (3.32) into a complex one and again we try to find solutions using a complex ansatz

$$z_k(s, t) = e^{vt} \zeta_k(s), \quad k \in \{5, 6\} \quad (3.54)$$

by choosing $v \in \mathbb{C}$ in such a way that the ordinary differential equation system

$$\forall s \in [0, 1] : \begin{cases} \zeta_5' = \frac{1}{\|\mathbf{p}_0\|} \zeta_6, \\ \zeta_6' = \left[v^2 \zeta_5 + \frac{2c}{\|\mathbf{p}_0\|} v \zeta_6 - \frac{c^2 \|\mathbf{p}_0\|'}{\|\mathbf{p}_0\|^2} \zeta_6 \right] \frac{1}{\gamma}, \end{cases} \quad (3.55)$$

fulfills the boundary conditions

$$\zeta_5(0) = 0, \quad (3.56)$$

$$\zeta_5(1) = 0, \quad (3.57)$$

and the normalization-phase condition

$$\|\zeta_6(0)\|^2 = 1, \quad \zeta_6(0) = \bar{\zeta}_6(0) \in \mathbb{R}, \quad (3.58)$$

which is equal to $\zeta_6(0) = \pm 1$. After separating real- and imaginary- part in

$$\zeta_k(s) = \xi_k(s) + i \eta_k(s), \quad k \in \{5, 6\},$$

$$v = \bar{\lambda} + i \bar{\omega},$$

and also in the eqs. (3.55)-(3.57), we get the following *four* coupled real ordinary differential equations:

$$\begin{aligned} \xi_5' &= \frac{1}{\|\mathbf{p}_0\|} \xi_6, \\ \xi_6' &= \left[(\bar{\lambda}^2 - \bar{\omega}^2) \xi_5 + \left(\frac{2c\bar{\lambda}}{\|\mathbf{p}_0\|} - \frac{c^2 \|\mathbf{p}_0\|'}{\|\mathbf{p}_0\|^2} \right) \xi_6 - 2\bar{\lambda} \bar{\omega} \eta_5 - \frac{2c\bar{\omega}}{\|\mathbf{p}_0\|} \eta_6 \right] \frac{1}{\gamma}, \\ \eta_5' &= \frac{1}{\|\mathbf{p}_0\|} \eta_6, \\ \eta_6' &= \left[(\bar{\lambda}^2 - \bar{\omega}^2) \eta_5 + \left(\frac{2c\bar{\lambda}}{\|\mathbf{p}_0\|} - \frac{c^2 \|\mathbf{p}_0\|'}{\|\mathbf{p}_0\|^2} \right) \eta_6 + 2\bar{\lambda} \bar{\omega} \xi_5 + \frac{2c\bar{\omega}}{\|\mathbf{p}_0\|} \xi_6 \right] \frac{1}{\gamma}, \end{aligned} \quad (3.59)$$

and with the right values of $\bar{\lambda}$ and $\bar{\omega}$, these *four* boundary conditions

$$\xi_5(0) = 0, \quad (3.60)$$

$$\eta_5(0) = 0, \quad (3.61)$$

$$\xi_5(1) = 0, \quad (3.62)$$

$$\eta_5(1) = 0 \quad (3.63)$$

are fulfilled. Using the normalization-phase convention (3.58) in the form

$$\xi_6(0) = \pm 1 , \quad (3.64)$$

$$\eta_6(0) = 0 \quad (3.65)$$

instead of eqs. (3.62)-(3.63) for the boundary value problem will help us to find the right values for $\bar{\lambda}$ and $\bar{\omega}$, simply by testing if $\xi_5(1)$ and $\eta_5(1)$ vanish, and the solution is:

$$\begin{aligned} u_3 &= e^{\bar{\lambda}t} (\xi_5 \cos \bar{\omega}t - \eta_5 \sin \bar{\omega}t), \\ q_3 &= e^{\bar{\lambda}t} (\xi_6 \cos \bar{\omega}t - \eta_6 \sin \bar{\omega}t). \end{aligned} \quad (3.66)$$

Plugging the expression for u_3 into the x_3 -component of eq. (3.19), we get for the linear correction $\mathbf{r}_1 = \mathbf{r}_1^{(\text{out})}$ of the out-of-plane motion

$$\begin{aligned} \mathbf{r}_1^{(\text{out})} &= u_3 \mathbf{e}_3 \\ &= e^{\bar{\lambda}t} [(\xi_5 \mathbf{e}_3) \cos \bar{\omega}t - (\eta_5 \mathbf{e}_3) \sin \bar{\omega}t] \end{aligned}$$

Also here for a particular eigenvalue $\bar{\lambda} + i\bar{\omega}$ the linear correction $\mathbf{r}_1^{(\text{out})}$ has the two independent amplitudes which are the coefficients of $e^{\bar{\lambda}t} \cos \bar{\omega}t$ and of $e^{\bar{\lambda}t} \sin \bar{\omega}t$:

$$\begin{aligned} \mathbf{A}^{(\text{out})} &= \xi_5 \mathbf{e}_3 , \\ \mathbf{B}^{(\text{out})} &= \eta_5 \mathbf{e}_3 . \end{aligned}$$

Since the steady-state configurations lie within the x_1, x_2 -plane, every out-of-plane eigenmode is represented by these two components:

$$\begin{aligned} \bar{a} \mathbf{A}^{(\text{out})}, \quad \bar{a} \in \mathbb{R} , \\ \bar{b} \mathbf{B}^{(\text{out})}, \quad \bar{b} \in \mathbb{R} , \end{aligned}$$

where \bar{a} and \bar{b} are again arbitrary constants.

3.2.3 Remarks

Since in our model no damping mechanism is included, we can expect that λ , the real part of the eigenvalue, vanishes. However, from a mathematical point of view this is not obvious, because the governing equations of motions (3.28)-(3.30) include first order time derivations.

As we shall see in chapter 4, if we take rolls instead of eyelets as boundaries, the linear correction term \mathbf{r}_1 vanishes at the points where the steady-state configuration touches the rolls tangentially. Therefore in this case the boundary conditions of the linearized problem turn out to be the same as if there were two eyelets on the surfaces of the two rolls.

3.2.4 Example

We now extend example 3.1.5 and calculate the lowest eigenvalue of the in-plane motion for the ropeway-span problem without gondolas using the equations of sec. 3.2.1. In fact it turns out that the real part of the eigenvalue, λ , is at least numerically equal to zero. From the imaginary part ω of the dimensionless eigenvalue we get the dimensional eigenfrequency

$$f = \frac{1}{2\pi} \sqrt{\frac{g}{l}} \omega .$$

In Fig. 3.4 the lowest eigenfrequency f_1 is plotted as a function of the cable line speed v which

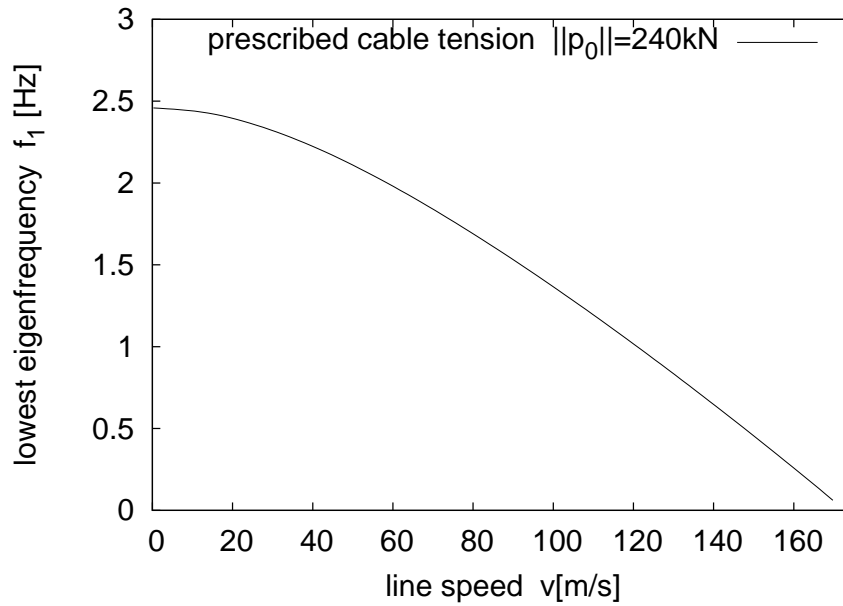


Figure 3.4: The lowest eigenfrequency of the cable span in the ropeway of example 3.2.4 (or 3.1.5) in dependence on the line speed.

is given in the steady-state configuration. The frequency achieves a global minimum at the limiting speed of $v = 169.74 \text{ m/s}$ (see also example 3.1.5). In Fig. 3.5 the dimensional version of the component (3.52) from the lowest in-plane eigenmode is plotted with a suitable chosen constant scaling factor a for the line speeds $v = 0 \text{ m/s}$, $v = 105 \text{ m/s}$ and $v = 169.74 \text{ m/s}$. Additionally the corresponding steady-state configuration is plotted, so that the nodes - the zeros of the linear correction term - in this eigenmode are visible. With increasing line speed v , the node moves monotonously towards the inlet or inlet roll. The other component, (3.53), which is plotted in Fig. 3.6, is even more interesting to observe, since in this case not only the initial node of the component moves monotonously towards the inlet, but also a second node appears above a certain line speed ($v \approx 40 \text{ m/s}$). Looking at the lowest ten eigenfrequencies depending on the line speed v in Fig. 3.7, we notice that for constant v the spectrum is similar to the spectrum of the tensioned but not axially moving elastic string, where the increment

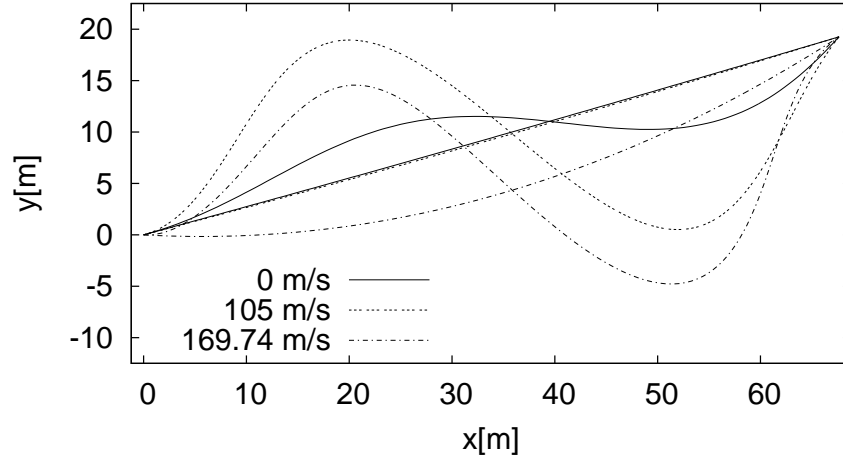


Figure 3.5: Example 3.2.4: The first component (3.52) of the lowest eigenmode and the corresponding steady-state configuration for three different line speeds v .

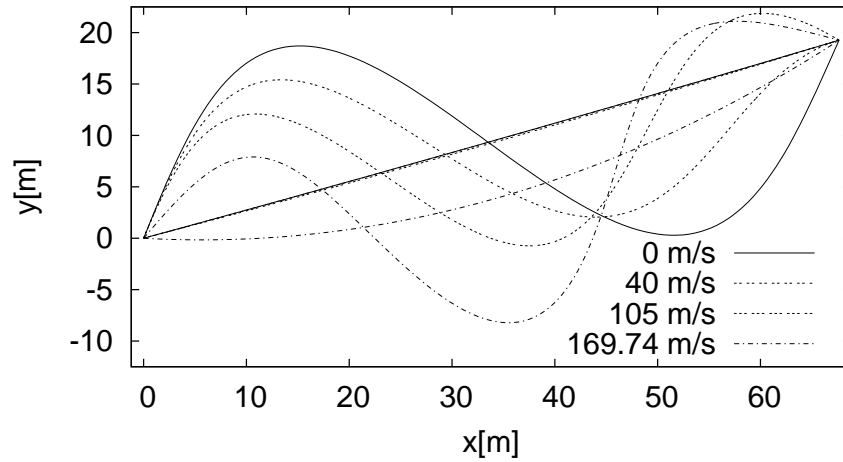


Figure 3.6: Example 3.2.4: The second component (3.53) of the lowest eigenmode and the corresponding steady-state configuration for four different line speeds v .

between two sequent eigenfrequencies is a constant f_0 . However, the crucial difference is that in our case the lowest eigenfrequency is not around f_0 - as it would be in the elastic string case - but it is around $2f_0$ - quite an octave higher. As it is visible in Fig. 3.5 and 3.6, the lowest eigenmode has at least one node - unlike the elastic string, which has no nodes in its lowest eigenmode. The reason for this is also evident, because an eigenmode without nodes implies extensibility, which is excluded in our model for the cable. We can compare our results, at least qualitatively with results of similar problems such as the elastic travelling cable of Perkins and Mote in [18]. Their mechanical model differs from the above-mentioned model with regard to two properties: Firstly, the cable is elastic and therefore the length of the cable configuration is not conserved. Secondly, not the cable tension at the inlet is prescribed like in example 3.2.4, but

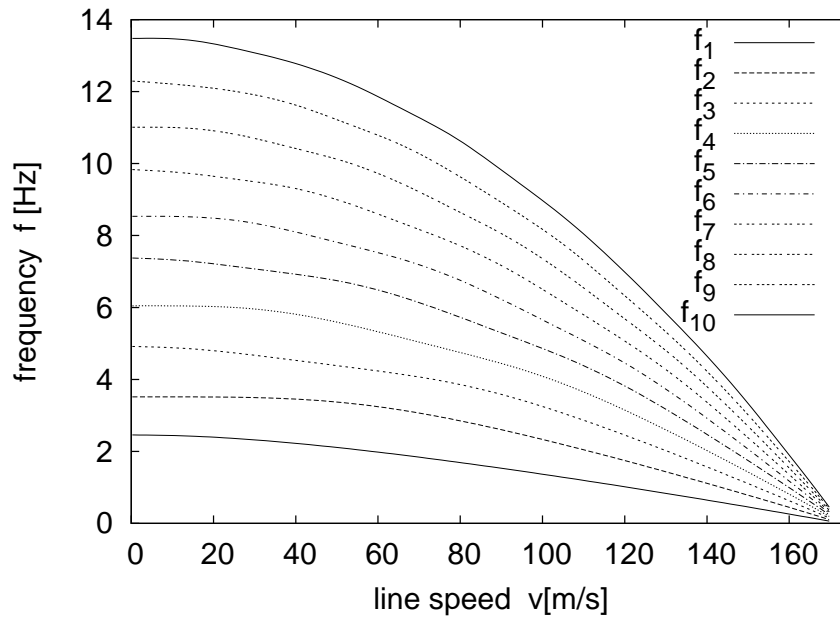


Figure 3.7: Example 3.2.4: The lower part of the eigenfrequency-spectrum varying with the line speed v .

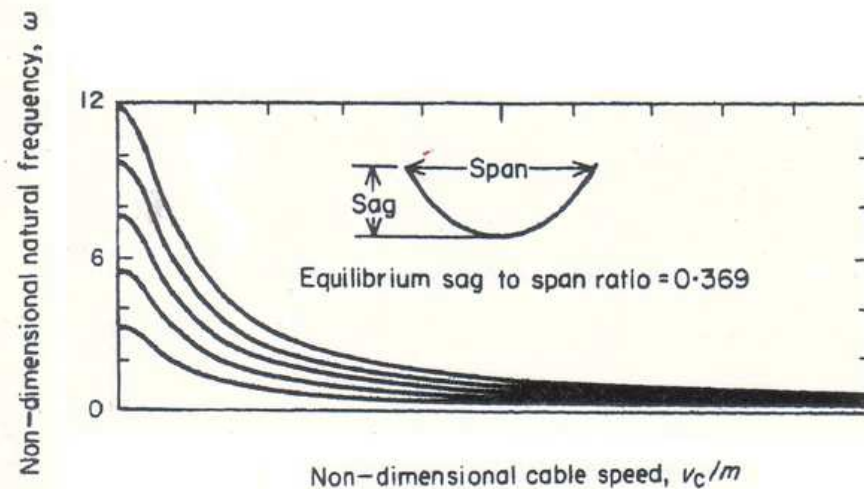


Figure 3.8: Example of Perkins and Mote in [18]: The figure shows the lowest non-dimensional in-plane eigenfrequencies of an elastic cable in dependency on the non-dimensional line speed. Here the cable mass between the in- and the outlet is conserved.

the total cable mass between the fixed inlet and outlet is conserved and in particular independent of the cable line speed. In our case, the eigenfrequencies decrease monotonically as functions of cable speed and also the tangents for vanishing cable speed are always horizontal. Due to the

different boundary conditions, there is no limiting cable velocity in the elastic cable example, and therefore all the eigenfrequencies approach asymptotically zero.

3.2.5 Remarks

The lowest eigenmode of a cable in a constant gravitational field for low axial velocity can be illustrated best in the following way.

Imagine the outlet nearby the inlet and the cable configuration with a huge sag, in such a way that from far away it looks like a single down-hanging folded chain or pendulum. Then the simplest motion would be a motion of the whole chain similar to the one of a mathematical pendulum. And exactly this motion is described by an oscillation with an asymmetric eigenmode, which has an odd number of nodes.

As we stated at the end of chapter 2, there is a remarkable analogy between the cable and a fluid conveying tube. Holmes and Marsden showed in [7] that such a fluid conveying tube with pinned ends is *not* a *self-exciting* system. Therefore we expect that in particular the phenomenon of violent sag-oscillations of the cable [12] in certain cable spans of a ropeway (s. chapter 1) is *not* caused by self-excitation, but solely by *external* excitation. For instance the equidistantly attached cabins or chairs excite periodically in time the cable configuration in a certain span.

Chapter 4

Rolls as boundaries

In many technical applications - not only in aerial ropeways - the cable is either hanging in the air or in contact with rolls. Thus again we take a look at the dynamics of a cable in a constant gravitational field like in chapter 3, but now we let the cable configuration be bounded by rolls instead of eyelets (s. Fig.4.1). The contact between the cable and the roll can be either with or without friction. If there is friction, the roll surface shall have the same velocity as the cable. For vanishing friction we assume that the roll is at rest. In any case of contact the cable shall touch the roll tangentially. The equations of motions are the same as in chapter 3, but the boundary conditions are different. To give a first survey, we only study the planar problem. Let \mathcal{C}_A be the circle line representing the roll that we have now instead of the inlet, and in the same way let \mathcal{C}_B be the circle line that replaces the outlet. The kinematic boundary condition is that the cable touches both of the rolls tangentially with the velocity v . In Fig. 4.2 we see the left or inlet roll. The cable first is in contact with the roll \mathcal{C}_A , where the cable configuration has the shape of a circle segment. At the point denoted by the arclength s_A the cable loses the contact with the roll, but still has the same tangent. Of course the location of this point as well as s_A are time-dependent.

Fixing a reference length l and using the transformation (3.1) of chapter 3, we have for all t the

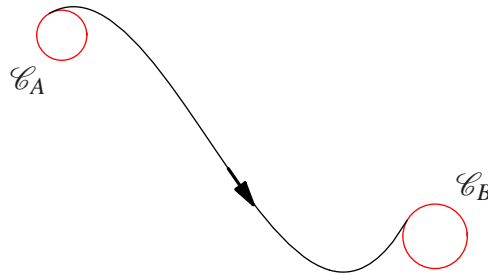


Figure 4.1: In many technical applications - not only in aerial ropeways - the cable at the boundaries moves over rolls.

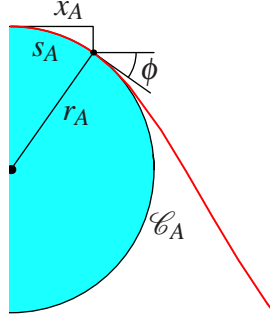


Figure 4.2: The left roll: the location of the cable configuration point where the cable loses contact with the roll is time-dependent.

dimensionless problem¹

$$\begin{aligned} \forall s \in [s_A(t), s_B(t)] : \begin{cases} \frac{D^2}{Dt^2} \mathbf{r}(s, t) = -\mathbf{e}_2 + \frac{\partial}{\partial s} \mathbf{p}(s, t), \\ \frac{\partial}{\partial s} \mathbf{r}(s, t) = \frac{\mathbf{p}(s, t)}{\|\mathbf{p}(s, t)\|}, \end{cases} \\ \mathbf{r}(s_A(t), t) \in \mathcal{C}_A, \quad \mathbf{r}'(s_A(t), t) \in T\mathcal{C}_A|_{\mathbf{r}(s_A(t), t)}, \\ \mathbf{r}(s_B(t), t) \in \mathcal{C}_B, \quad \mathbf{r}'(s_B(t), t) \in T\mathcal{C}_B|_{\mathbf{r}(s_B(t), t)}. \end{aligned} \quad (4.1)$$

4.1 The Steady-State Problem

Since for our applications concerning ropeways only the convex steady-state plays a significant role (see ex. 3.1.4 in chapt. 3), we will confine here the problem to this case. Therefore let χ_0 be the convex steady-state configuration solution of

$$\begin{aligned} \forall s \in [s_{A,0}, s_{B,0}] : \begin{cases} c^2 \mathbf{r}_0''(s) = -\mathbf{e}_2 + \mathbf{p}_0'(s), \\ \mathbf{r}_0'(s) = \frac{\mathbf{p}_0(s)}{\|\mathbf{p}_0(s)\|}, \end{cases} \\ \mathbf{r}(s_{A,0}, t) \in \mathcal{C}_A, \quad \mathbf{r}'(s_{A,0}, t) \in T\mathcal{C}_A|_{\mathbf{r}(s_{A,0}, t)}, \\ \mathbf{r}(s_{B,0}, t) \in \mathcal{C}_B, \quad \mathbf{r}'(s_{B,0}, t) \in T\mathcal{C}_B|_{\mathbf{r}(s_{B,0}, t)}. \end{aligned} \quad (4.2)$$

The points on the rolls where the cable configuration touches them tangentially are denoted by the arclengths $s_{A,0}$ and $s_{B,0}$ which initially are unknown. These points can be determined by a numerical iteration procedure.

¹By $T\mathcal{M}|_{\mathbf{x}}$ we denote the tangential vectorspace on the manifold \mathcal{M} at the point $\mathbf{x} \in \mathcal{M}$.

4.2 The linearized problem

As in section 3.2 of chapter 3, we will now study the dynamics of the cable if it is almost but not exactly in the steady-state motion of the convex steady-state configuration of problem (4.1). Let ε be again the distance between the state of a general configuration $\chi(t)$ and the state of χ_0 . Assuming that ε is very small, we can use the same ansatz as in section 3.2 of chapter 3. Additionally, for the left role (s. Fig.4.2) we make the ansatz

$$s_A(t) = s_{A,0} + \varepsilon s_{A,1}(t) + O(\varepsilon^2)$$

so that on the one hand

$$\begin{aligned} \mathbf{r}(s_A(t), t) &= \mathbf{r}_0(s_A(t)) + \varepsilon \mathbf{r}_1(s_A(t), t) + O(\varepsilon^2) , \\ &= \mathbf{r}_0(s_{A,0}) + (s_A(t) - s_{A,0}) \mathbf{r}'_0(s_{A,0}) + \varepsilon \mathbf{r}_1(s_{A,0}, t) + O(\varepsilon^2) , \\ &= \mathbf{r}_0(s_{A,0}) + \varepsilon (s_{A,1}(t) \mathbf{r}'_0(s_{A,0}) + \mathbf{r}_1(s_{A,0}, t)) + O(\varepsilon^2) . \end{aligned} \quad (4.3)$$

On the other hand we have the circle line

$$\mathcal{C}_A = \left\{ \mathbf{x} \mid \mathbf{x} = \mathbf{m}_A + r_A \begin{pmatrix} \sin(s/r_A) \\ \cos(s/r_A) \end{pmatrix}, s \in (-r_A\pi, r_A\pi] \right\}$$

and its tangent manifold²

$$T\mathcal{C}_A = \left\{ \mathbf{x} \mid \mathbf{x} = \lambda \begin{pmatrix} \cos(s/r_A) \\ -\sin(s/r_A) \end{pmatrix}, s \in (-r_A\pi, r_A\pi], \lambda \in \mathbb{R} \right\}$$

so that if we expand

$$\begin{aligned} \sin\left(\frac{s_A(t)}{r_A}\right) &= \sin\left(\frac{s_{A,0}}{r_A}\right) + \varepsilon s_{A,1}(t) \frac{1}{r_A} \cos\left(\frac{s_{A,0}}{r_A}\right) + O(\varepsilon^2) , \\ \cos\left(\frac{s_A(t)}{r_A}\right) &= \cos\left(\frac{s_{A,0}}{r_A}\right) - \varepsilon s_{A,1}(t) \frac{1}{r_A} \sin\left(\frac{s_{A,0}}{r_A}\right) + O(\varepsilon^2) , \end{aligned}$$

we can write

$$\begin{aligned} \mathbf{r}(s_A(t), t) \in \mathcal{C}_A &\Leftrightarrow \mathbf{r}(s_A(t), t) = \mathbf{m}_A + r_A \begin{pmatrix} \sin(s_A(t)/r_A) \\ \cos(s_A(t)/r_A) \end{pmatrix} \\ &= \underbrace{\mathbf{m}_A + r_A \begin{pmatrix} \sin(s_{A,0}/r_A) \\ \cos(s_{A,0}/r_A) \end{pmatrix}}_{=\mathbf{r}_0(s_{A,0}) \in \mathcal{C}_A} + \varepsilon s_{A,1}(t) \underbrace{\begin{pmatrix} \cos(s_{A,0}/r_A) \\ -\sin(s_{A,0}/r_A) \end{pmatrix}}_{=\mathbf{r}'_0(s_{A,0}) \in T\mathcal{C}_A|_{\mathbf{r}_0(s_{A,0})}} + O(\varepsilon^2) . \end{aligned}$$

Comparing the last equation with eq.(4.3) we conclude that

$$\mathbf{r}_1(s_{A,0}, t) = \mathbf{0} \quad (4.4)$$

²The tangent manifold $T\mathcal{M}$ is the union of all tangent vectorspaces of the manifold \mathcal{M}

and therefore

$$\begin{aligned}
 \mathbf{r}_1(s_A(t), t) &= \underbrace{\mathbf{r}_1(s_{A,0}, t)}_{\mathbf{0}} + \underbrace{(s_A(t) - s_{A,0})}_{\varepsilon s_{A,1}(t) + O(\varepsilon^2)} \mathbf{r}'_1(s_{A,0}, t) + O(\varepsilon^2) \\
 &= \varepsilon s_{A,1}(t) \mathbf{r}'_1(s_{A,0}, t) + O(\varepsilon^2) \\
 \varepsilon \mathbf{r}_1(s_A(t), t) &= O(\varepsilon^2)
 \end{aligned}$$

or rather

$$\mathbf{r}(s_A(t), t) = \mathbf{r}_0(s_A(t)) + O(\varepsilon^2) .$$

Of course the same applies to $s_B(t)$ on the right roll. Hence we can summarize the linearized problem in the following way:

$$\begin{aligned}
 \forall s \in [s_{A,0}, s_{B,0}] : \quad & \begin{cases} \frac{D^2}{Dt^2} \mathbf{r}_1 = \mathbf{p}'_1, \\ \mathbf{r}'_1 = \frac{\mathbf{p}_1}{\|\mathbf{p}_0\|} - \frac{\mathbf{p}_0}{\|\mathbf{p}_0\|} \left(\frac{\mathbf{p}_0}{\|\mathbf{p}_0\|} \cdot \frac{\mathbf{p}_1}{\|\mathbf{p}_0\|} \right), \end{cases} \\
 \mathbf{r}_1(s_{A,0}, t) &= \mathbf{0}, \\
 \mathbf{r}_1(s_{B,0}, t) &= \mathbf{0}.
 \end{aligned} \tag{4.5}$$

Up to a scaling length factor, the linearized problem is equal to the eyelet problem (3.18) in chapter 3. We conclude that if the cable is almost but not exactly in the steady-state motion ($0 < \varepsilon \ll 1$), we first have to find the arclengths $s_{A,0}$ and $s_{B,0}$ or the points on the rolls where the cable loses the contact in the steady-state motion. By taking these points as fixed eyelets, we then get the right eigenfrequencies and eigenmodes.

4.3 A Not Perfectly Flexible Cable

In this section we analyse, in how far the planar steady-state solution of the cable between two rolls in a constant gravitational field changes if the cable is not perfectly flexible. As a consequence, additionally to the tangential section force P_0 there is now a non-vanishing transversal section force component Q_0 , so that the cable tension \mathbf{p}_0 can be written as

$$\mathbf{p}_0 = P_0 \mathbf{t}_0 + Q_0 \mathbf{n}_0 .$$

The curvature of the steady-state configuration is defined by

$$\alpha'_0 = \kappa_0 ,$$

where α_0 is the inclination angle of the tangential vector

$$\mathbf{t}_0 = \begin{pmatrix} x'_0 \\ y'_0 \end{pmatrix} = \begin{pmatrix} \cos \alpha_0 \\ \sin \alpha_0 \end{pmatrix}$$

of the steady-state configuration of the inextensible cable. The corresponding normal vector is

$$\mathbf{n}_0 = \begin{pmatrix} -\sin \alpha_0 \\ \cos \alpha_0 \end{pmatrix}.$$

Like in eq. (2.5) of chapter 2 we get from Newton's law

$$\rho A \frac{D^2}{Dt^2} \mathbf{r}_0(s) = \mathbf{f} + \mathbf{p}'_0(s), \quad \forall s \in I, \quad (4.6)$$

with the external force per unit length $\mathbf{f} = -\rho A g \mathbf{e}_2$ and the arclength interval $I = [s_{A,0}, s_{B,0}]$ which is apriori unknown due to the geometry of the boundaries. Eq. (4.6) is equal to

$$(\rho A v^2 \mathbf{t}_0)' = \mathbf{f} + (P_0 \mathbf{t}_0)' + (Q_0 \mathbf{n}_0)'$$

and can be written as

$$\mathbf{0} = \mathbf{f} + (P_0^* \mathbf{t}_0)' + (Q_0 \mathbf{n}_0)'$$

with the fictitious tangential cable section force

$$P_0^* = P_0 - \rho A v^2.$$

Thus eq. (4.6) corresponds to a fictitious statical problem

$$\mathbf{0} = \mathbf{f} + \mathbf{p}'_0, \quad \forall s \in I, \quad (4.7)$$

with the cable tension

$$\mathbf{p}_0^* = P_0^* \mathbf{t}_0 + Q_0 \mathbf{n}_0,$$

which also can be written in terms of cartesian components:

$$\mathbf{p}_0^* = H_0^* \mathbf{e}_1 + V_0^* \mathbf{e}_2.$$

The transformation between the two bases is

$$\begin{pmatrix} P_0^* \\ Q_0 \end{pmatrix} = \begin{pmatrix} \cos \alpha_0 & \sin \alpha_0 \\ -\sin \alpha_0 & \cos \alpha_0 \end{pmatrix} \begin{pmatrix} H_0^* \\ V_0^* \end{pmatrix}. \quad (4.8)$$

From eq. (4.7) follows:

$$\begin{aligned} H_0^{*'} &= 0, \\ V_0^{*'} &= \rho A g. \end{aligned}$$

Hence H_0^* is a constant. From eq. (4.8) we deduce

$$\begin{aligned} Q_0' &= (-H_0^* \sin \alpha_0 + V_0^* \cos \alpha_0)', \\ &= -\kappa_0 (H_0^* \cos \alpha_0 + V_0^* \sin \alpha_0) + \rho A g \cos \alpha_0, \end{aligned}$$

as well as

$$V_0^* = (Q_0 + H_0^* \sin \alpha_0) / \cos \alpha_0 .$$

Combining the last two equations yields:

$$Q_0' = -\kappa_0 (H_0^* + Q_0 \sin \alpha_0) / \cos \alpha_0 + \rho A g \cos \alpha_0 .$$

Now we also have to take care of the non-vanishing sectional bending moment:

$$\mathbf{M}_0 = M_0 \mathbf{e}_3 .$$

Applying the angular momentum law on a cable segment like we did with Newton's law in chapter 2 and neglecting rotary inertia terms, we get further equations of motion, namely

$$\rho A \frac{D}{Dt} \left(\mathbf{r}_0(s) \times \frac{D}{Dt} \mathbf{r}_0(s) \right) = \mathbf{r}_0(s) \times \mathbf{f} + (\mathbf{r}_0(s) \times \mathbf{p}_0(s))' + \mathbf{M}_0'(s) , \quad \forall s \in I , \quad (4.9)$$

for the cable configuration. Eq. (4.9) is equal to

$$\rho A v (\mathbf{r}_0 \times \mathbf{v} \mathbf{t}_0)' = \mathbf{r}_0 \times \mathbf{f} + (\mathbf{r}_0 \times \mathbf{p}_0)' + \mathbf{M}_0'$$

and this yields:

$$\begin{aligned} \mathbf{0} &= \mathbf{r}_0 \times \mathbf{f} + (\mathbf{r}_0 \times \mathbf{p}_0^* + \mathbf{M}_0)' \\ &= \mathbf{r}_0 \times \underbrace{(\mathbf{f} + \mathbf{p}_0^{*'})}_{=\mathbf{0}} + \underbrace{\mathbf{t}_0 \times \mathbf{p}_0^*}_{=Q_0 \mathbf{e}_3} + M_0' \mathbf{e}_3 . \end{aligned}$$

Therefore we have:

$$M_0' = -Q_0 . \quad (4.10)$$

Since the cables in our applications to ropeways are steelwire-ropes or of similar material quality, it makes sense to assume that the cable has elastic bending characteristics - that is in dimensional quantities:

$$M_0 = B \kappa_0 , \quad (4.11)$$

where the constant B denotes the bending stiffness. The combination of eqs. (4.10) and (4.11) leads to

$$B \kappa_0' = -Q_0 .$$

We summarize the equations of motions:

$$\forall s \in [s_{A,0}, s_{B,0}] : \begin{cases} x_0' &= \cos \alpha_0 \\ y_0' &= \sin \alpha_0 \\ \alpha_0' &= \kappa_0 \\ \kappa_0' &= -Q_0/B \\ Q_0' &= -\kappa_0 (H_0^* + Q_0 \sin \alpha_0) / \cos \alpha_0 + \rho A g \cos \alpha_0 \end{cases} .$$

After choosing an appropriate reference length l - like for instance the cable length between the rolls if the bending stiffness vanishes - we bring the system into a dimensionless form by substituting

$$\begin{aligned} s &= \hat{s}l, & s_{A,0} &= \hat{s}_{A,0}l, & s_{B,0} &= \hat{s}_{B,0}l, & x_0 &= \hat{x}_0l, \\ y_0 &= \hat{y}_0l, & \kappa_0 &= \hat{\kappa}_0/l, & H_0^* &= \hat{H}_0^* \rho A g l, & Q_0 &= \hat{Q}_0 \sqrt{\rho A g B/l} \end{aligned}$$

and dropping afterwards the " ^ " -symbol. We introduce the dimensionless bending stiffness parameter

$$\beta = \sqrt{\frac{B}{\rho A g l^3}}$$

and get the dimensionless equations of motions:

$$\forall s \in [s_{A,0}, s_{B,0}] : \begin{cases} x'_0 &= \cos \alpha_0 \\ y'_0 &= \sin \alpha_0 \\ \alpha'_0 &= \kappa_0 \\ \beta \kappa'_0 &= -Q_0 \\ \beta Q'_0 &= -\kappa_0(H_0^* + \beta Q_0 \sin \alpha_0) / \cos \alpha_0 + \cos \alpha_0 \end{cases} . \quad (4.12)$$

In the system (4.12) we have on the one hand five first order equations for the five unknown and depending variables x_0 , y_0 , α_0 , κ_0 and Q_0 . On the other hand we have the three parameters $s_{A,0}$, $s_{B,0}$ and H_0^* , which have to be chosen iteratively in such a way that the boundary conditions

$$\begin{aligned} x_0(s_{A,0}) &= x_A, & y_0(s_{A,0}) &= y_A, & \alpha_0(s_{A,0}) &= \phi, & \kappa_0(s_{A,0}) &= -1/r_A, \\ x_0(s_{B,0}) &= x_B, & y_0(s_{B,0}) &= y_B, & \alpha_0(s_{B,0}) &= \psi, & \kappa_0(s_{B,0}) &= -1/r_B \end{aligned} \quad (4.13)$$

on the rolls (s. Fig. 4.2) can be fulfilled. Although the solution of (4.12) & (4.13) has to be found iteratively - in a similar manner as in sec. 4.1 - for every step the boundary conditions are of the same type as (4.13). For instance, in the k -th step, where besides r_A and r_B the quantities $s_{A,0}^{(k)}$, $s_{B,0}^{(k)}$, $x_A^{(k)}$, $x_B^{(k)}$, $y_A^{(k)}$, $y_B^{(k)}$, $\phi^{(k)}$ and $\psi^{(k)}$ are given, we have to solve (4.12) with the boundary conditions

$$\begin{aligned} x_0(s_{A,0}^{(k)}) &= x_A^{(k)}, & y_0(s_{A,0}^{(k)}) &= y_A^{(k)}, & \alpha_0(s_{A,0}^{(k)}) &= \phi^{(k)}, & \kappa_0(s_{A,0}^{(k)}) &= -1/r_A, \\ x_0(s_{B,0}^{(k)}) &= x_B^{(k)}, & y_0(s_{B,0}^{(k)}) &= y_B^{(k)}, & \alpha_0(s_{B,0}^{(k)}) &= \psi^{(k)}, & \kappa_0(s_{B,0}^{(k)}) &= -1/r_B. \end{aligned} \quad (4.14)$$

One should bear in mind that the parameter H_0^* is modified from step to step in such a way that these boundary conditions can be fulfilled best. From eq. (4.14) we also see that $x_0(s)^{(k)}$ is given by integration:

$$x_0(s)^{(k)} = x_A^{(k)} + \int_{s_{A,0}^{(k)}}^s \cos \alpha_0(t) dt,$$

and (4.12) reduces to a fourth-order system in the variables y_0 , α_0 , κ_0 and Q_0 . Moreover, since \mathcal{C}_A is a circleline (s. Fig.4.2), we can express $x_A^{(k)}$ by $y_A^{(k)}$ and r_A as well as $\phi^{(k)}$ by $s_{A,0}^{(k)}$ and r_A . Of course, for the circleline \mathcal{C}_B the situation is similar and therefore only four of the eight equations in (4.14) remain as necessary boundary conditions for the boundary value problem in the k -th iteration step, into which we also introduce the new parameter $l^{(k)} = s_{B,0}^{(k)} - s_{A,0}^{(k)}$ as well as a new independent variable $t = (s - s_{A,0}^{(k)})/l^{(k)}$, so that with the abbreviation $(\cdot)' = d(\cdot)/dt$ we finally have the following problem in the k -th iteration step:

$$\forall s \in [0, 1] : \begin{cases} y_0' &= l^{(k)} \sin \alpha_0, \\ \alpha_0' &= l^{(k)} \kappa_0, \\ \beta \kappa_0' &= -l^{(k)} Q_0, \\ \beta Q_0' &= l^{(k)} (-\kappa_0(H_0^* + \beta Q_0 \sin \alpha_0) / \cos \alpha_0 + \cos \alpha_0), \end{cases} \quad (4.15)$$

$$y_0(0) = y_A^{(k)}, \quad \kappa_0(0) = -1/r_A,$$

$$y_0(1) = y_B^{(k)}, \quad \kappa_0(1) = -1/r_B.$$

The other equations in (4.14), which are not used for the boundary value problem, remain important since they are necessary for the iteration procedure which is performed in the same way as in sec. 4.1.

If we are interested in the case of almost perfect flexible cables, we can consider the slight bending stiffness as a small perturbation of the completely flexible cable. This is the case for $\beta \ll 1$ and hence the problem (4.15) becomes:

4.3.1 A Singularly Perturbed Boundary Value Problem

We try to derive a formal approximation of the solution of (4.15) in the form of a matched asymptotic expansion (s. a. O'Malley [14]). First we have to check whether the problem is a *regular* singularly perturbed boundary value problem (s. a. appendix A). The problem (4.15) has the form

$$\forall t \in [0, 1] : \begin{cases} \beta \mathbf{y}' &= \mathbf{f}(\mathbf{y}, \mathbf{z}, \beta), \\ \mathbf{z}' &= \mathbf{g}(\mathbf{y}, \mathbf{z}), \end{cases}$$

$$\mathbf{0} = \mathbf{b}(\mathbf{y}(0), \mathbf{z}(0), \mathbf{y}(1), \mathbf{z}(1)),$$

with $\mathbf{y} = (\kappa_0, Q_0)$ and $\mathbf{z} = (y_0, \alpha_0)$. For $\beta = 0$, the reduced equation $\mathbf{0} = \mathbf{f}(\bar{\mathbf{y}}, \bar{\mathbf{z}}, 0)$ is:

$$\begin{pmatrix} 0 \\ 0 \end{pmatrix} = \begin{pmatrix} -l^{(k)} \bar{Q}_0 \\ l^{(k)} (-\bar{\kappa}_0 H_0^* / \cos \bar{\alpha}_0 + \cos \bar{\alpha}_0) \end{pmatrix},$$

which can be uniquely solved with respect to $\bar{\mathbf{y}} = \varphi(\bar{\mathbf{z}})$:

$$\begin{pmatrix} \bar{\kappa}_0 \\ \bar{Q}_0 \end{pmatrix} = \begin{pmatrix} \cos^2 \bar{\alpha}_0 / H_0^* \\ 0 \end{pmatrix}. \quad (4.16)$$

The matrix $\mathbf{f}_y(\varphi(\bar{\mathbf{z}}), \bar{\mathbf{z}}, 0)$ that is

$$\begin{pmatrix} 0 & -l^{(k)} \\ -l^{(k)}H_0^*/\cos\bar{\alpha}_0 & 0 \end{pmatrix},$$

has the negative (stable) eigenvalue μ_- with the corresponding eigenvector \mathbf{e}_- ,

$$\mu_- = -l^{(k)}\sqrt{H_0^*/\cos\bar{\alpha}_0}, \quad \mathbf{e}_- = \begin{pmatrix} 1 \\ \sqrt{H_0^*/\cos\bar{\alpha}_0} \end{pmatrix},$$

as well as the positive (unstable) eigenvalue μ_+ with the corresponding eigenvector \mathbf{e}_+ ,

$$\mu_+ = l^{(k)}\sqrt{H_0^*/\cos\bar{\alpha}_0}, \quad \mathbf{e}_+ = \begin{pmatrix} 1 \\ -\sqrt{H_0^*/\cos\bar{\alpha}_0} \end{pmatrix}.$$

If the unperturbed configuration is curved, then $\cos\bar{\alpha}_0 > 0$. Furthermore, if the configuration is the convex one - that is the case in our ropeway applications (s. sec. 3.1.1 of chapter 3) - then $H_0^* > 0$ and the eigenvalues are real. Consequently the eigenvectors \mathbf{e}_- and \mathbf{e}_+ have a transversal component to the hyperplanes of the phase-space where κ is constant. Hence the boundary conditions $\kappa_0(0) = -1/r_A$ and $\kappa_0(1) = -1/r_B$ can be fulfilled for sure. Therefore we have a

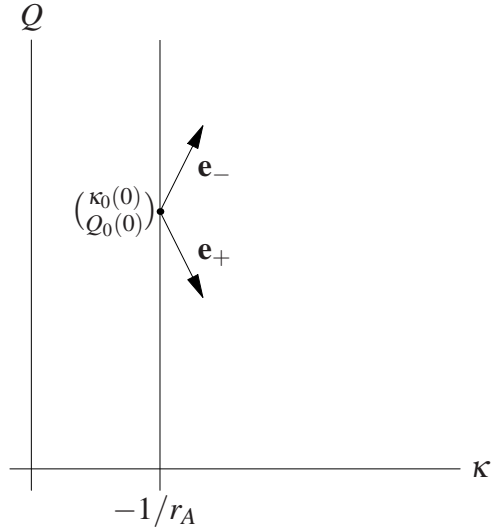


Figure 4.3: The eigenvector \mathbf{e}_- (\mathbf{e}_+) of the linearized problem at $t=0$ ($t=1$) has a component transversal to the hyperplane $\kappa = -1/r_A$ ($\kappa = -1/r_B$). Thus the problem (4.15) is well posed.

regular singularly perturbed problem, and based on the theory that was developed by Vasileva & Butuzov [39], Esipova [6] as well as Schmeiser [27], a formal asymptotic approximation for the solution of (4.15) can be constructed using the following ansatz for the solution:

$$\begin{aligned} \mathbf{y}(t, \beta) &= \varphi(\bar{\mathbf{z}}(t)) + \mathbf{L}\mathbf{y}(\tau) + \mathbf{R}\mathbf{y}(\sigma) + O(\beta), \\ \mathbf{z}(t, \beta) &= \bar{\mathbf{z}}(t) + O(\beta), \end{aligned}$$

that is

$$\begin{pmatrix} \kappa_0(t, \beta) \\ Q_0(t, \beta) \end{pmatrix} = \begin{pmatrix} \cos^2 \bar{\alpha}_0 / H_0^* \\ 0 \end{pmatrix} + \begin{pmatrix} L\kappa_0(\tau) \\ LQ_0(\tau) \end{pmatrix} + \begin{pmatrix} R\kappa_0(\sigma) \\ RQ_0(\sigma) \end{pmatrix} + O(\beta),$$

$$\begin{pmatrix} y_0(t, \beta) \\ \alpha_0(t, \beta) \end{pmatrix} = \begin{pmatrix} \bar{y}_0(t) \\ \bar{\alpha}_0(t) \end{pmatrix} + O(\beta),$$

In the last formulas, the *boundary layer variables* $\tau = t/\beta$ and $\sigma = (1-t)/\beta$ for the left ($t = 0$) and the right ($t = 1$) boundary were introduced. The left and the right layer terms, \mathbf{Ly} and \mathbf{Ry} , have to fulfill $\mathbf{Ly}(\infty) = \mathbf{Ry}(\infty) = \mathbf{0}$:

$$L\kappa_0(\infty) = R\kappa_0(\infty) = 0, \quad (4.17)$$

$$LQ_0(\infty) = RQ_0(\infty) = 0. \quad (4.18)$$

From the first of the two equations in (4.15) and from (4.16) we get $\bar{\mathbf{z}}' = \mathbf{g}(\varphi(\bar{\mathbf{z}}(t)), \bar{\mathbf{z}})$:

$$\begin{pmatrix} \bar{y}_0' \\ \bar{\alpha}_0' \end{pmatrix} = l^{(k)} \begin{pmatrix} \sin \bar{\alpha}_0 \\ \cos^2 \bar{\alpha}_0 / H_0^* \end{pmatrix}. \quad (4.19)$$

The equation for the left layer term, $\frac{d}{d\tau} \mathbf{Ly}(\tau) = \mathbf{f}(\varphi(\bar{\mathbf{z}}(0)) + \mathbf{Ly}(\tau), \bar{\mathbf{z}}(0), 0)$, is:

$$\frac{d}{d\tau} \begin{pmatrix} L\kappa_0(\tau) \\ LQ_0(\tau) \end{pmatrix} = l^{(k)} \begin{pmatrix} -LQ_0(\tau) \\ -L\kappa_0(\tau) H_0^* / \cos \bar{\alpha}_0(0) \end{pmatrix}, \quad (4.20)$$

and the equation $\frac{d}{d\sigma} \mathbf{Ry}(\sigma) = \mathbf{f}(\varphi(\bar{\mathbf{z}}(1)) + \mathbf{Ry}(\sigma), \bar{\mathbf{z}}(1), 0)$ for the right layer term is:

$$\frac{d}{d\sigma} \begin{pmatrix} R\kappa_0(\sigma) \\ RQ_0(\sigma) \end{pmatrix} = l^{(k)} \begin{pmatrix} RQ_0(\sigma) \\ R\kappa_0(\sigma) H_0^* / \cos \bar{\alpha}_0(1) \end{pmatrix}. \quad (4.21)$$

Finally, the boundary condition $\mathbf{b}(\varphi(\bar{\mathbf{z}}(0)) + \mathbf{Ly}(0), \bar{\mathbf{z}}(0), \varphi(\bar{\mathbf{z}}(1)) + \mathbf{Ry}(0), \bar{\mathbf{z}}(1)) = \mathbf{0}$ yields:

$$\cos^2 \bar{\alpha}_0(0) / H_0^* + L\kappa_0(0) + 1/r_A = 0, \quad (4.22)$$

$$\bar{y}_0(0) - y_A^{(k)} = 0, \quad (4.23)$$

$$\cos^2 \bar{\alpha}_0(1) / H_0^* + R\kappa_0(0) + 1/r_B = 0, \quad (4.24)$$

$$\bar{y}_0(1) - y_B^{(k)} = 0. \quad (4.25)$$

The eqs. (4.19), (4.23) and (4.25) together lead to the same result as the equations of the catenary problem that we discussed in sec. 4.1. As we said above one should not forget that the parameter H_0^* varies from step to step in such a way that in every step we have a different unperturbed or steady-state solution as well as a different boundary layer term. Since the second-order system (4.20) is linear and with constant coefficients, we can integrate it fulfilling the boundary conditions (4.17) and (4.22). Thus we have:

$$\begin{pmatrix} L\kappa_0(\tau) \\ LQ_0(\tau) \end{pmatrix} = -\frac{1/r_A + \cos^2 \bar{\alpha}_0(0) / H_0^*}{\exp(l^{(k)} \sqrt{H_0^* / \cos \bar{\alpha}_0(0)} \tau)} \begin{pmatrix} 1 \\ \sqrt{H_0^* / \cos \bar{\alpha}_0(0)} \end{pmatrix}.$$

In the same way we get from the eqs. (4.21), (4.17) and (4.24):

$$\begin{pmatrix} R\kappa_0(\sigma) \\ RQ_0(\sigma) \end{pmatrix} = -\frac{1/r_B + \cos^2 \bar{\alpha}_0(1) / H_0^*}{\exp(l^{(k)} \sqrt{H_0^* / \cos \bar{\alpha}_0(1)} \sigma)} \begin{pmatrix} 1 \\ -\sqrt{H_0^* / \cos \bar{\alpha}_0(1)} \end{pmatrix}.$$

4.3.2 Example

We now apply the formulas of sec. 4.3.1 to an example. Let l , the reference length, be the length of the (unique) convex configuration connecting the highest points of the two rolls \mathcal{C}_A and \mathcal{C}_B , which shall have the same radius, $r = r_A = r_B$, and which are at the same elevation (y-value) (s. Fig. 4.4). Therefore the steady-state solution is a symmetric one and has a reflectional

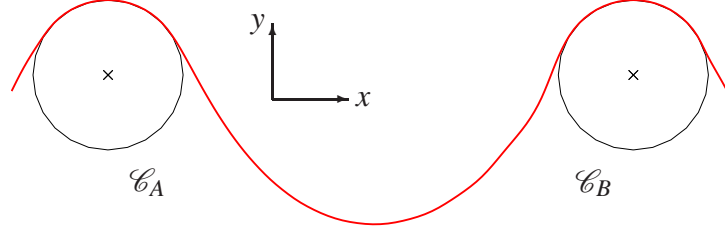


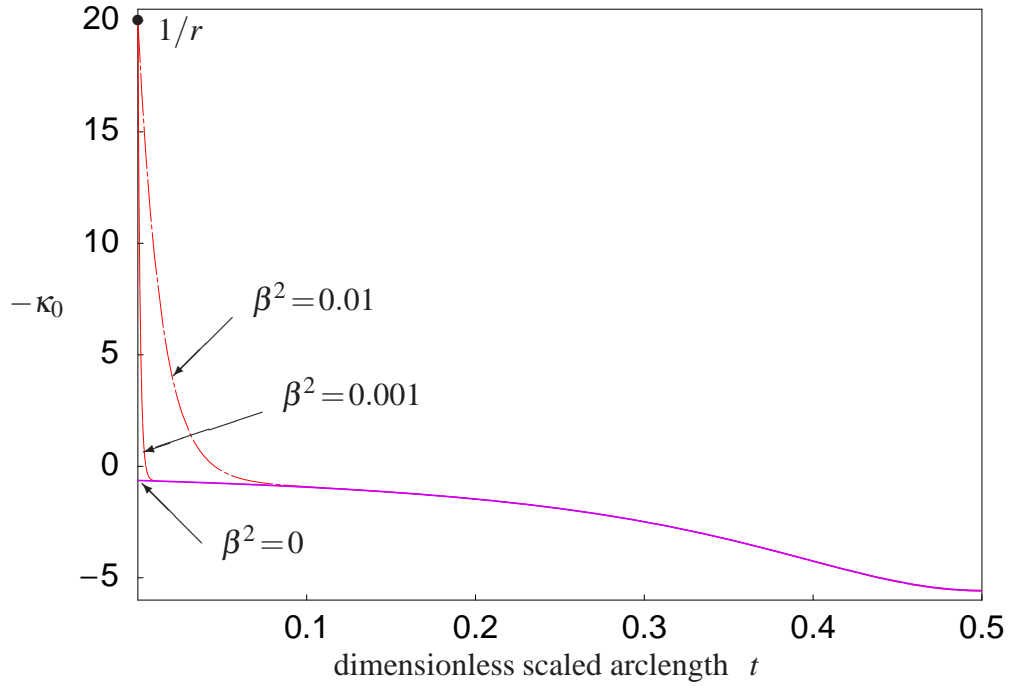
Figure 4.4: Example 4.3.2: A slightly bending-stiff cable moves axially between two rolls which have the same radius and are at the same elevation.

symmetry with respect to the vertical axis that goes through the lowest point of the cable. In the k -th step we get the matched approximation:

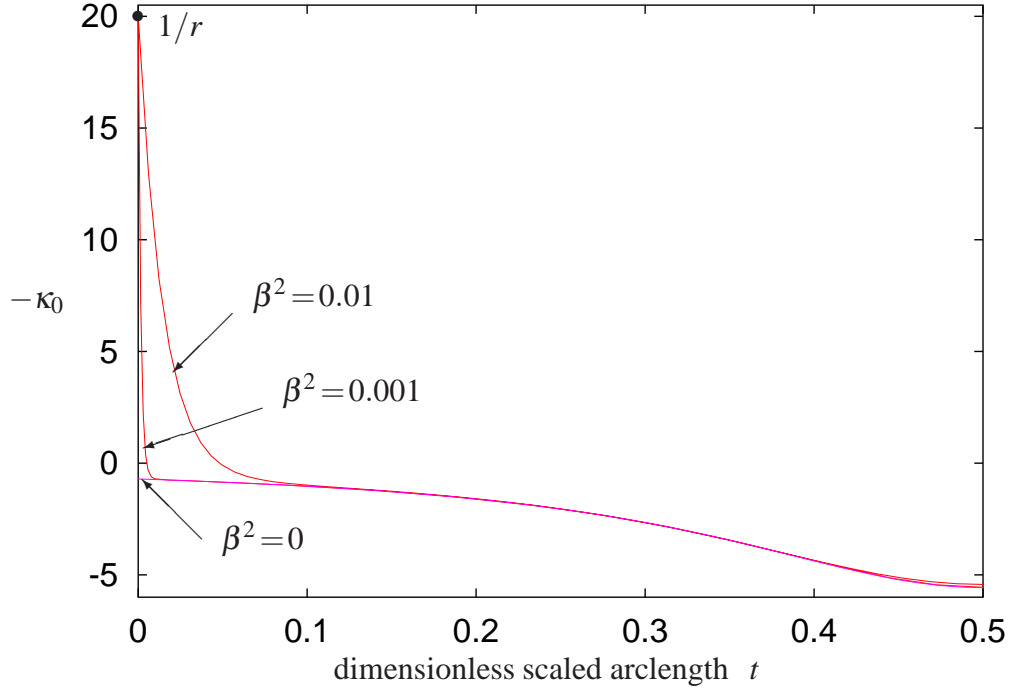
$$\begin{aligned}
 x_0 &= x_A^{(k)} + H_0^* \left(\operatorname{arsinh} \left[\frac{l^{(k)}}{2H_0^*} \right] + \operatorname{arsinh} \left[\frac{l^{(k)}}{H_0^*} \left(t - \frac{1}{2} \right) \right] \right) + O(\beta) \\
 y_0 &= y_A^{(k)} + H_0^* \left(\sqrt{1 + \left[\frac{l^{(k)}}{2H_0^*} \right]^2} - \sqrt{1 + \left[\frac{l^{(k)}}{H_0^*} \left(t - \frac{1}{2} \right) \right]^2} \right) + O(\beta) \\
 \alpha_0 &= \arctan \left[\frac{l^{(k)}}{H_0^*} \left(t - \frac{1}{2} \right) \right] + O(\beta) \\
 \kappa_0 &= \frac{H_0^*}{H_0^{*2} + \left[l^{(k)} \left(t - \frac{1}{2} \right) \right]^2} - \frac{\frac{2}{r} + \frac{2H_0^*}{H_0^{*2} + (l^{(k)}/2)^2}}{e^{\frac{l^{(k)}}{2\beta} \sqrt{H_0^{*2} + (l^{(k)}/2)^2}}} \cosh \left[\frac{l^{(k)} \left(t - \frac{1}{2} \right)}{\beta} \sqrt{H_0^{*2} + (l^{(k)}/2)^2} \right] + O(\beta) \\
 Q_0 &= \sqrt[4]{H_0^{*2} + (l^{(k)}/2)^2} \frac{\frac{2}{r} + \frac{2H_0^*}{H_0^{*2} + (l^{(k)}/2)^2}}{e^{\frac{l^{(k)}}{2\beta} \sqrt{H_0^{*2} + (l^{(k)}/2)^2}}} \sinh \left[\frac{l^{(k)} \left(t - \frac{1}{2} \right)}{\beta} \sqrt{H_0^{*2} + (l^{(k)}/2)^2} \right] + O(\beta)
 \end{aligned} \tag{4.26}$$

In Fig. 4.5(a) the two leading terms for κ_0 given in (4.26) are plotted for three different values of the bending stiffness β . The solution depicted is the result of the iterative process. The accuracy of the analytically found asymptotic solution presented in Fig. 4.5(a) has been checked by a numerically calculated solution of the iterative non-linear boundary value problem (4.15) with COLSYS [2]. This solution is shown in Fig. 4.5(b). Obviously for small β very good agreement is achieved. The only perspicuous difference is visible for $t = 0.5$. The reason for this is that in contrast to the numerical solution, the matched asymptotic expansion disregards the inextensibility of the cable.

Per definition, the integration of the curvature κ_0 respective to the arclength s yields the inclination angle α_0 of the steady-state configuration. Therefore we get a new, by the boundary layers corrected angle through integration. But the resulting new configuration will a priori not match the boundary conditions. Hence the fictitious horizontal force - the parameter H_0^* - has to be modified until the remaining boundary conditions can be fulfilled with sufficient accuracy. Thus the iteration procedure for the not completely flexible but completely inextensible cable with constant cable length l between the two rolls also implies a variation of the parameter H_0^* that depends on the line speed. The configurations resulting from such a force adaptive iteration procedure, applied to our example, are plotted for the dimensionless bending stiffnesses $\beta^2 = 0.001$ in Fig. 4.6(a) and $\beta^2 = 0.01$ in Fig. 4.6(b). In both pictures the corresponding completely flexible configuration is plotted with a dashed line. It is interesting to observe in these figures how the point on the roll where the cable loses contact is varying when the bending stiffness is increasing. Therefore, in Fig. 4.7(a) we zoom in the left roll and observe this point for different β^2 -values, but now as the numerical result of the iterative boundary value problem (4.15) with COLSYS. Finally, the same numerical integration for different β^2 yields the steady-state angle α_0 that is plotted in Fig. 4.7(b).



(a) Leading two terms in the matched asymptotic curvature expansion in (4.26).



(b) Curvature resulting from the numerical solution of the iterative boundary value problem (4.15) with COLSYS [2].

Figure 4.5: Steady-state curvature κ_0 of the symmetric ex. 4.3.2 with the roll-radius $r = l/20$ and the bending stiffnesses β . The different solution methods yield very well coinciding results.

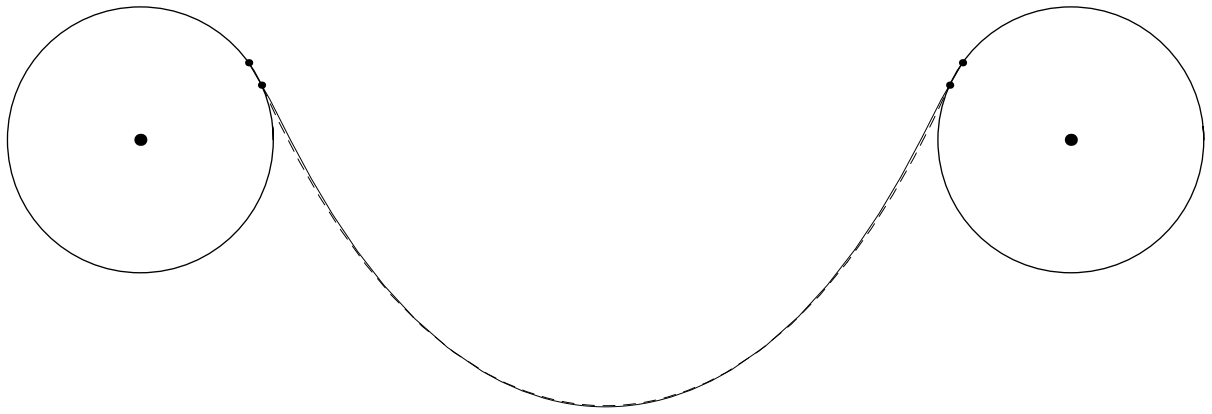
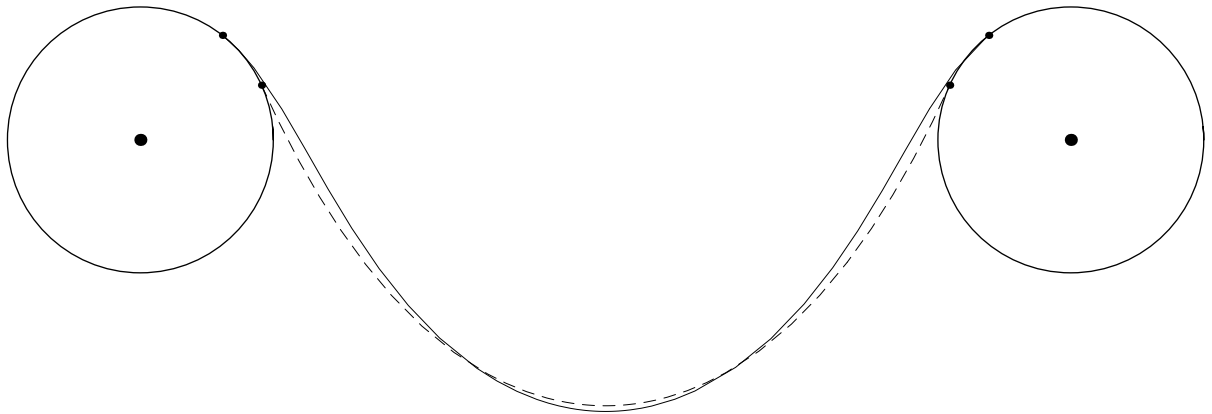
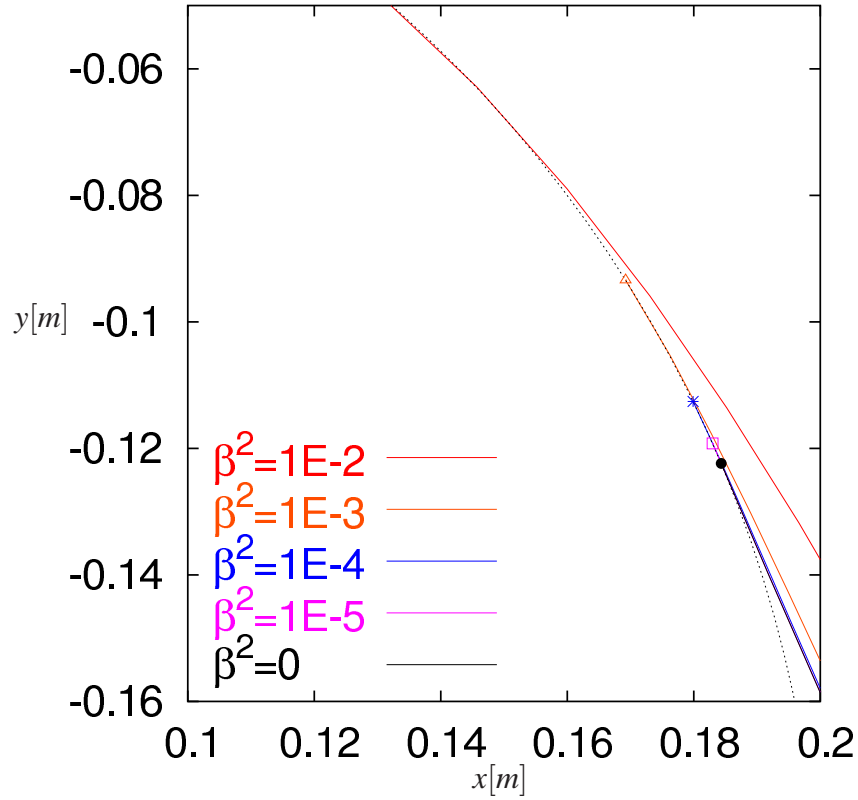
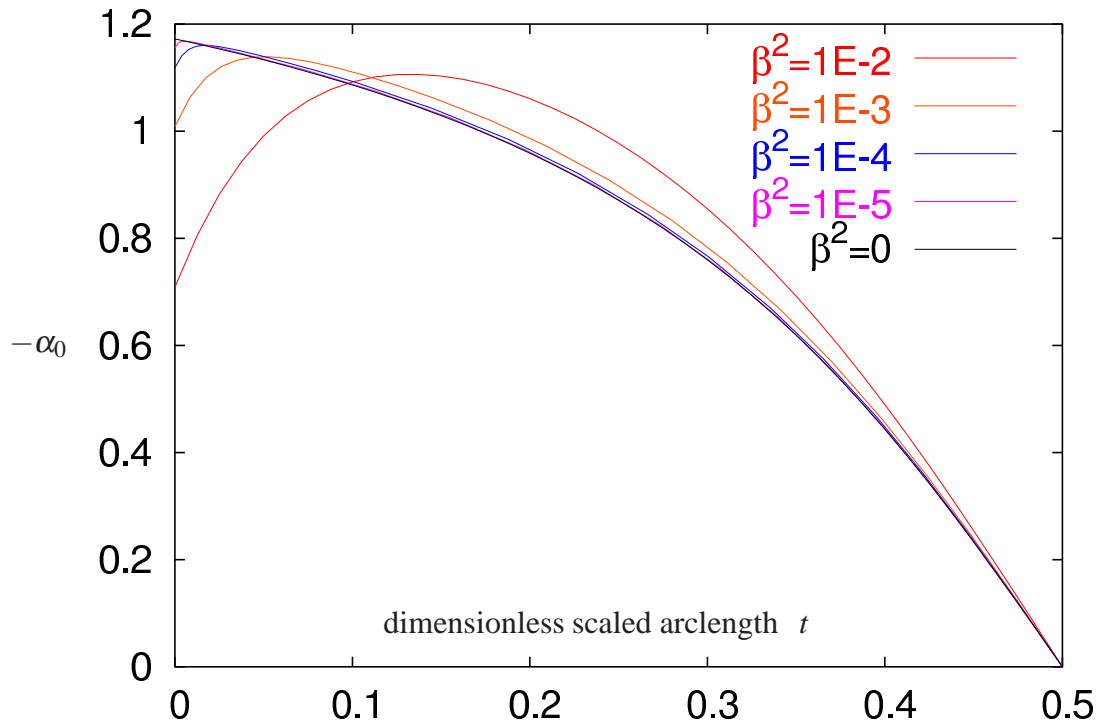
(a) $\beta^2 = 0.001$ (solid line) and $\beta^2 = 0$ (dashed line)(b) $\beta^2 = 0.01$ (solid line) and $\beta^2 = 0$ (dashed line)

Figure 4.6: Example 4.3.2: The figure shows how the steady-state shape of the configuration varies when the curvature in (4.26) is integrated and consequently a matching iteration procedure is performed. The configurations with ($\beta^2 > 0$, solid line) and without ($\beta^2 = 0$, dashed line) bending stiffness are depicted. It also becomes clear how the bending stiffness forces the variation of the point on the roll where it loses contact.



(a) The steady-state configuration on the left roll for different bending stiffness values - the point where the cable loses contact is tagged.



(b) The inclination angle of the steady-state configuration.

Figure 4.7: Results of the iterative boundary value problem (4.15) using COLSYS [2].

Chapter 5

Numerical Simulation of the Steady-State Solution between Two Rolls

In this chapter we describe one of the Finite Element simulations that we performed in order to check the steady-state results from chapter 4. For this purpose we used *ABAQUS/Standard* Vers. 6.4.1 which incorporates an implicit time-integrator for the direct method in dynamical applications. In particular we are interested in surveying the influence of a slight bending stiffness in the two-dimensional problem.

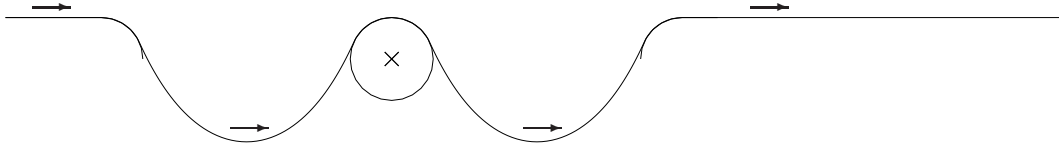
The axial motion implies a large displacement of the cable structure that may have an arbitrary sag between the rolls. Therefore the problem is in a geometrical sense highly non-linear. Since the inextensible cable with a slight bending stiffness is modelled by two-dimensional beam elements that have a very high axial stiffness and a very low bending stiffness, the stiffness matrix is numerically ill-conditioned. The supports of the cable as well as the rolls are modelled as two-dimensional 'rigid bodies', which are bordered by rigid and analytically defined line segments in the plane. The contact between the cable and the rigid bodies is frictionless and the impacts of the cable elements on the 'surface' of the rigid bodies are completely inelastic. Moreover, the special geometry of the supports and the rolls increase the complexity of this non-linear contact problem. A sufficient period of time has to pass by until the cable motion tunes in a more or less axial steady-state motion. Consequently a large number of elements is necessary, if the cable does not have a cyclic structure.

All the facts mentioned above affect in a crucial manner the complexity of the numerical problem, resulting in a long simulation time even for the planar problem. Furthermore we noticed that if the cable is not a closed or cyclic structure the use of more than one CPU in a parallel mode does not appreciably improve the computing time. To optimize the choice of elements as well as the settings of the time integrator, a large number of numerical tests is required.

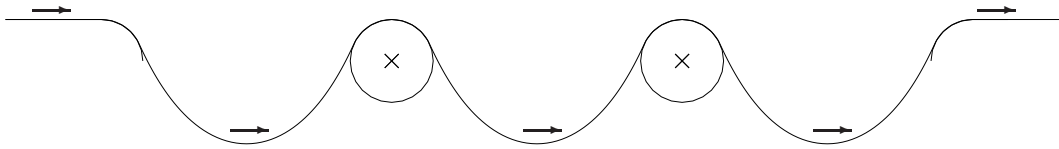
In Fig. 5.1 we see different models that were tested to simulate the steady-state case. There are basically two types of models depending on the cable structure: either a closed one (e.g. Fig. 5.1(e)) or an open one. The advantage of closed structures is that they get by with few elements, the disadvantage is that due to the initial curvature of the elements the relaxed configuration is not a straight one and thus the steady-state configuration is periodically disturbed. Another problem with the cyclic structures is that due to the inelastic impacts between the cable elements and the rigid bodies, a drive mechanism is necessary. The simplest open model is depicted in



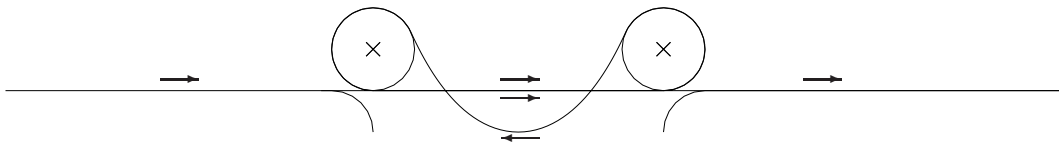
(a) A cable hanging between two 'tables' is drawn on the one end and pushed on the other end.



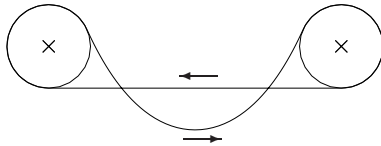
(b) Similar model to 5.1(a), but now there is a roll between the two tables.



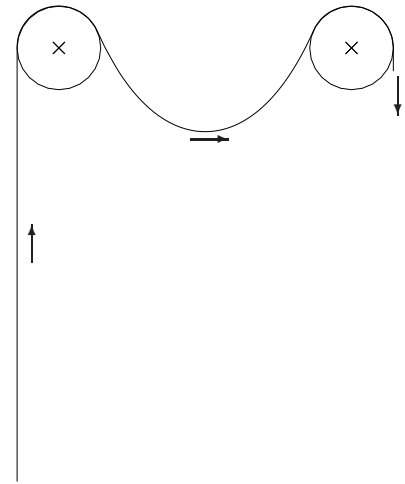
(c) Like 5.1(b), but with two rolls.



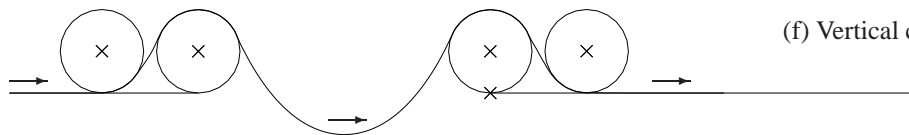
(d) A crossed cable.



(e) A crossed and closed cable.



(f) Vertical cable feed-in.



(g) Model with a curvature prescribing inlet and outlet.

Figure 5.1: Different two-dimensional FE-models used to simulate a steady-state cable motion over rolls. The cable is modelled as a combination of hybrid truss- and beam- Elements. The latter have a slight bending stiffness. The rolls and tables are modelled as analytical rigid bodies. The contact between this bodies and the cable is frictionless. The cable has no self-contact.

Fig. 5.1(a). The cable has on the one hand an initial position at which it is hanging between two rigid flat 'tables' and on the other hand a constant and purely axial initial velocity. As the arrows shall indicate, the cable moves from left to right. Therefore the major part of it lies initially on the left table and at the end of the simulation the whole cable is located on the right table. In order to keep the axial velocity of the elements approximately constant during the whole simulation, the velocity is permanently prescribed on both endpoints of the cable. The edges of the tables are formed roundly to make the borders of the hanging cable similar to rolls. Nevertheless the cable behaves there in a different way than on rolls, since the bending stiff cable loses already contact before it passes the edge and thus the curvature cannot be freely prescribed. For this reason the border has to match more the shape of a roll. The model in Fig. 5.1(b) has such a roll in the middle and therefore two spans that are the model domains where the cable is hanging without having contact. The disadvantage here is that each of the spans is asymmetric due to the two different boundary conditions. This problem is improved in the model that is depicted in Fig. 5.1(c). The span in the middle is now symmetric, but the stability of the equilibrium of the system consisting of three coupled cable spans must be checked. Besides, the simulation time increases drastically. The models shown in Figs. 5.1(d)-5.1(g) have only a single span which is bordered by two rolls. The model in Fig. 5.1(d) is based on the assumption that no self-contact is defined for the cable. Hence the cable can be crossed without a problem. The disadvantage here is that the sag must be large enough. Also in the models of the Figs. 5.1(e) and 5.1(f) the sag cannot be chosen arbitrarily. The model displayed in Fig. 5.1(g) seems to be most convenient for our purpose. There are two rolls fixed at the border of each of the tables. During the simulation the straight part of the cable that is initially lying on the left table (plotted in red in Fig. 5.2) has to pass a small hole under the first roll (from the left) and then another small hole between the first and the second roll. Thus the cable is forced to have contact with the second roll before it gets into the span. Similar is the situation on the right table where the cable after having contact with the roll and passing two small holes is finally horizontally drawn away along the table. The pairs of rolls on each of the tables can be regarded as eyelets that additionally prescribe the curvature of the rolls. Fig. 5.2 shows the model at the beginning of the simulation. The cable structure consists of two parts: the first part (blue) to which 160 hybrid truss elements T2D2H are assigned, models a completely flexible and nearly inextensible cable and has a length of approximately $3.25m$. The sequent part (red) to which 492 hybrid beam elements B21H are assigned, models a nearly inextensible cable with a slight bending stiffness ($EJ = 0.0025Nm^2$) and has a length of approximately $10m$. Both element types have the same mass density ($4400kg/m^3$) and belong to the linear and hybrid formulated two-node-elements. Since the cable has a relatively high axial stiffness ($EA = 1040kN$), it is reasonable to use elements in a hybrid formulation. At the beginning of the simulation to every node a tangential velocity of $10m/s$ is assigned, so that the cable moves from the left to the right. In the same manner if it is possible ¹ an initial cable tension corresponding to the steady-state case is assigned to every element of the cable. During the entire simulation time ($T = 1s$) the horizontal velocity of $10m/s$ at both endpoints is prescribed. In the last third of this time period the configuration within the span fluctuates slightly around a 'steady-state' curve (s. Fig. 5.3).

¹In version 6.4.1 of *ABAQUS/Standard* unexpected severe problems arise when an initial stress to beam elements is assigned. The support service of this commercial software promised this shortcoming would disappear in one of the following versions.

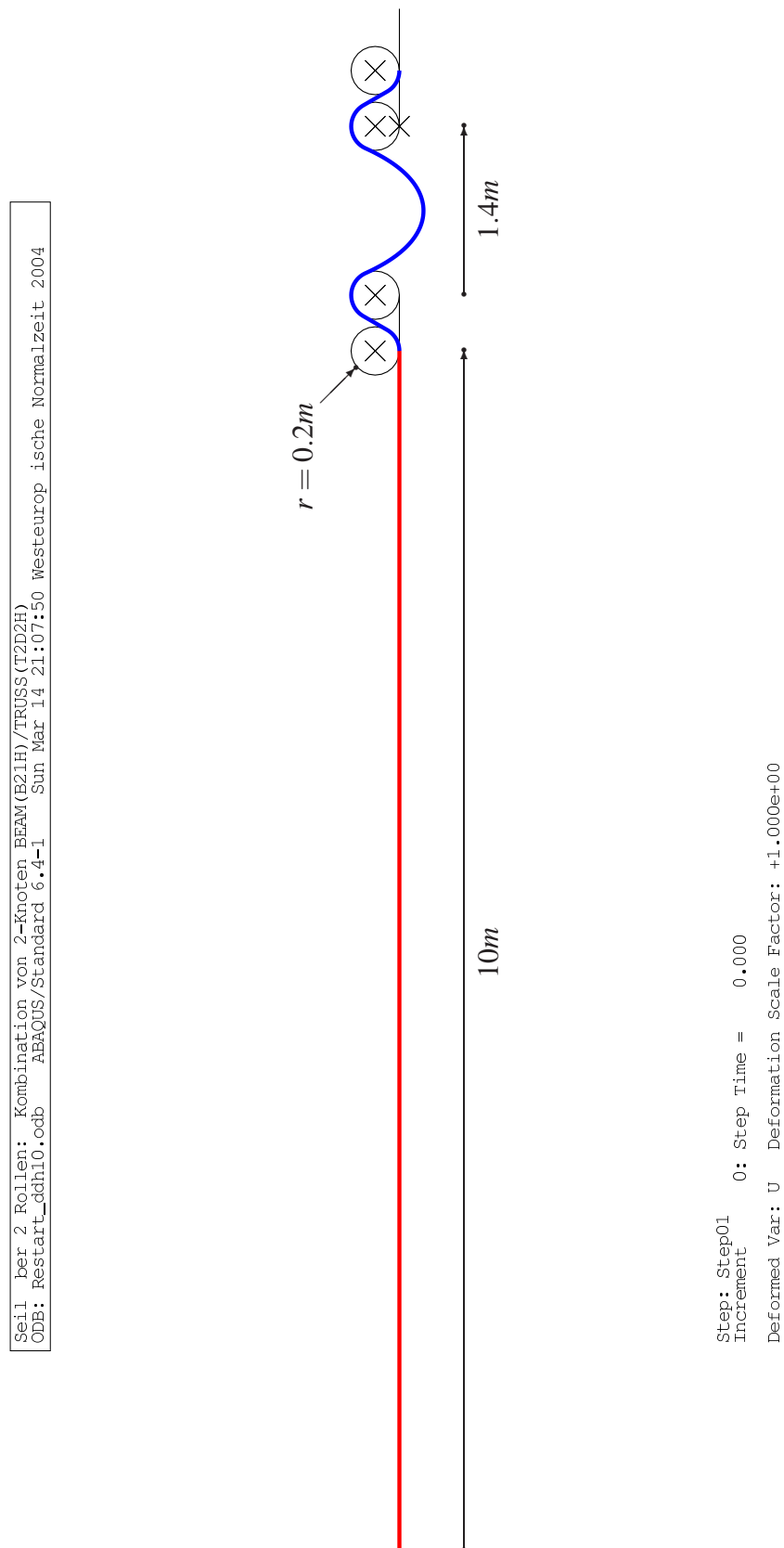


Figure 5.2: Initial configuration of the FE-Simulation with the model of Fig. 5.1(g). The red part of the cable is built up of two-dimensional hybrid beam elements B21H.

The transient dynamical configuration is kind of asymmetric and can be compared with the corresponding symmetric result of the matched asymptotic expansion in chapter 4 (s. Fig. 5.4). Besides, we can also check the simulation configuration against the results of the solution of the iterative non-linear boundary value problem (4.15) with COLSYS [2] for different bending stiffness values. (s. Fig. 5.5). We are not able to give a clear answer to the question of why the configuration of the Finite Element Simulation is asymmetric. One reason may be that this happens because of discretization errors, another could be the inelastic interaction between the cable and the rigid surface. It should be underlined that neither a material damping was included in the model nor was any numerical damping in the implicit time integration method (Hilber-Hughes-Taylor) added.

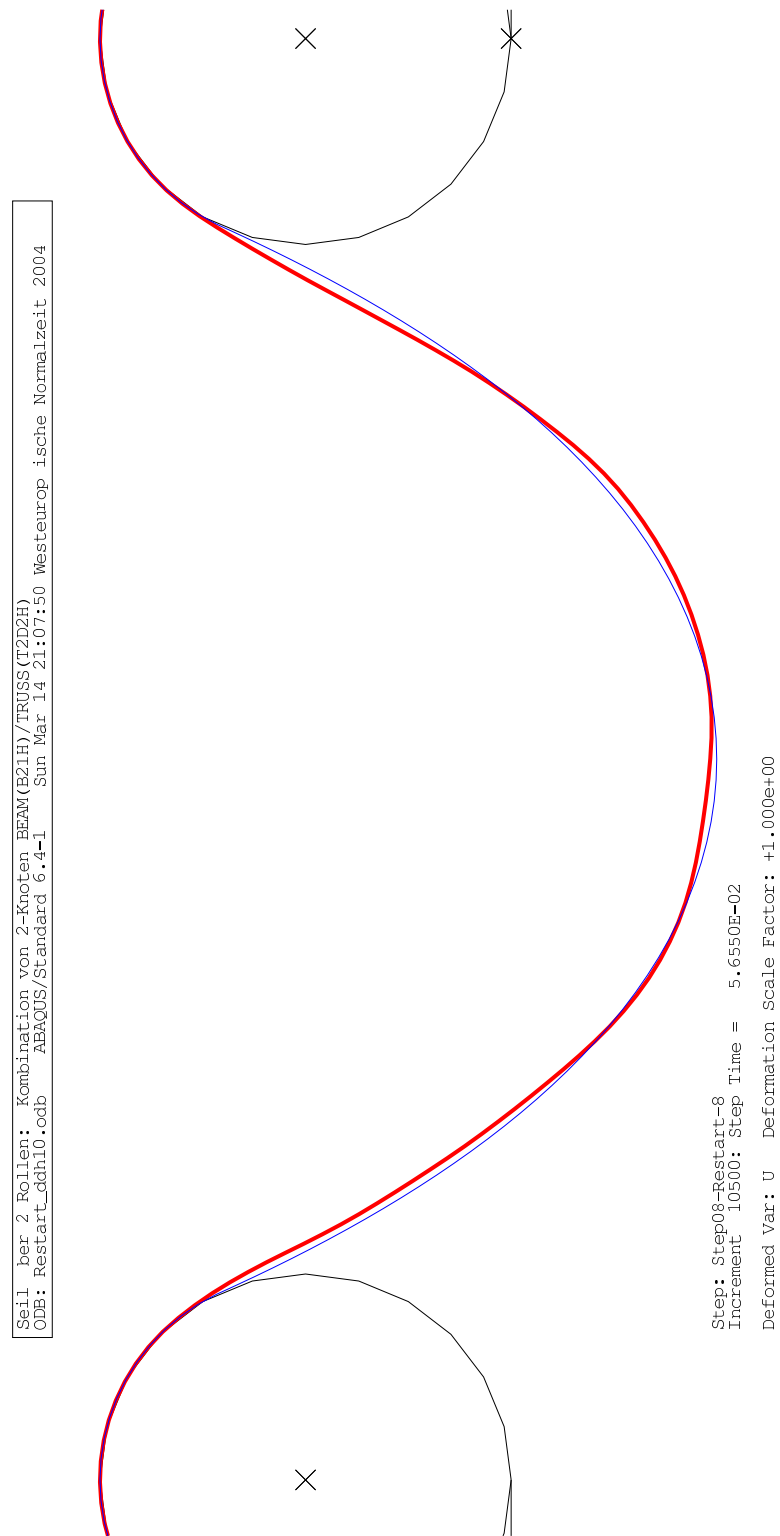


Figure 5.3: The cable in the span: the configuration after 0.86s of the simulation time is depicted in red, the completely flexible initial configuration in blue.

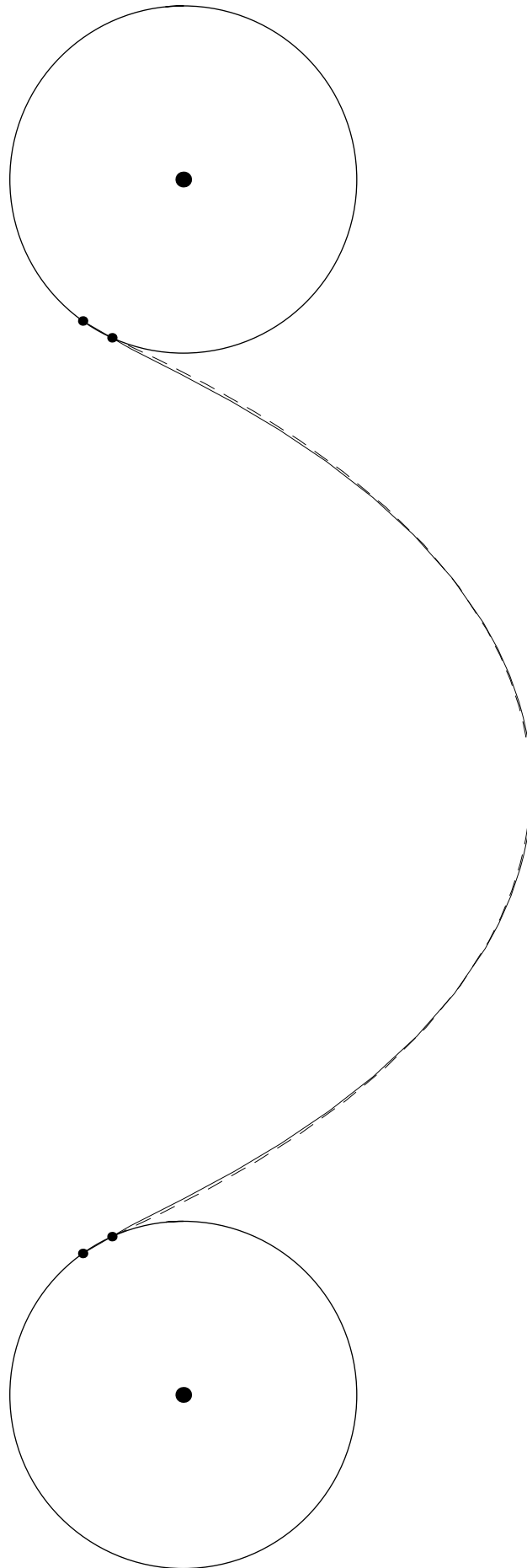


Figure 5.4: The configuration with bending stiffness approximated by a matched asymptotic expansion.

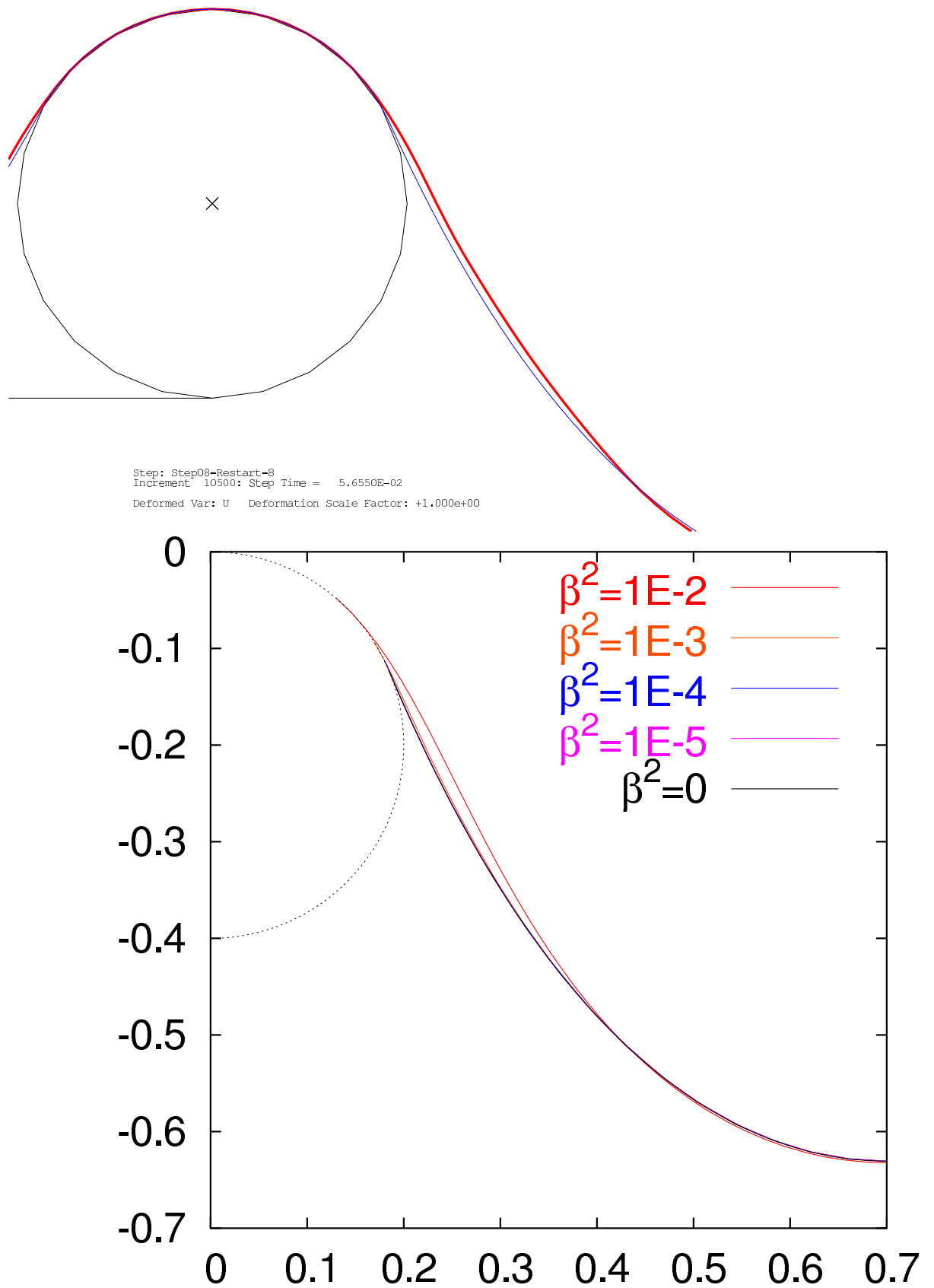


Figure 5.5: Comparison between the FE-simulation configuration after 0.86s and the numerical steady-state solution with COLSYS [2] for different bending stiffness values β .

Chapter 6

Coupled Cable Spans

Up to now we were only looking at the motion of a cable between two eyelets or two rolls. As we mentioned in the introduction, the cable of a monocable circulating ropeway is a closed loop and moves either through the air or over rolls. The sections, where the cable moves through the air over a more or less wide distance, are called the cable spans. Since it is a single cable that passes through different spans, the dynamics of the cable-configurations in all cable spans of the ropeway are coupled.

As we stated in eq. (3.14) of chapter 3, the steady-state cable tension in a constant gravitational field is a linear function of height. We can generalize this statement to be valid for the entire cable loop of the whole ropeway by assuming that there is no friction and no damping mechanism between the spans. Hence in every point of the cable loop the section force is determined if we know the prescribed cable tension in the haulage device. This device is normally located in one of the ropeway terminals where loading and unloading takes place. Let us number the spans all the way through, denoting the adjacent span to the haulage device with the outgoing rope as the first one. Thus the prescribed cable tension in the haulage device regulates the sag of the steady-state cable configuration in the first and in the last span. Then the cable tension is transmitted over a tower from the first span to the second span where it determines the sag of the second span. Over the next tower the cable tension is directed to the third span etc. Since the knowledge about this 'force-interaction' between two neighbouring cable spans is also important for the calculation of the initial configuration in a numerical simulation, we now take a look at:

6.1 How the Cable Tension at the Border of a Span Influences the Sag

Let there be a convex steady-state configuration of an axially moving cable connecting two eyelets with a given cable tension at the inlet. We use the parametrization of the catenary where the y -value is given as a function of the x -value, that is the function Y_0 with $Y_0(x_0(s)) = y_0(s)$. Then we choose the horizontal distance x_B between the inlet and the outlet as reference length l in order to apply the transformation (3.1) of chapter 3. Hence the eqs. (3.10), (3.11) and (3.14) yield the following dimensionless problem: The constants c_x , c_y and a have to be chosen in such

a way that the function $Y_0(x_0) = c_y + a \cosh[(x_0 - c_x)/a]$ fulfills the boundary conditions

$$Y_0(0) = 0, \quad (6.1)$$

$$Y_0(1) = y_B, \quad (6.2)$$

$$(\|\mathbf{p}_0\| - c^2) \Big|_{x=0} = Y_0(0) - c_y = p_A, \quad (6.3)$$

with the given parameters y_B , c and p_A . Plugging (6.1) into (6.3) we get $c_y = -p_A$. Therefore, by substituting

$$Y_0(x_0) = a \cosh\left(\frac{x_0 - c_x}{a}\right) - p_A \quad (6.4)$$

into (6.1) and (6.2) as well as defining the function

$$f(a, c) = a \cosh\left(\frac{c}{a}\right), \quad (6.5)$$

we get the two equations

$$\begin{aligned} f(a, c_x) &= p_A, \\ f(a, c_x - 1) &= p_A + y_B. \end{aligned} \quad (6.6)$$

Hence the pairs (a, c_x) that fit in (6.4) lie in the intersection of the two one-dimensional manifolds

$$\begin{aligned} \mathcal{M}_0 &= \{(a, c_x) \mid f(a, c_x) = p_A\}, \\ \mathcal{M}_1 &= \{(a, c_x) \mid f(a, c_x - 1) = p_A + y_B\}. \end{aligned} \quad (6.7)$$

The function $f(a, c)$ is discussed in detail in appendix B. Due to the convexity of each of the domains enclosed by \mathcal{M}_0 and \mathcal{M}_1 , the set $\mathcal{M}_0 \cap \mathcal{M}_1$ can only consist of no (s. Fig. 6.1(a)), one (s. Fig. 6.1(b)) or two (s. Fig. 6.1(c)) intersection points in the open half-plane $a > 0$. In Fig. 6.1 we also see how the number of intersection points depends on p_A . For $0 \leq p_A < p_{crit}$ there are no intersection points (s. Fig. 6.1(d)). Then for $p_A = p_{crit}$ the two cone-sections \mathcal{M}_0 and \mathcal{M}_1 touch each other in the only intersection point (s. Fig. 6.1(d)). And finally for $p_A > p_{crit}$ there are always two intersection points (s. Fig. 6.1(d)).

Thus for fixed eyelet-elevation y_B , the cable tension p_A at the left eyelet is a function of the catenary parameter a (s.a. Fig. 6.2):

$$p_A = p(a).$$

Due to the convex and conical properties of $f(a, c)$ (s. app. B) the function $p(a)$ has for any y_B the following characteristics: Firstly, there are two asymptotes, one for $a \searrow 0^+$ and one for $a \rightarrow \infty$. Secondly, there is a positive parameter a_{crit} in such a way that

$$\begin{aligned} \frac{dp}{da} &< 0, & 0 < a < a_{crit}, \\ \frac{dp}{da} &= 0, & a = a_{crit}, \\ \frac{dp}{da} &> 0, & a_{crit} < a. \end{aligned}$$

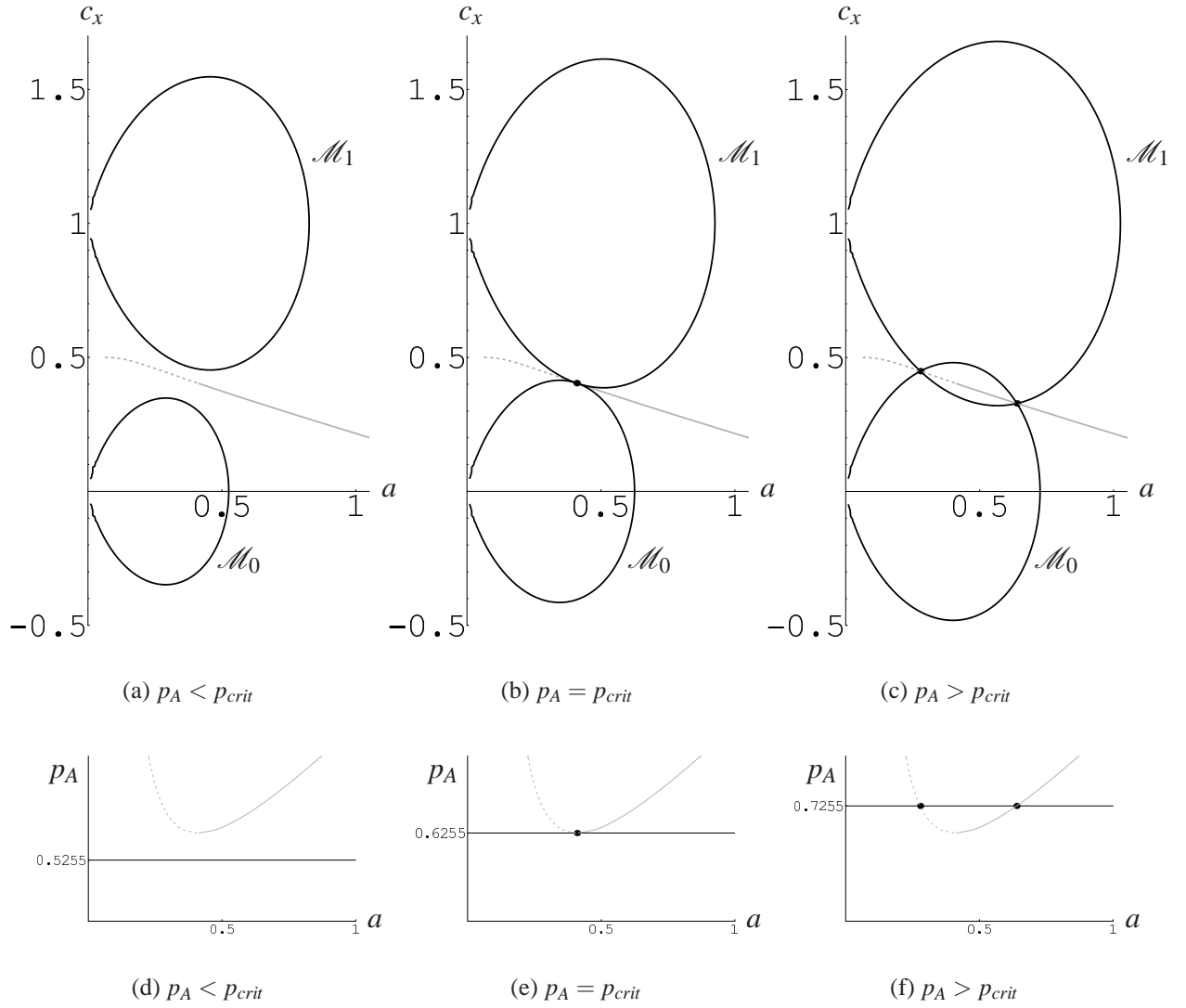


Figure 6.1: The two eqs. in (6.6) define implicitly the two curves \mathcal{M}_0 and \mathcal{M}_1 (s. Figs. 6.1(a)-6.1(c)) in the a, c_x -plane. Here the curves are depicted for $y_B = 0.3$ and intersect only if p_A , the prescribed cable tension at the left eyelet is equal to (s. Fig. 6.1(b)) or greater than (s. Fig. 6.1(c)) a critical value $p_{crit} = 0.6255$. The figures 6.1(d)-6.1(f) show the dependence of a on p_A .

Thus for $0 < a < a_{crit}$ the cable tension p increases if a decreases - the latter is for instance the case if caused by a slight perturbation the sag increases and the cable length between the eyelets becomes longer. If in this case the prescribed cable tension p_A is kept constant, the sag will increase perpetually. An analogous acceleration, but in the other direction, takes place if by a slight perturbation a is increased. Therefore the steady-state solutions for $0 < a < a_{crit}$ are mechanically *unstable*. In the other case that is $a_{crit} < a$ we notice that p decreases if a decreases. Consequently a perturbing small enlargement of the sag would decrease the necessary cable tension p so that a constant p_A would work against the perturbation. In this

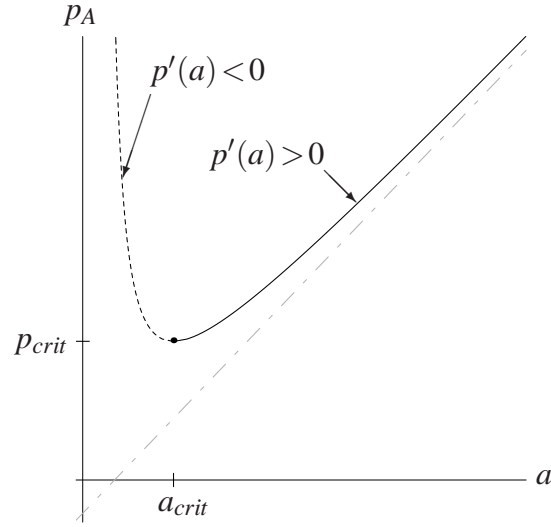
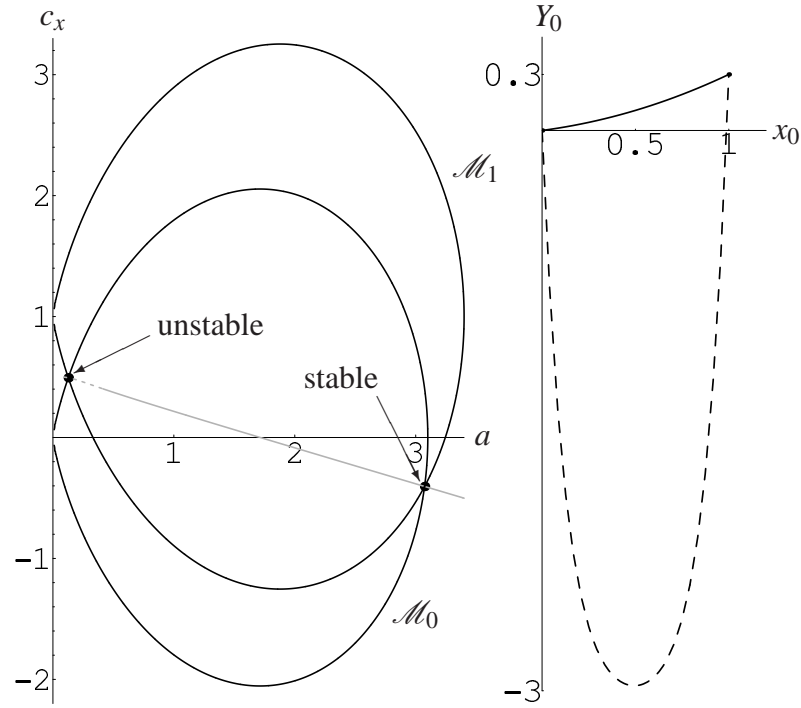


Figure 6.2: The convex function $p(a)$ is enclosed by two asymptotes and has a local minimum at $a = a_{crit}$. The steady-state solutions for $0 < a < a_{crit}$ are the unstable solutions and the solutions for $a_{crit} < a$ are stable.

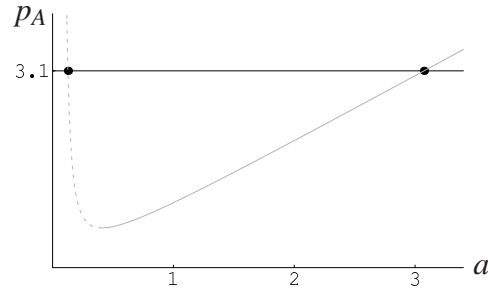
sense the equilibrium solutions for $a_{crit} < a$ are *stable*. In Fig. 6.3(b) we see as an example how the stable and the unstable configurations look like if $y_B = 0.3$ and $p_A \approx 5p_{crit}$.

In ropeway applications of course the interesting steady-state configuration is the mechanically stable one. The corresponding intersection point of \mathcal{M}_0 and \mathcal{M}_1 is found by a Newton-iteration in which due to the convex and conical properties of $f(a, c)$ 'successful' initial values can be given easily. Finally, this procedure is applied to every span of the ropeway and a stable steady-state configuration of the entire cable loop of the ropeway is determined. Since in every span there is such a critical cable tension p_{crit} so that the prescribed cable tension p_A at the bordering tower of this span has to fulfill $p_A > p_{crit}$, we necessarily also get a minimal prescribed cable tension in the haulage device of the aerial ropeway.



(a) The two intersection points of \mathcal{M}_0 and \mathcal{M}_1 correspond to a stable and an unstable configuration.

(b) The stable and the unstable (dashed) configuration.



(c) For $p_A > p_{crit}$ there are two a -branches, a stable and an unstable (dashed) one.

Figure 6.3: In this plots for $y_B = 0.3$ and $p_A = 3.1$ we see how different the resulting steady-state configurations are if p_A is perspicuously higher than p_{crit} (here $p_{crit} = 0.6255$). In particular one of the solutions is always mechanically stable and the other unstable.

Chapter 7

Numerical Simulation of The Dynamics of Ropeways with Finite Elements

In this chapter we describe a way to simulate the three-dimensional dynamics of a circulating monocable aerial ropeway using the Finite Element Method. For this purpose we used *ABAQUS/Explicit* Vers. 6.5.3 which incorporates an explicit time-integrator for the direct method in dynamical applications. Just as in chapter 5, the mainly axial motion of the cable implies large displacements. Therefore the problem is in a geometrical sense non-linear. The special geometry of the pulleys and the sheave assemblies increase the complexity of this non-linear contact problem.

7.1 The components of the model

In chapter 6 we saw how the steady-state configuration of coupled cable spans of the ropeway can be determined. By applying this method successively to all the cable spans, a steady-state configuration for the whole cable loop is obtained. This yields the initial positions and initial velocities of the nodes of the cable loop elements as well as their initial stresses. The cable is modelled by three-dimensional truss elements. In fact the use of more realistic beam elements instead of truss elements would demand a prescription of the initial bending moment in every node. Hence the inclusion of a bending stiffness of the cable would require a steady-state bending moment calculation (s. chapter 4) of the whole cable loop before the Finite Element Analysis can start. In this model there is no self-contact of the cable.

On the towers of a ropeway the cable is in contact with rolls that are gathered in a sheave assembly. As we saw in chapter 1 (Fig. 1.2), the cable passes such sheave assemblies above or beneath and sometimes also above and beneath. In most of the cases the shape of a carrying or holding-down sheave assembly with many rolls can be sufficiently well approximated by an enveloping circular cylinder surface part. The corresponding cylinder radius would be much larger than the radius of the involved rolls. All the different types of sheave assemblies can be modelled by a *generalized sheave assembly*. This is a symmetric hyperbolically bent surface which is generated by a semicircle that rotates around a non-intersecting axis of the same plane (s. Fig. 7.1). The contact between this funnel-shaped rigid surface and the cable, which slides through it like through a three-dimensional eyelet (s. Fig. 7.2(a)), is defined as frictionless. The

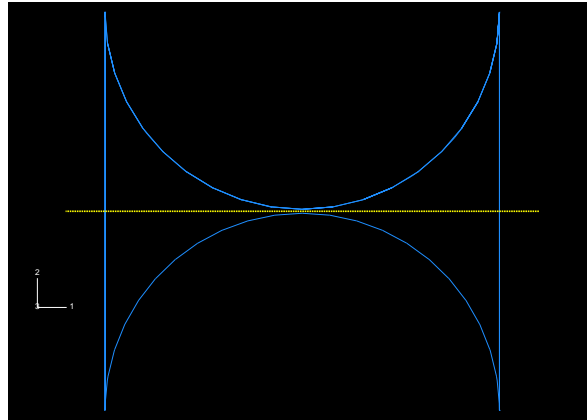


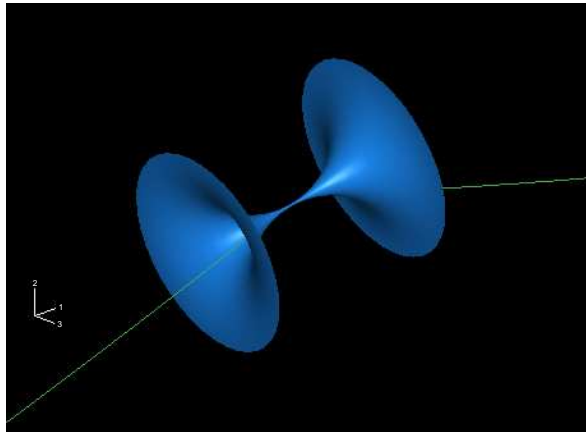
Figure 7.1: A generalized sheave assembly can be modelled by a three-dimensional surface of revolution: a semicircle that has a radius which depends on the envelope of the rolls rotates around a non-intersecting axis of the same plane.

generalized sheave assembly prevents the cable from leaving the track whenever the mesh of the cable loop is sufficiently fine enough. This retention of the cable track on the sheave assembly is nowadays still a very practical safety-problem for which several investigations have to be carried out [5].

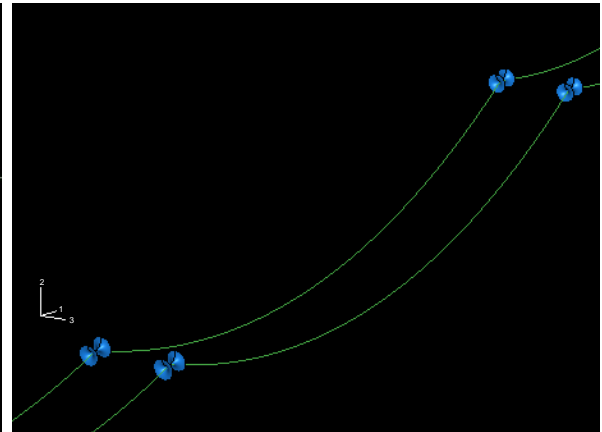
The haulage pulley is the part of the ropeway where the cable tension is prescribed and controlled. It is normally a sheave with an unconstrained vertical rotation axis and it is pulled pneumatically or by a weight perpendicularly to this axis. Usually it is situated in one of the terminals or where the cable has to turn round an angle of 180 degrees. The drive pulley is the part of the ropeway where the axial cable line speed is stipulated. It is also a sheave with a vertical rotation axis, but normally it cannot move horizontally like the haulage pulley. If the haulage pulley and the drive pulley coincide in this terminal, a differential gear has to be installed.

We model the pulleys as rigid circular cylinders with a vertical axis, combined with a cylindric bearing surface or horizontal ramp that keeps the cable in the same height (s. Figs.7.2(c) & 7.2(d)). For the sake of cable routing, at each terminal two eyelets or generalized sheave assemblies for the incoming and the outgoing rope are necessary. The contact between the cable and the circular cylinder surface of the haulage pulley, as well as the contact between the cable and the ramps is frictionless. Only along the segment where the cable contacts the drive pulley, friction is necessary.

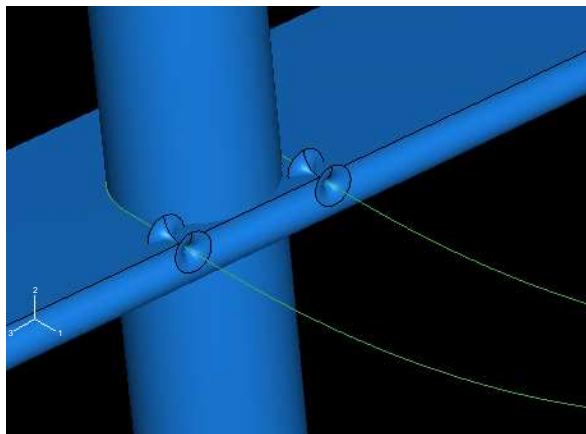
Finally, the cabins or gondolas that are attached to the cable, can be modelled in two ways: either they are simply attached to the cable in certain nodes as combinations of concentrated mass elements with concentrated inertia elements, or they are attached as rigid bodies with shape, mass and inertia tensor of a circular cylinder. In the latter case the cabins are connected to the cable by spring-dashpot elements.



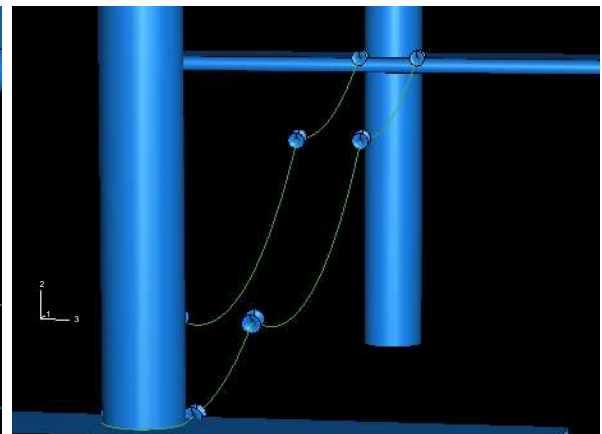
(a) Basically the generalized sheave assembly...



(b) ... acts like a three-dimensional eyelet.



(c) The haulage pulley and the drive pulley...



(d) ... are modelled by cylindrical surfaces.

Figure 7.2: The generalized sheave assemblies on the towers and the haulage and drive pulleys of the bottom and top terminals are modelled by analytical rigid surfaces.

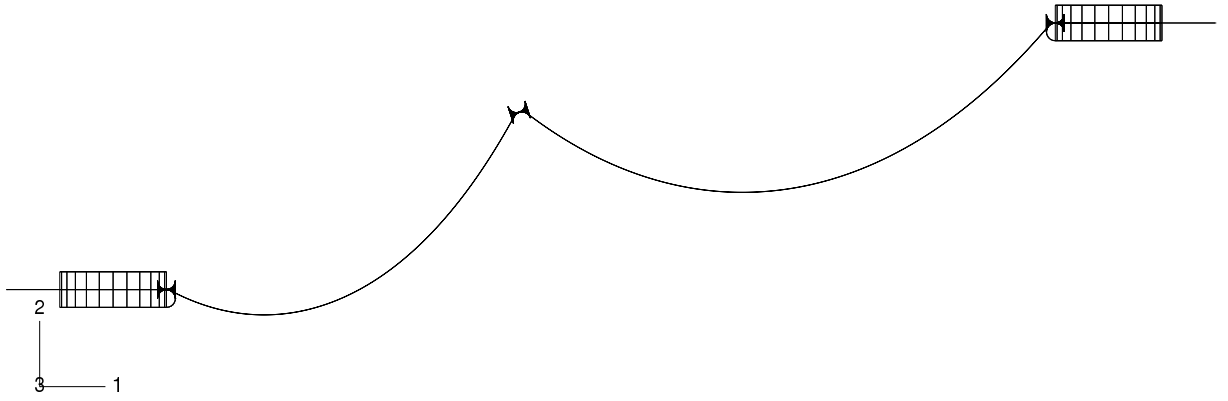


Figure 7.3: An illustrative Finite Element model of a ropeway with two spans used to simulate sag-oscillations. The drive pulley is located in the top terminal (on the right).

7.2 Sag-Oscillations due to Resonances

At the end of chapter 3 it was remarked that sag-oscillations can be expected only if the cable is externally excited.

A periodic external excitation of the cable happens for instance when the line speed v of the monocabre ropeway is kept constant and the cabins or chairs are attached to the cable in equidistant positions. If d is the distance between two adjacent cabins, then $f = v/d$ is the frequency of cabins entering the span from the outmost roll of a sheave assembly. Since $d = N/l$, where N is the total number of cabins attached to the cable loop of length¹ l , we have:

$$f = Nv/l \quad (7.1)$$

In Fig. 7.3 a ropeway model with two spans for the limited purpose of illustration of sag-oscillations is depicted. The first span has a horizontal distance of $20m$ and a vertical distance of $10m$, the second span located next to the drive pulley has a horizontal distance of $30m$ and a vertical distance of $5m$. The cable loop with a mass density $\rho = 8895kg/m^3$, a section area $A = 9.05 \cdot 10^{-4}m^2$ and a Young's modulus $E = 2 \cdot 10^{11}Pa$ has an undistorted length of $l = 149.3m$ and is modelled by thousand 2-node truss elements. The cabins are modelled by a combination of concentrated mass elements ($m_{cab} = 10kg$) with spherically symmetric rotary inertia elements ($I_{ij} = \delta_{ij}m_{cab}^2/2 kg m^2$). They are connected to the cable loop by connector elements. The initial sags correspond to a prescribed cable tension of $928.53N$ in the cable when it turns around the haulage pulley.

The Figs. 7.4–7.6 show a series of Finite Element simulations with this model. In Fig. 7.4 we see eight simulations for $v = 4.5m/s$ after the elapsed simulation time $t = 40.4s$. During the whole simulation the most violent sag-oscillations are visible for the model with four cabins ($N = 4$). Then, in Fig. 7.5 the simulations for $v = 6m/s$ after an elapsed simulation time $t = 40.9s$ can be seen. The most violent sag-oscillations are observed in the model with three cabins ($N = 3$). Finally, in Fig. 7.6 we see eight simulations for $v = 9m/s$ after an elapsed

¹If the cabins are detached in the terminals, l is not exactly the cable loop length but still well defined.

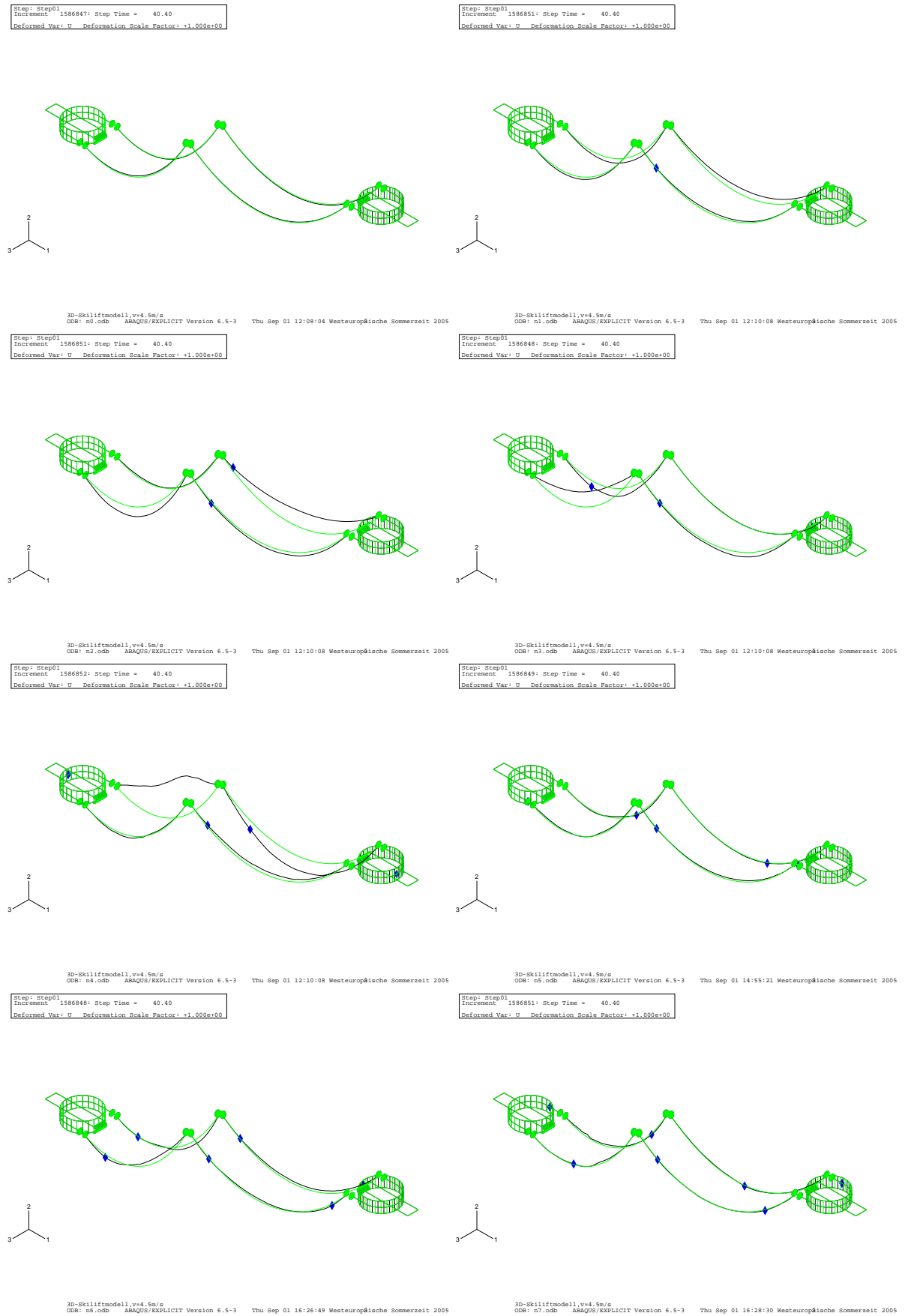


Figure 7.4: The model from Fig. 7.3 with different numbers of cabins ($N=0, 1, 2, \dots, 7$) after an elapsed simulation time $t=40.4s$. In this series of simulations the line speed is $v=4.5m/s$.

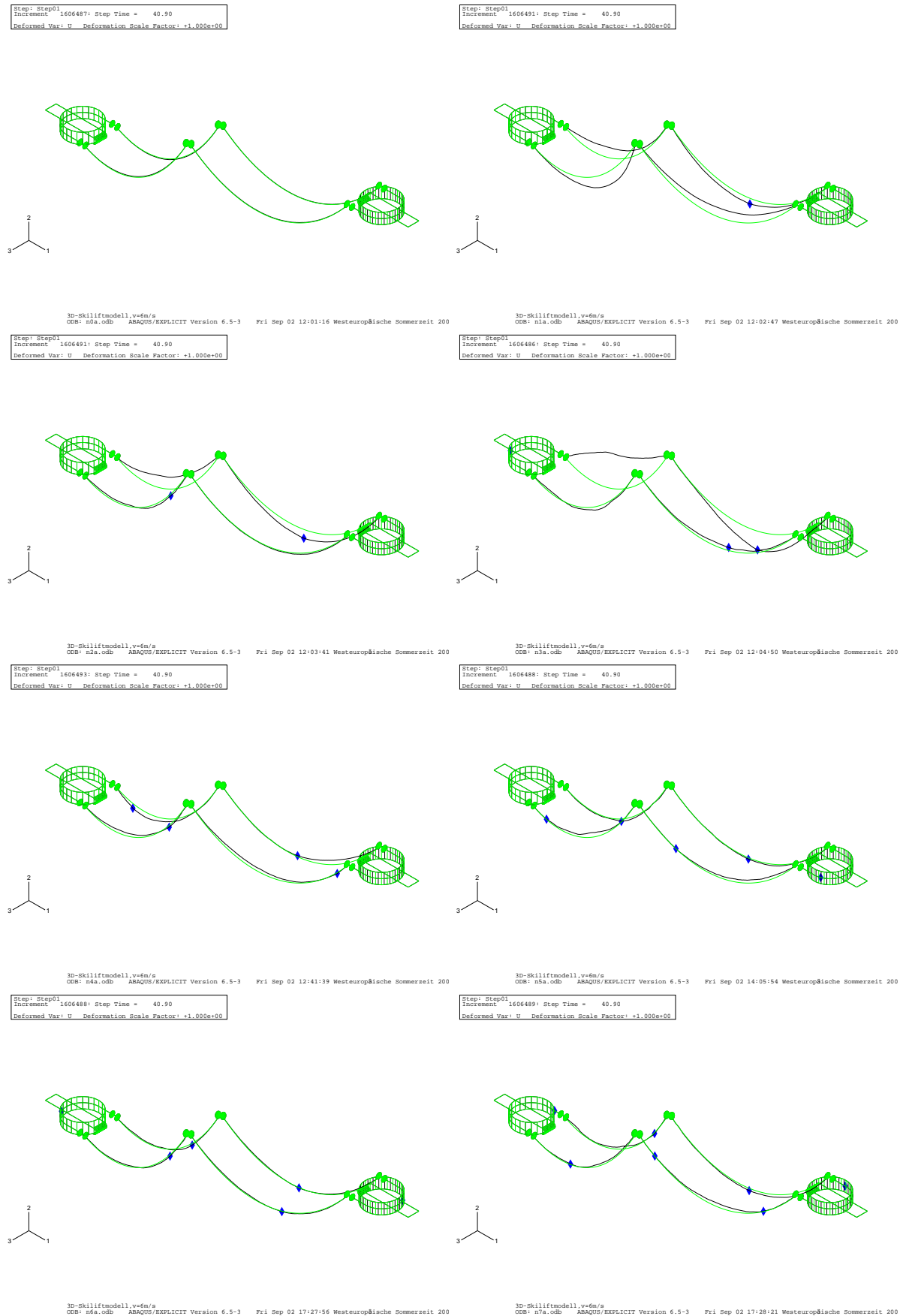


Figure 7.5: Like Fig. 7.4, but now after an elapsed simulation time $t = 40.9s$ and for a line speed $v = 6m/s$.

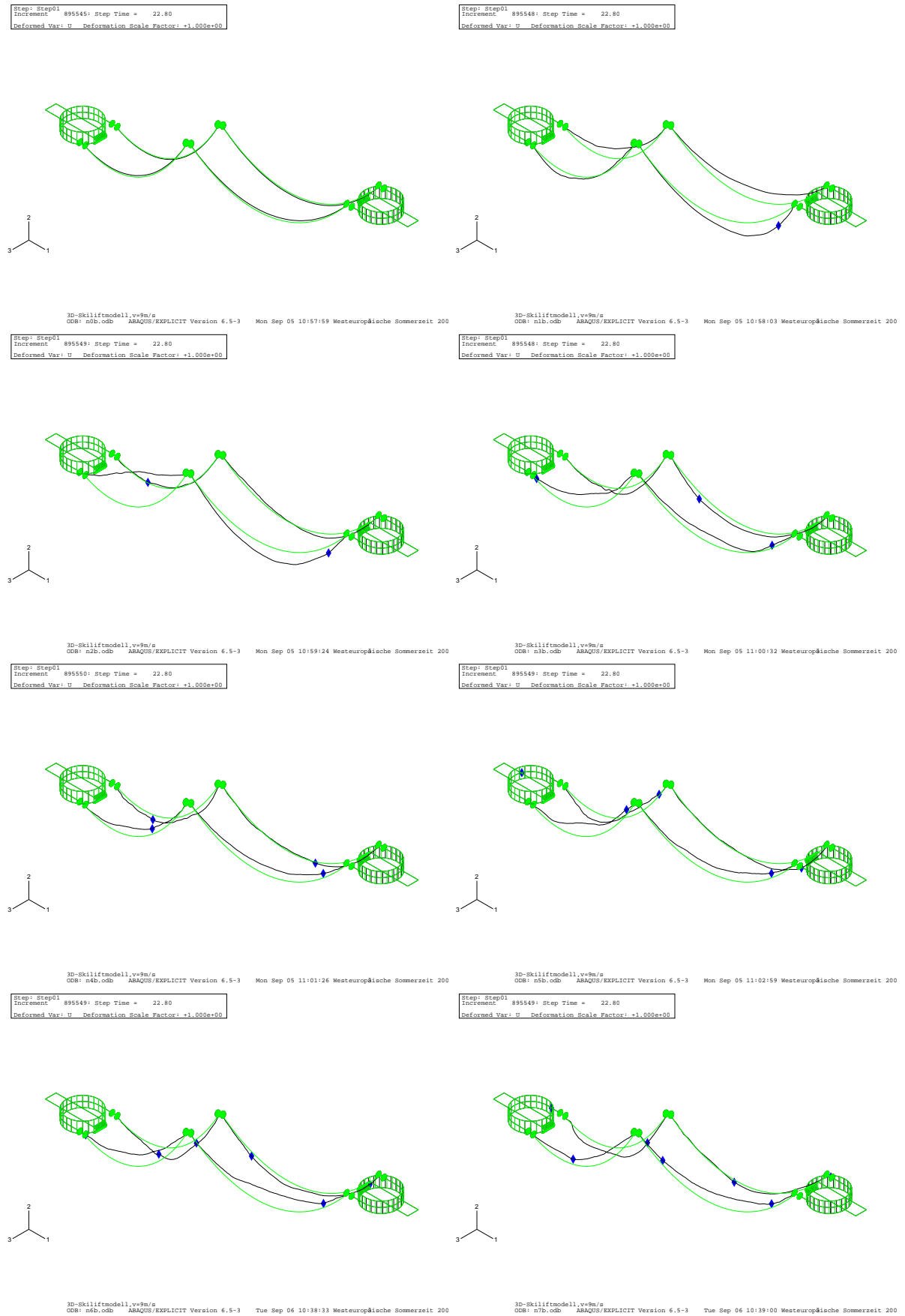


Figure 7.6: Like Fig. 7.4, but now after an elapsed simulation time $t = 22.8\text{ s}$ and for a line speed $v = 9\text{ m/s}$.

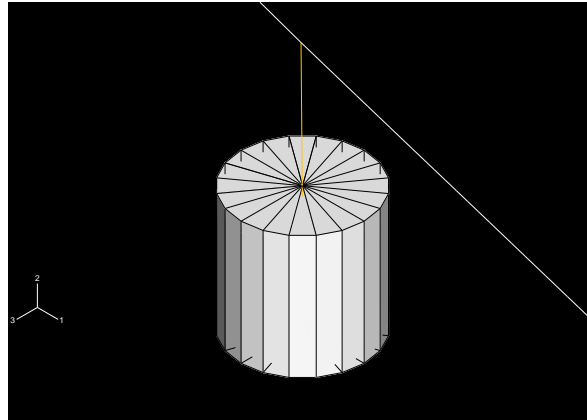


Figure 7.7: The preprocessor program *fiat* for ABAQUS/Explicit attaches cabins or gondolas to the cable that are modelled as cylindrical rigid bodies with a prescribed mass and inertia tensor. They are connected to the cable by spring-dashpot elements.

simulation time $t = 22.8s$. In this case the most violent sag-oscillations are visible for the model with four cabins ($N = 2$).

For all the three different velocities the maximal sag-oscillations in this test series happen if $Nv = 18 \text{ m/s}$, that is due to eq. (7.1) for the same frequency f of cabins which leave a span bordering tower. Hence the example of the series of simulations suggests that sag-oscillations are a resonance phenomenon due to external excitations.

7.3 Preprocessing

Whenever circulating monocable aerial ropeways are projected, it might be very helpful to predict sag-oscillations due to resonances. Therefore we developed a program *fiat* which generates input files for a direct dynamic analysis of such a ropeway model with *ABAQUS/Explicit* 6.5.3. The user feeds the program with important parameters such as the positions of the towers and the pulleys, the material constants, the number of truss elements and the number of cabins (s. Fig. 7.7) which are equidistantly attached to the cable. Theoretically there is no limitation for the size of the model, but of course it is a moot point whether it is reasonable to simulate the whole ropeway.

7.4 Example

As an example we produce with *fiat* the Finite Element model of the Silvrettabahn in Ischgl (Austria) [12] (s. Fig. 7.8). This is a monocable ropeway which comprises 21 cable spans, and each gondola carries six persons.

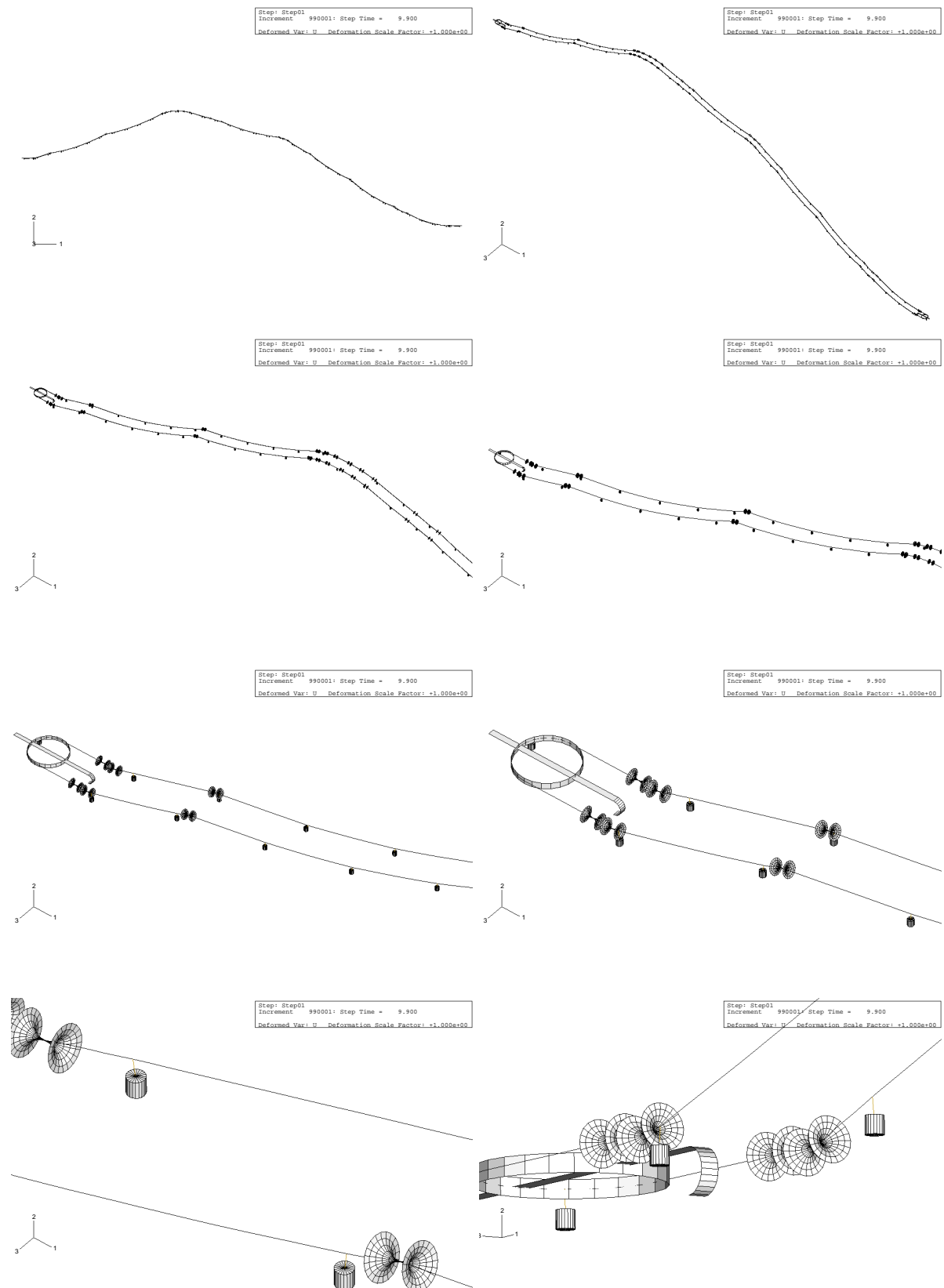


Figure 7.8: Finite Element model of the Silvrettaabahn in Ischgl (Austria) [12]

7.5 Remarks

As mentioned above, it is questionable whether the simulation of a whole ropeway is reasonable. For instance the ski lift in Fig. 7.8 comprises 21 cable spans and has an undistorted cable length of 3790.4m. Attaching 70 gondolas to the cable loop, which we model by 20000 linear truss elements, we can simulate the operation of the lift with a line speed of $v = 5m/s$. If we limit the time increment to $\Delta t_{max} = 10^{-5}s$, ABAQUS/Explicit Vers. 6.5.3 requires seven days² for the simulation time $t = 9.9s$. Hence in this time the gondola covers a distance less than 49.5m. Since some of the cable spans are longer than 200m it would take more than a month to simulate the path of a cabin from one tower to another.

7.6 Example

Fig. 7.9 shows another example of how the model produced by the program *fiat* can be used to simulate realistic situations. The produced ABAQUS input-file was modified in such a way that a similar situation like the tragical accident that took place in Soelden (Austria) in the summer of 2005 could be re-enacted. A helicopter that was flying 200m over an aerial ropeway lost a concrete hopper with a load of 750kg. Unfortunately the cable was hit by the hopper not far away from a gondola (s. Fig. 7.9(b)). Due to the impact the coupling mechanism of the gondola opened in such a way that the cabin fell down. Subsequently, this caused oscillations which were so violent that even persons in the adjacent gondolas were thrown out through the windows.

²computing on a cluster node with four Alpha-EV68 processors (1 GHz, 8 MB Cache/CPU)

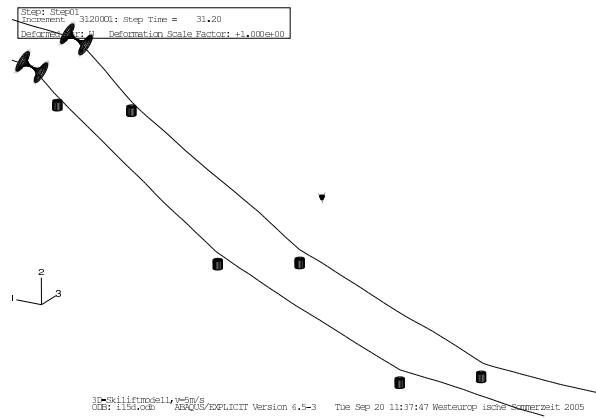
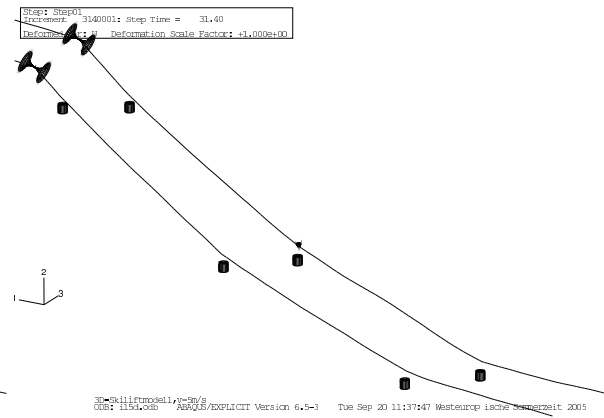
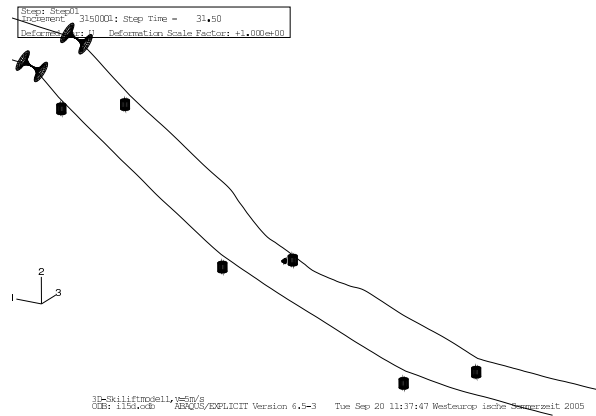
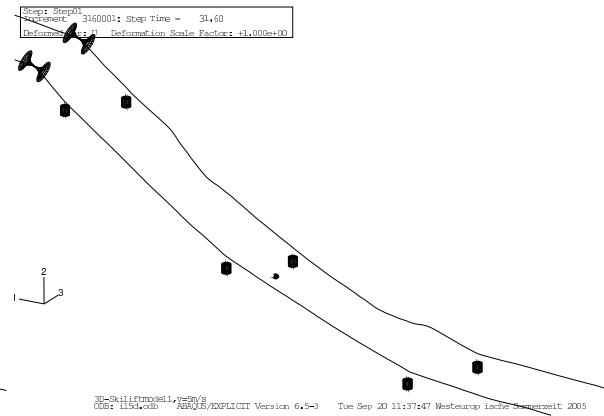
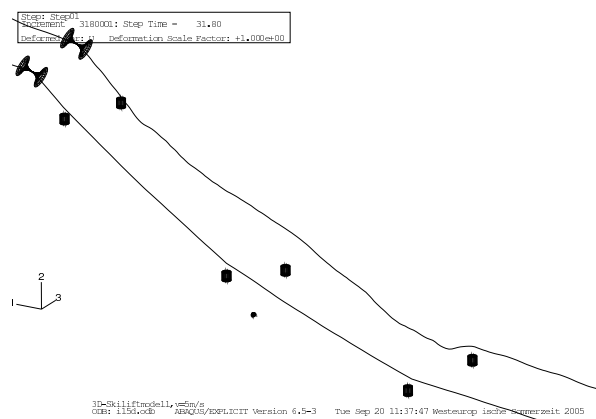
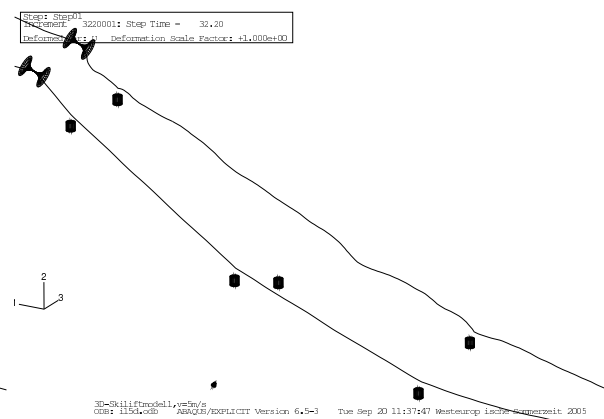
(a) $t = 31.2s$ (b) $t = 31.4s$ (c) $t = 31.5s$ (d) $t = 31.6s$ (e) $t = 31.8s$ (f) $t = 32.2s$

Figure 7.9: The cable of the ropeway is hit by a hopper not far away from a gondola (s. Fig. 7.9(b)). Due to the impact the coupling mechanism of the gondola opens in such a way that the cabin falls down.

Chapter 8

Conclusion

In our investigation on sag-oscillations of circulating monocable aerial ropeways we primarily looked at the dynamics of axially moving cables.

After deriving the equations of motions for the cable that moves in an external force field in a three-dimensional space, we observed that the same system of forces is acting on the cable as it is acting on the fluid within a massless tube. Hence the motion of the cable configuration is the same as of the centerline of such a fluid conveying tube.

In a constant gravitational field the steady-state configuration between two eyelets is in general either a convex or a concave catenary. Due to the inextensibility of the cable, the corresponding catenary parameter is independent of the cable line speed. Unlike in the static case, a concave configuration can be mechanically stable.

We discussed the steady-state configuration in dependence on the cable line speed if the cable tension is prescribed in one of the eyelets. Hence we made two observations for typical contemporary ropeway applications: on the one hand that the concave steady-state configuration is not a relevant one, and on the other hand that the sag does practically not depend on the line speed. As a matter of fact the cable-tension is linearly dependent on the height and thus in the same way as the hydrostatical pressure depends on height in fluid mechanics.

We analysed the eigenfrequencies and eigenmodes of the in-plane motion in dependence on the cable line speed if the cable tension is prescribed in one of the eyelets. Hence we saw that for typical contemporary ropeway applications the lowest eigenfrequencies and eigenmodes are practically independent of the line-speed. Nevertheless we saw that the line speed still remains to be an important parameter since it is proportional to the external excitation frequency that is acting on the cable caused by the equidistantly attached gondolas or chairs.

We showed that if we take rolls instead of eyelets as boundaries, the linear correction term vanishes at the points, where the steady-state configuration touches the rolls tangentially. Therefore in this case the boundary conditions of the linearized problem turn out to be the same as if there were two eyelets on the surfaces of the two rolls.

Moreover, we discussed the relationship between the shape of the lowest eigenmode and the inextensibility of the cable.

Based on the analogy between the cable configuration and the fluid conveying tube, we stated that there is no self-excitation of the axially moving cable between two eyelets. In particular we came to the conclusion that violent sag-oscillations of aerial ropeways are caused by external

oscillations.

In addition, we saw to what extent the planar steady-state solution of the cable between two rolls in a constant gravitational field changes if the cable is not perfectly flexible. Thus, in the case of almost perfect flexible cables we considered the slight bending stiffness as a small perturbation of the completely flexible cable. We showed that this is a regular singularly perturbed boundary value problem and after introducing boundary layer variables, we derived a formal approximation for the solution that is a matched asymptotic expansion. This analytical results were compared with numerical results that were computed in Fortran90 using the boundary value solver COLSYS. Especially at the boundaries where the bending stiffness plays a crucial role, the two different methods showed very good agreement.

We described various two-dimensional Finite Element simulations with ABAQUS/Standard that were performed in order to check the results concerning the steady-state motion of the cable.

Then we looked at the cable of a circulating monocable aerial ropeway which is actually a cable loop. We observed that if we prescribe the cable tension on a tower in the adjacent cable span, there might be two, one or no possible steady-state configuration. In the case of two solutions, one is mechanically stable and the other one is mechanically unstable.

Between two neighbouring cable spans of a ropeway there is always a certain 'force-interaction' over the sheave assemblies of the common tower. Thus if the prescribed cable tension in the haulage device of the ropeway is high enough, a mechanically stable steady-state configuration of the cable loop can be determined. This configuration is for instance necessary if a three-dimensional Finite Element model of a ropeway has to be performed.

Furthermore we showed an illustrative series of simulations that indicate how sag-oscillations could be caused by resonance due to a periodic excitation of an axially moving cable. Basically the phenomenon of sag-oscillations can be explained without elasticity. Crucial, however, is the fact that two or more cable spans have to be involved. Obviously the configuration length in one cable span increases while simultaneously the configuration length in an adjacent span decreases.

Finally, for the purpose of testing ropeways we developed a program in C++ that helps to generate input-files for ABAQUS/Explicit.

Acknowledgements

I do not take it for granted that I live in an age and in a place in which knowledge is that easily accessible. I feel very thankful for this and also for the many people around me who gave me the opportunity for studies and for scientific work. Some of them are: my doctoral advisor Ao.Univ.Prof. Dipl.-Ing. Dr.techn. Alois Steindl for his helpfulness in so many occasions, the manager of the scientific project I worked on O.Univ.Prof. Dipl.-Ing. Dr.techn. Dr.h.c. Hans Troger for his cordiality, my co-advisor O.Univ.Prof. Dipl.-Ing. Dr.techn. Franz G. Rammerstorfer for his cooperativeness when I started to learn the Finite Element Method, my father Dr.techn. Wolfgang Renezeder for his patience and the many fruitful discussions on mechanics, my friend Dipl.-Ing. Helga Allmer for advising and helping me with the figures, my friend Dipl.-Ing. Dr.techn. Bernhard Barkow for also helping me with the figures and with Latex, my sister in law Mag.phil. Dr.phil. Ulrike Renezeder for her helpfulness and patience correcting my grammatical mistakes in English, Mr. Michael Dahms for allowing me to use his photos, the expert advisor Dipl.-Ing. Dr.techn. Rudolf Knasmillner for explaining me so many things about ropeways, the computer advisor of the Central Service for Informatics of our university Ing. Josef Beiglböck for his cooperativeness in helping me to perform Finite Element programs, the Austrian Science Fund (FWF) for financing the project P15825 which I worked on and last but not least my dear family for their love.

Appendix A

Regular Singularly Perturbed Boundary Value Problem

In the subsection 4.3.1 of chapter 4 we perturbed the perfectly flexible cable with a slight bending stiffness and saw that the steady-state configuration turned out to be a regular singularly perturbed boundary value problem. Since there are also singular singularly perturbed boundary value problems, we want to state now more precisely how a regular singularly perturbed boundary value can be defined and how a formal approximation of the solution is derived in the form of a matched asymptotic expansion (s. a. O'Malley [14]). Furthermore we also will go through the existence and the uniqueness of the solution (s. Schmeiser [27, 28] for more details). Consider a singularly perturbed boundary value problem of the form

$$\begin{aligned}\varepsilon y' &= f(y, z, t, \varepsilon), \\ z' &= g(y, z, t, \varepsilon), \\ 0 &= b(y(0), z(0), y(1), z(1)),\end{aligned}\tag{A.1}$$

where $(.)' = d(.) / dt$ and $t \in [0, 1]$. Furthermore, y is a $(n_+ + n_-)$ -vector, z is an n_0 -vector and f , g and b are appropriate mappings. Let the reduced equations

$$0 = f(\bar{y}, \bar{z}, t, 0)$$

be uniquely solvable with respect to $\bar{y} = \phi(\bar{z}, t)$. Suppose that the matrix $f_y(\phi(\bar{z}, t), \bar{z}, t, 0)$ has n_- (stable) eigenvalues with strictly negative real parts and n_+ (unstable) eigenvalues with strictly positive real parts for all t in the closed interval $[0, 1]$. For a solution of (A.1) we make the ansatz

$$\begin{aligned}y(t, \varepsilon) &= \phi(\bar{z}(t), t) + Ly(\tau) + Ry(\sigma) + O(\varepsilon) \\ z(t, \varepsilon) &= \bar{z}(t) + O(\varepsilon),\end{aligned}\tag{A.2}$$

where $\tau = t/\varepsilon$, $Ly(\infty) = Ry(\infty) = 0$. Substituting in (A.1) yields

$$\begin{aligned}
 \bar{z}' &= g(\phi(\bar{z}, t), z, t, 0), \\
 \frac{d}{d\tau} Ly &= f(\phi(\bar{z}(0), 0) + Ly, \bar{z}(0), 0, 0), \\
 \frac{d}{d\sigma} Ry &= -f(\phi(\bar{z}(1), 1) + Ry, \bar{z}(1), 1, 0), \\
 0 &= b(\phi(\bar{z}(0), 0) + Ly(0), \bar{z}(0), \phi(\bar{z}(1), 1) + Ry(0), \bar{z}(1)), \\
 Ly(\infty) &= Ry(\infty) = 0.
 \end{aligned} \tag{A.3}$$

Schmeiser [27] deduced the following theorem about existence and uniqueness from the papers of Vasileva & Butuzov [39] and Esipova [6]:

Theorem 1. *Let f , g and b be continuously differentiable with respect to all variables. Let problem (A.3) have a stable solution (\bar{z}, Ly, Ry) , i.e. the linearization of (A.3) at (\bar{z}, Ly, Ry) is invertible. Then there are constants $\varepsilon_0, \delta > 0$, in such a way that for $0 < \varepsilon \leq \varepsilon_0$ a solution $(y(t, \varepsilon), z(t, \varepsilon))$ of (A.1) exists, which satisfies (A.2) and is unique in a ball with radius δ and centre $(\phi(\bar{z}, t) + Ly(\tau) + Ry(\sigma), \bar{z}(t))$ in the space $C^1[0, 1]$.*

Appendix B

Properties of $f(a, c) = a \cosh(c/a)$

In eq. (6.5) of chapter 6 we defined $f(a, c)$ and used some characteristics of this function, which we will discuss now more in detail.

The function $f(a, c)$ is asymmetric with respect to the variable a and symmetric with regard

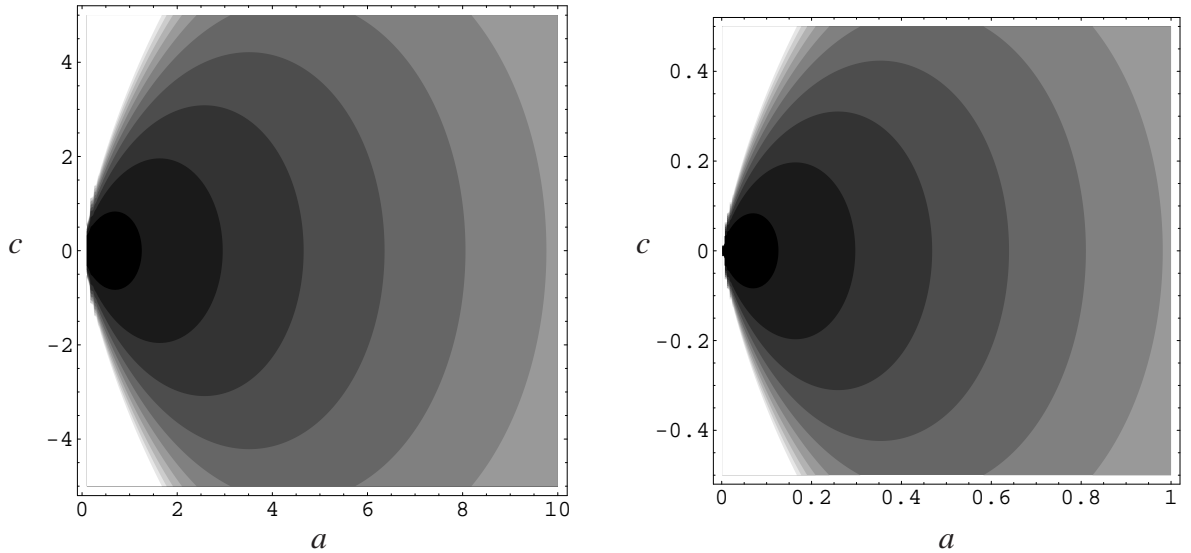


Figure B.1: Contour-plots of the function $f(a, c)$ in eq. (6.5) - light color means high value. The similarity between the two pictures of different 'zoom'-factor is typical for the parallel plane sections of a geometrically three-dimensional cone $\Gamma \subset \mathbb{R}^3$ for which $\Gamma \subset \lambda \Gamma$ holds with $\lambda > 0$.

to the variable c (s. Fig. B.1) and fulfills for all λ the equation

$$f(\lambda a, \lambda c) = \lambda f(a, c).$$

Thus all the curves $\mathcal{C} = \{(a, c) | f(a, c) = p\} \cup (0, 0)$ with different p are similar to each other and f is more a homogeneous function of order one. In other words the graph of f is geometrically a conical surface with its vertex in $(0, 0)$. Hence it becomes also clear that for non-zero

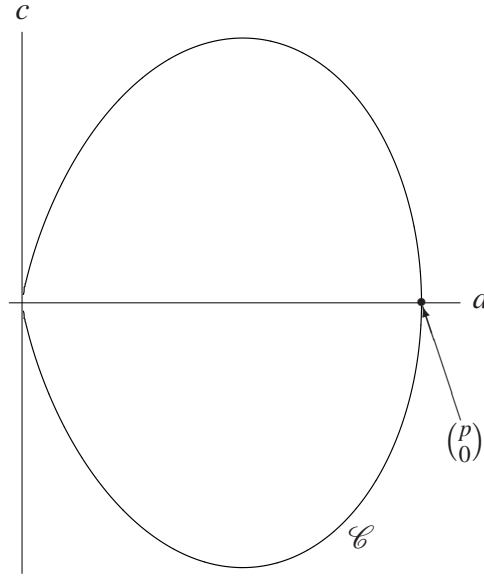


Figure B.2: The domain enclosed by the line $\mathcal{C} = \{(a, c) | f(a, c) = p\} \cup (0, 0)$ has the area p^2 .

a one of the eigenvalues of the Hessian matrix of $f(a, c)$ in the a, c -plane is zero and that at the point (a, c) the eigenvector to the zero-eigenvalue is (a, c) . The other eigenvalue, representing the other main curvature, is positive for positive a . As a consequence for constant non-zero p the closed line \mathcal{C} where $f(a, c) = p$ (s. Fig. B.2), encloses a convex domain in the (a, c) -plane with an area A . The implicitly given function of \mathcal{C} can be integrated analytically resulting in $A = p^2$.

Finally, for the sequence $g_n(x) = n / \cosh(nx)$ with $n \in \mathbb{N}$ it can be easily shown that $\int_{-\infty}^{\infty} g_n(x) dx = \pi$ for every n and moreover that $\lim_{n \rightarrow \infty} g_n(x) = \pi \delta(x)$. Hence we have

$$\lim_{a \searrow 0^+} \frac{1}{f(a, c)} = \pi \delta(c),$$

so that the behaviour of $f(a, c)$ for $a \searrow 0^+$ becomes comprehensible.

Bibliography

- [1] S. S. ANTMAN, Nonlinear Problems of Elasticity, Springer-Verlag, New York – Berlin – Heidelberg
- [2] U. M. ASHER, J. CHRISTIANSEN AND R. D. RUSSELL, A collocation solver for mixed order systems of boundary value problems, *Math. Comp*, **33**: 659 – 679, (1978).
- [3] K.-J. BATHE, Finite Elemente Methoden, 2.Auflage - Berlin [u.a.], Springer, 2002
- [4] E. CZITARY, Über die Schwingungen des Zugseiles von Seilschwebbahnen, *Österr. Ing.-Archiv*, **15**(2), 34–53. (1961).
- [5] E. ENGEL UND N. OSTERMANN, Förderseil-Entgleisungsschutz, *Arbeiten d. Inst. f. Eisenbahnwesen, Verkehrswirtschaft u. Seilbahnen*, **31**, 15–18. (2003).
- [6] V. B. ESIPOVA, The asymptotic behaviour of solutions of the general boundary value problem for singularly perturbed systems of ordinary differential equations of conditionally stable type, *Diff. Eqns* **11**, 1457-1465 (1975).
- [7] P. HOLMES AND J. MARSDEN, Bifurcations to divergence and flutter in flow-induced oscillations: an infinite dimensional analysis, *Automatica* **14**, 367-384 (1978).
- [8] H. M. IRVINE AND T. K. CAUGHEY, The linear theory of free vibrations of a suspended cable, *Proceedings of the Royal Society London* (1974) **A341**, 299-315.
- [9] H. M. IRVINE, Free vibrations of inclined cables, *American Society of Civil Engineers, Journal of the Structural Division* (1978) **104**, 343-347.
- [10] H. M. IRVINE, Cable Structure, Cambridge, Massachusetts: MIT Press.
- [11] S. LIEDL, Motions and forces in the rope system of aerial ropeways during operation, *8th International Congress for Transportation by Rope (OITAF)*, 381–392 (1999).
- [12] R. LÖSCHER, Pumpschwingungen bei Einseilumlaufbahnen, Dissertation a. d. TU Wien, Fak. f. Bauingenieurwesen, Inst. f. Eisenbahnwesen (1997).
- [13] R. MIROSHNIK, The Phenomenon of Steady-State String Motion, *Journal of Applied Mechanics* (2001) **68**(7), 568-574.
- [14] R. E. O'MALLEY, Introduction to Singular Perturbations, New York – London: Academic Press, Applied Mathematics And Mechanics Vol. 14, 1974

-
- [15] O. M. O'REILLY AND P. VARADI, Elastic Equilibria of Translating Cables, *Acta Mechanica* (1995) **118**, 189-206.
- [16] O. M. O'REILLY, Steady Motions of a Drawn Cable, *Journal of Applied Mechanics* (1996) **63**(3), 180-189.
- [17] N. C. PERKINS, Three dimensional theory and analysis of travelling sagged cable dynamics, Ph.D. Dissertation, University of California, Berkeley.
- [18] N. C. PERKINS AND C. D. MOTE, JR., Three-dimensional vibration of travelling elastic cables, *Journal of Sound and Vibration* (1987) **114**(2), 325-340.
- [19] N. C. PERKINS AND C. D. MOTE, JR., Theoretical and experimental stability of two translating cable equilibria, *Journal of Sound and Vibration* (1989) **128**(3), 397-410.
- [20] F. G. RAMMERSTORFER, Grundzüge Finite Elemente und andere Numerische Ingenieurmethoden, Skriptum zur gleichnamigen Vorlesung an der TU Wien (2002).
- [21] F. G. RAMMERSTORFER, Nichtlineare Finite Elemente Methoden, Skriptum zur gleichnamigen Vorlesung an der TU Wien (2002).
- [22] G. REGA ET AL., Experimental Investigation of the Nonlinear Response of a Hanging Cable. Part I: Local Analysis, *Nonlinear Dynamics* **14**, 89-117 (1997).
- [23] H. C. RENEZEDER, A. STEINDL AND H. TROGER, On the dynamics of axially moving strings, *Proc. Appl. Math. Mech.*, **4**: 201–202, (2004).
- [24] H. C. RENEZEDER, A. STEINDL AND H. TROGER, On the dynamics of circulating monocable aerial ropeways, *Proc. Appl. Math. Mech.*, **5**: 123–124, (2005).
- [25] J. H. ROHRS, On the oscillations of a suspension cable, *Transactions of the Cambridge Philosophical Society* (1851) **9**, 379-389.
- [26] E. J. ROUTH, Advanced Rigid Dynamics, New York: MacMillan, fifth edition.
- [27] C. SCHMEISER, Finite Deformations of Thin Beams. Asymptotic Analysis by Singular Perturbation Methods, *Journal of Applied Mathematics* **34**, 155-164 (1985).
- [28] C. SCHMEISER, Angewandte Mathematik, Skriptum zur gleichnamigen Vorlesung an der TU Wien (2003).
- [29] A. SIMPSON, Determination of the inplane natural frequencies of multispans transmission lines by a transfer matrix method, *Proceedings of the Institution of Electrical Engineers* (1966) **113**, 870-878.
- [30] A. SIMPSON, On the Oscillatory Motions of Translating Elastic Cables, *Journal of Sound and Vibration* (1972) **20**, 177-189.
-

-
- [31] R. SKUTCH, Über die Bewegung eines gespannten Fadens, welcher gezwungen ist, durch zwei feste Punkte mit einer constanten Geschwindigkeit zu gehen, und zwischen denselben in Transversal-Schwingungen von geringer Amplitude versetzt wird, *J. Ann. Phys. Chem.* (1897) **61**, 190-195.
- [32] A. I. SOLER, Dynamic response of single cables with initial sag, *Journal of the Franklin Institute* (1970) **290**, 377-387.
- [33] U. STAROSSEK, Die Dynamik des durchhängenden Seiles, Instiut für Tragwerksentwurf und -konstruktion der Universität Stuttgart.
- [34] A. STEINDL, Nonlinear Three-Dimensional Oscillations of a Fluid Conveying Tube with Symmetric Elastic Support, Habilitationsschrift, TU Wien, 1996
- [35] R. D. SWOPE AND W. F. AMES, Vibrations of a moving threadline, *Journal of the Franklin Institute* (1963) **275**, 36-55.
- [36] M. S. TRIANTAFYLLOU, Linear dynamics of cables and chains, *Shock and Vibration Digest* (1984) **16**, 9-17.
- [37] M. S. TRIANTAFYLLOU, The dynamics of translating cables, *Journal of Sound and Vibration* (1985) **103**, 171-182.
- [38] H. TROGER AND A. STEINDL, Nonlinear Statbility and Bifurcation Theory, Wien, New York, Springer, 1991
- [39] V. B. VASILEVA AND V. F. BUTUZOV, Asymptotic Expansions of Solutions of Singularly Perturbed Equations, *Nauka* (in Russian) (1973).
- [40] H. H. WEST, L. F. GESCHWINDNER AND J. E. SUHOSKI, Natural vibrations of suspension cables, *American Society of Civil Engineers, Journal of the Structural Division* (1975) **101**, 2277-2291.
- [41] P. WOLFE: Vibration of Translating Cables, *Acta Mechanica - Springer Verlag* **158**, 1-14 (2002).
-

Curriculum Vitae

Personal Information

Name: Dipl.-Ing. Hans Christian Renezeder
Address: Davidgasse 39/28
A – 1100 Wien
Date of Birth: October 4th, 1975
Nationality: Austria

Education

3/2002-1/2006 PhD-student at the Institute of Mechanics and Mechatronics,
Vienna University of Technology
10/1993-6/2001 Student of Physics, Vienna University of Technology,
master's thesis "Thermodynamical Properties of Model Systems"
at the Institute of Theoretical Physics
9/1985-6/1993 Secondary School, Schottengymnasium of the Benedictines, Vienna
9/1981-6/1985 Primary School, Marianum, Vienna

Professional Experience

since 7/2005 Programmer in the civil engineer office Renezeder, Vienna.
7/2002-6/2005 Research assistant at the Institute of Mechanics and Mechatronics,
Vienna University of Technology

Military Service

7/2001-2/2002 Staff-Company of the Vienna Military Command